An Experimental Study on the Influence of the Particle Size of Chemically Active Inhibitors in Turbulent Combustion

Erlend Wangsholm

Dissertation for the degree of Master of Science
on the subject of Process Safety Technology

Department of Physics and Technology
University of Bergen
Norway
June 2012

Abstract

Accidental gas leaks pose a great danger in the process industries. To reduce the consequences, should such a gas leak ignite, mitigating measures are needed. One such measure, involving the introduction of water deluge upon confirmed gas detection, has been successfully applied on larger offshore production platforms. The use of water deluge is a promising effort, but due to the large amounts of water needed, it is ill-suited for inland facilities. A possible alternative, involving chemically active inhibitors, has been investigated by Total Petrochemicals and GexCon AS in the recent years.

The concept is to use pressurized containers to release chemically active inhibitors into a detected gas leak. Since combustion consists of chain-reactions involving radicals it is possible to slow the combustion, or even quench it, by using inhibitors that react with those same radicals.

To verify the potential of this concept, laboratory and large-scale experiments were conducted at GexCon AS. A wide variety of potential inhibitors were tested on a variety of combustible hydrocarbon-air mixtures. It was found that potassium carbonate had the highest general effect. When added at concentrations of up to 50g/m^3, it led to a drastic reduction of the laminar burning velocity for most of the combustible mixtures tested. At higher inhibitor concentrations, the added effect varied depending on the type of fuel and the equivalence ratio tested.

There was however, no investigation into the possible effect of the inhibitor particle size. Due to the larger surface area to mass ratio, and the increased rate of particle decomposition as it is exposed to heat, smaller particles should be more efficient at inhibiting combustion. This tendency has been seen in experiments involving laminar combustion, but has yet to be confirmed for turbulent combustion.

The aim of this thesis is therefore to investigate the influence of particle size in the chemically active inhibitor, potassium carbonate. Three parameters commonly used to describe the violence of explosions are examined using a 20 liter USBM vessel. The particle size, concentration of inhibitor, and equivalence ratio of the combustible mixture are varied. The parameters examined are the maximum pressure, the maximum rate of pressure rise and the calculated laminar burning velocity, of the explosion.

The research was conducted at the laboratories of the University of Bergen and at GexCon AS. Funding for the project was provided by the University of Bergen, GexCon AS and Total Petrochemicals.

The overall conclusion from the conducted experiments is that the particle size of the chemically active inhibitor, potassium carbonate, influences its ability to function as an inhibitor in turbulent combustion. It was also discovered that the grinding effect caused, as the potassium carbonate is dispersed from the reservoir in the 20 liter USBM vessel, is concentration dependent. Neither observation has been found in other scientific literature.

Acknowledgements

As most experimental assignments, this one has also had its share of obstacles along the way. Fortunately I've had many able minds to turn to and I'd like to take this opportunity to thank those who've contributed. First and foremost I would like to thank my three supervisors; associate Professor Bjørn J. Arntzen at the University of Bergen, Professor emeritus Rolf K. Eckhoff, and Kees van Wingerden at GexCon AS. They provided staunch support while I wrestled with the thesis and kept a close eye on the progression of my work.

I would also like to extend a general thanks to the staff at GexCon AS who contributed with helpful guidance on various issues in the early stages of my work.

At the *Elektronmikroskopisk felleslaboratorium* of the University of Bergen I would like to thank senior engineer Egil S. Erichsen for hours of help with the scanning electron microscope. His contribution was essential for the work related to the particle size of my samples.

I would like extend my gratitude to Tor Ivar Sellevold for leaving me a solid foundation to build on with his master thesis and for showing me how to operate the 20 liter USBM vessel and its software, at the explosion laboratory of the University of Bergen.

I would also like to thank my fellow students at the safety technology discipline, for making my years at the University of Bergen memorable. A special thanks to Kjetil L. Olsen, for valuable discussions and feedback on subjects related to my thesis.

I would also like to thank all my friends for their companionship and inspiration over the years. The annual trips abroad were a brilliant idea and are much cherished.

I would like to thank my parents, Arne and Berit, for their continuing support, even when I must have seemed clueless as to what I wanted to study next. Without you, the power company would have turned off the electricity in my apartment years ago. I would also like to thank my brothers, Terje and Sindre, for inspiration in exploring the world outside my window.

Last, but not least, I would like to thank my wonderful wife, Sandra. Her everlasting love and support is valued beyond words.

Erlend Wangsholm

Table of Contents

Nomenclature

C: rate constant
A: collision frequency
E_a: activation energy
P: pressure
t: time
V: volume
T: temperature
n: mol
R: gas constant
S_L: laminar burning velocity
S_T: turbulent burning velocity
τ: time scale
k: turbulent kinetic energy
λ: wave number
u: velocity
x: velocitiy
ε: turbulent energy dissipation rate
ρ: density
H: enthalpy
E: energy
c: heat capacity
ɣ: isentropic expansion factor (c_p/c_v)
μ: dynamic viscosity
Re: Reynolds number
δ : Flame thickness
Da: Damköhler number
Ka: Karlovitz number
K: Karlovitz stretch factor
v: kinematic viscosity
r: radius
α: thermal diffusivity

Subscript

I: integral scale
c: chemical scale
T: Taylor scale
O: macroscopic scale
rms: root mean square
ex: explosion
ci: chemical igniter
fl: flame
v: vessel
i: initial
f: final
b: burned
u: unburned

Abbreviations

UoB: University of Bergen
CFD: Computational Fluid Dynamics
FLACS: FLame ACcelerator Simulator
USBM: Unites States Bureau of Mines
rms: root mean square
EQ: Equivalence ratio

Survey of the Thesis

Chapter 1 presents an introduction on how the risk related to accidental explosions in industrial situations can be managed. It also gives an introduction on how standardized experiments can be used to evaluate the consequences in case of an accidental explosion. At the end of the chapter, the aim of the current project is highlighted.

Chapter 2 presents the basic theory on combustion and the effect of inhibitors required to fully understand the thesis.

Chapter 3 presents relevant scientific publications. These cover the sensitivity of the burning velocity, the use of powders in the 20 liter vessel, and the calculation of a laminar burning velocity from turbulent combustion in closed volumes.

Chapter 4 presents the experimental work conducted in relation to the thesis. It covers the preparation of the samples, the experimental setup and the experimental procedures.

Chapter 5 presents the experimental results separated into two separate subsections. The first section contains pictures, taken with the scanning electron microscope, of the inhibitor particles. The second section contains graphs illustrating the effect of the inhibitors on the turbulent combustion.

Chapter 6 presents the discussion of the experimental results. The main focus is on the problems related to the grinding effect of the 20 liter vessel and on the effect of the inhibitor on the combustion.

Chapter 7 presents the conclusion of the conducted work.

Chapter 8 presents suggestions for further research.

1. Introduction

The world consumption of natural gas is at an all-time high and steadily increasing. Combustible mixtures of hydrocarbon gases and air can constitute a severe safety hazard during processing, transport and usage. Examples of the devastating effect accidental ignition of hydrocarbon gas leaks in petrochemical industries include Pasadena (1989), Pajaritos (1991), Deer Park (1997), Münchmünster (2005) and Texas (2006). As this list clearly illustrates, there is still work to be done for the use and handling of hydrocarbon gases to be safe. As industrial development continues to spread to new parts of the world, the challenges with regards to safety become increasingly complex. The demand for flexible and innovative solutions, to established challenges, will therefore not diminish in the foreseeable future.

This thesis constitutes part of a larger project where the aim is to develop a new method for preventing and mitigating accidental gas explosions through the use of chemically active inhibitors. Experiments are conducted with a 20 liter constant volume explosion vessel with inhibitor applied to a combustible propane-air mixture shortly before ignition. The inhibitor is dispersed by a pressurized air burst, which at the same time causes generation of turbulence. With the aid of pressure sensors and the KSEP 6.0 software, a pressure-time diagram of the explosion can be used to calculate explosion parameters. One such parameter is the laminar burning velocity, which is a key parameter in the CFD-code FLACS. This is a follow-up study of a previous investigation conducted at the University of Bergen which failed to produce conclusive results.

1.1 Managing Risk

To understand how to manage risk, an agreement as to what defines risk is of crucial importance. According to [1] risk can be defined as *"the threat an unwanted incident constitutes to persons, the environment and materials"*. This is often expressed quantitatively with the formula

$$Risk = f(Frequency, Consequence) \tag{1.1}$$

Thus recurring accidents with low consequence can constitute the same amount of risk as rare accidents with larger consequences. This interpretation has led to the development of two different, but complementary, approaches to managing risk. Prevention, which focuses on preventing an unwanted incident from happening, and mitigation, which focuses on limiting the consequences should an unwanted incident first occur.

The main aspects of each of these approaches are covered extensively in [2] and [3]. A summary of the main principles is presented in Table 1.

Table 1: Summary of means to prevent and mitigate accidental gas explosions.

<table>
<tr><th colspan="2">Prevention</th><th rowspan="2">Mitigation</th></tr>
<tr><th>Ignition Sources</th><th>Formation of Explosible Atmosphere</th></tr>
<tr><td rowspan="2">Open flames</td><td rowspan="2">Gas/dust concentration outside combustible range</td><td>Ventilation</td></tr>
<tr><td>Isolation</td></tr>
<tr><td>Hot surfaces</td><td rowspan="2">Inerting by adding inert dust (such as fine rock)</td><td>Automatic suppression</td></tr>
<tr><td>Accidental mechanical impacts</td><td>Partial inerting</td></tr>
<tr><td>Smoldering combustion</td><td rowspan="2">Inerting by adding inert gas (N_2, CO_2, Ar)</td><td>Pressure resistant design</td></tr>
<tr><td>Electrostatic discharges</td><td>Controlling turbulence generation</td></tr>
<tr><td>Rapid compression systems</td><td>Intrinsic inerting</td><td>Good housekeeping routines</td></tr>
<tr><td>Jets of hot combustion products</td><td colspan="2">Addition of chemically active inhibitors (Such as K_2CO_3)</td></tr>
</table>

1.2 Mitigation through Standards

In order to properly mitigate the effects of accidental explosions it is necessary to develop an understanding of the consequences should one occur. There are two ways of developing this understanding. One is to study earlier accidental explosions and to learn from the consequences. The other is through experimental research. The development of experimental standards enables validation of results and research cooperation between different institutions. It also simplifies research as the experimental setup is removed as a varying factor in the experiments. This allows for development of models based on experimental setups that all are familiar with. A short introduction to the development of the most common standard apparatus, for determining explosion parameters of an explosive atmosphere, is presented in Appendix A. For the work done in this thesis, a modified 20 liter USBM vessel was used. This vessel will be described in more detail in section 4.3.1.

1.3 Experimental Data

In experiments involving explosions, sensors are needed to gather reliable data. Signals from the sensors are interpreted by computer software, which then produce a graphic presentation of the results. For the experiments conducted in relation to this thesis, pressure sensors, mounted inside the USBM-vessel, were used to produce graphs. An illustration of a pressure-time graph, produced with the KSEP-software used for the thesis, is presented in Figure 1.

Key parameters, in this case describing the turbulent combustion, are extracted from the graph. The parameters available, which were extracted from the experimental work in this thesis, are listed in Table 2. Their definitions can also be found in the same table.

Most of the data available from the pressure-time curve, match the results from experiments with the $1m^3$ vessel. An exception is the maximum explosion pressure. Its deviation, from experiments with the $1m^3$ vessel, is the result of heat loss to the vessel wall. It is therefore necessary to calculate a corrected maximum explosion pressure when conducting experiments using the 20 liter vessel, in order to match findings with the $1m^3$ vessel.

Additionally, it is important to note that the inflection point on the pressure-time curve, W_p, is marked. This makes it easy to find the pressure at the inflection point and the time interval up to the inflection point. The importance of which will be clarified in section 3.3.

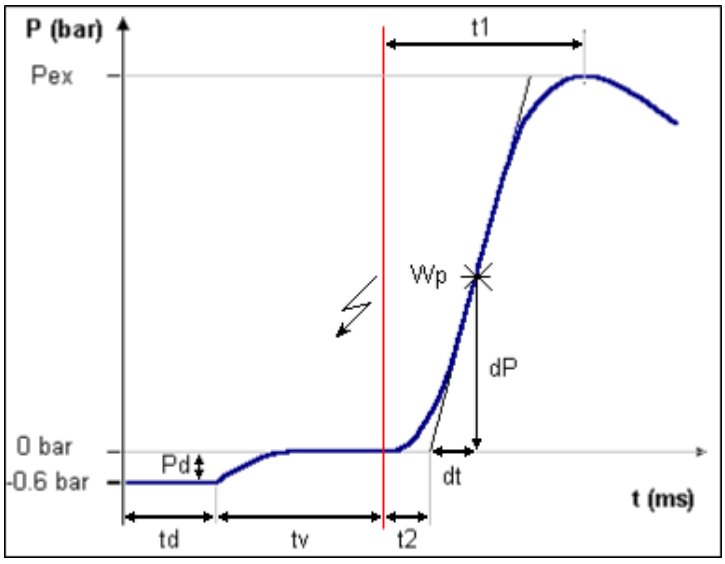

Figure 1: Example of a pressure-time curve. (From Cesana & Siwek, [4])

Table 2: Definition of the parameters available from the pressure-time graph. (From Cesana & Siwek, [4])

Symbol	Definition
P_{ex}	*Explosion overpressure:* The difference between the pressure at ignition and the pressure culmination.
P_m	*Corrected explosion overpressure:* A corrected overpressure after consideration is taken to wall cooling effects and any chemical igniter impact.
P_{max}	*Maximum explosion overpressure:* Maximum value of Pm for any given fuel.
$(dP/dt)_m$	*Rate of pressure rise with time:* The maximum slope of a tangent on the pressure-time curve.
$(dP/dt)_{max}$	*Maximum rate of pressure with time:* Maximum value of the pressure-time ratio for any given fuel.
t_1	*Duration of combustion:* Time from activation of the ignition to the culmination point.
t_2	*Induction time:* Time from activation of the ignition to the intersection of the tangent with the 0 bar line.
P_d	*Expansion pressure of reservoir:* Pressure difference between explosion vessel prior to and post dispersion.
t_d	*Time-delay of the outlet valve:* Time between activation of the pneumatic valve and the first pressure rise in the vessel. Should be 30-50ms.
t_v	*Ignition delay time:* The delay from dispersion to ignition. For the 20 liter vessel this should be 60ms.

1.4 The Cube-Root Law and the K_{st}-value

To adapt the results from laboratory experiments to large scale industrial situations, scaling is required. The cube-root law is a scaling concept developed for explosions in closed volumes. According to [2] it was first introduced by Bartknecht in 1971 (only available in German). The concept is illustrated by [5] through the use of a mathematical example. A summarized version of the mathematical example is found in Appendix D: Calculations. The relationship between the pressure rise and the volume, of two geometrically similar vessels, is seen in equation (1.2).

$$\left(\frac{dP}{dt}\right)_{max,1} \times V_1^{\frac{1}{3}} = \left(\frac{dP}{dt}\right)_{max,2} \times V_2^{\frac{1}{3}} = constant \equiv K_{ST} \tag{1.2}$$

According to [2], the existence of the K_{ST} constant, was further validated by Bartknecht in 1978, when he presented experimental results that seemingly confirmed the validity of the scaling law for dusts in vessels of volume 0.04m^3 or greater.

Over the past few decades, a wide range of experiments have been done to find the K_{ST} of different dusts. However, as illustrated in Table 3, the K_{ST} values from experiments vary greatly. This presents a challenge when trying to regulate safety measures. Another challenge, concerning the practical use of K_{ST} to set mitigation requirements, is that it is based on a fixed amount of turbulence. In a practical situation, however, the turbulence may vary greatly, depending on the geometry in the area.

Table 3: KST values measured from clouds of maize starch dust in air in different closed vessels. (Eckhoff, [2])

Investigator	$(dP/dt)_{max}$ **[bar/s]**	**Volume of vessel [m^3]**	K_{ST} **[bar*m/s]**
Bartknecht (1978)	680	0.0012	73
Nagy and Verakis (1983)	612	0.0012	66
Eckhoff et al. (1987)*	220	0.0012	23
Nagy and Verakis (1983)	413	0.009	86
Aldis, Lee, and Lai (1983)	320	0.020	87
Eckhoff et al. (1987)*	365	0.020	100
Yi Kang Pu (1988)	10-20	0.026	3-6
Yi Kang Pu (1988)	60-80	0.026	20-25
Nagy and Verakis (1983)	272	0.028	83
Bond, Knystautus, and Lee (1986)	50	0.33	34
Kauffman et al. (1984)	72	0.95	71
Kauffman et al. (1984)	20	0.95	20
Nagy and Verakis (1983)	136	3.12	200
Nagy and Verakis (1983)	110	6.7	209
Nagy and Verakis (1983)	55	13.4	131

*Arithmetic mean values, 11% moisture in starch

1.5 Computational Fluid Dynamics

In the 1990s computer development had reached a point where it became possible to use computers to simulate fluid dynamics. By utilizing the fact that fluid flow is governed by three fundamental principles;

1. The conservation of mass
2. Force = mass × acceleration (Newton's second law)
3. The conservation of energy

and that these principles can be expressed in terms of mathematical equations, it is possible to simulate fluid behavior through the use of control volumes [6].

With a powerful computer and the right software it would then be possible to simulate the effects of accidental spills, fires, explosions and any mitigating measures, in any specific industrial environment. This data should provide a far more realistic foundation for assessing consequences then can be achieved from direct scaling of experimental results.

GexCon AS has developed a program, FLame ACceleration Simulator (FLACS), based on fluid dynamics and validations from experiments, for simulations of gas leaks and explosions, which has been commercially available since 1996. The main parameters for calculating the burning velocity in any given area with the CFD-code are the laminar burning velocity and the turbulence intensity.

In 2002 a consortium including GexCon AS initiated a new simulation project called the Dust Explosion Simulation Code (DESC) project. The object was to develop a CFD code capable of simulating accidental dust explosions based on the CFD code from FLACS. Although the project ended in 2005 and the software is now commercially available, it is continually being improved. The research conducted for this thesis is part of this improvement process. The goal is to implement the effect of inhibitors on the combustion process into the coding by means of the laminar burning velocities.

1.6 Aim of the Current Work

As mentioned at the very beginning, this study is a follow-up on an earlier study at the University of Bergen on the effect of varying particle size of inhibitors in turbulent premixed combustion. That study concluded that particle size of inhibitor had no effect on the calculated laminar burning velocity. Although little research has been found on effect of inhibitor particle size in turbulent premixed combustion, quite a few journals have been found that study the effect of inhibitor particle size under other conditions. So far these show a marked increase in effect as the particle size is reduced, down to a minimum diameter [7-10]. This is, as would be expected, because heat absorption and heterogeneous recombination are surface processes. As the last study conducted at the University of Bergen provided no satisfactory explanation for the results, it was decided to conduct a second study. Thus the aim of this thesis depends on the experimental findings. It is either

1. Validate the findings of the last study and present an explanation for the findings and then conduct experiments with other inhibitors to see if the same effect is found.

   or

2. Find the source of the discrepancy from similar studies and conduct a new investigation into the effect of reducing the inhibitor particle size in turbulent combustion.

2. Theory

The following chapter is divided into four parts. The first section is a short introduction to the ideal gas law, which is assumed to be valid for any calculation in the thesis. The second and third section cover the theory on explosions and combustion required for full understanding of the thesis. The fourth section concerns the use of inhibitors and their effect on the combustion.

2.1 The Ideal Gas Law

The ideal gas law (2.4) is actually a combination of three basic laws for gases, namely Boyle's law (2.1), Charles' law (2.2), and Avogadro's law (2.3). These laws can be combined through the use of a proportionality constant, or gas constant, R. The unit of the constant varies according to the units used for the other values in the equation, but the most common variant is 8.314 $JK^{-1}mol^{-1}$. This gas constant is correct in calculations where the SI units Pascal, cubic meters, mole and Kelvin are used to denote pressure, volume, gas quantity and temperature, respectively.

$$V \propto \frac{1}{P} \ (at\ constant\ n\ and\ T) \tag{2.1}$$

$$V \propto T \ (at\ constant\ n\ and\ P) \tag{2.2}$$

$$V \propto n \ (at\ constant\ P\ and\ T) \tag{2.3}$$

$$V = R\frac{nT}{P}\ or\ PV = nRT \tag{2.4}$$

Thus an ideal gas is a hypothetical gas with pressure, volume and temperature behavior completely in accord with the ideal gas law. Although no such gas exists outside the theoretical world, real gases behave as proposed by the ideal gas law, within reasonable pressure and temperature scenarios.

2.2 Explosions

Explosions are rapid increases in pressure, due to a sudden release of energy, that lead to the formation of a pressure wave [3, 11].

The source of the energy could be chemical reactions or mechanical failure. As only the first type of source is relevant in this thesis, any further use of the word, explosion, will refer to the chemical type.

There are four basic requirements that must be fulfilled, for an explosion to occur. In addition to these, confinement is usually necessary to produce any large degree of pressure build-up. Thus the five factors associated with dangerous explosions are:

1. Fuel: Combustible gas, vapor or dust.
2. Ignition source: Any heat source capable or initiating an exothermic chain reaction.
3. Oxidizer: Usually air, but not limited to (as in the case of explosives).
4. Combustible mixture: Proper dispersion and concentrations for combustion.
5. Confinement: Not a necessity for an explosion, but its impact on the pressure build-up is vast. Because of this it is usually included as a requirement. I.e. the dust explosion pentagon.

2.2.1 Ignition

Any chemical reaction can be described by the general equation:

$$Reactant(s) \rightarrow Product(s) \tag{2.5}$$

This equation states that, during the course of a reaction, reactants are consumed to produce products. This is done through collisions between moving molecules. If they possess a high amount of kinetic energy when they collide, they may vibrate to such a degree that chemical bonds are broken. If this should happen, new molecules can be formed. A minimum kinetic energy requirement, for initiation of a chemical reaction, can thus be defined. This is called the activation energy, E_a.

By monitoring the concentrations of the reactants or the products, it is possible to determine the rate of chemical reactions over time. If two reactants combine to form a product, the rate will be proportional to the concentration of the two reactants. Since the rate varies depending on which reactants are involved, any rate-equation would have to include a reactant dependent constant. This constant is known as the rate constant, and is denoted, C. The term constant, however, is slightly misleading. It is misleading because a characteristic of chemical reactions is that they are greatly influenced by temperature. This is the reason that cooking an egg is quicker at the earth's surface, than at the top of the Himalayas (lower pressure causes the water to boil at a lower temperature).

In 1889, Arrhenius formulated an equation explaining the relationship between the temperature and the rate coefficient. The equation is called Arrhenius law, and is seen in equation (2.6).

$$C = A \times exp\left(-\frac{E_a}{RT}\right) \tag{2.6}$$

where A is the collision frequency (constant for a wide temperature range), E_a is the activation energy, T is the absolute temperature and R is the gas constant. Thus an increase in the temperature will result in an increased rate of chemical reactions.

In accordance with the two ignition factors previously mentioned (i.e. that for a reaction to occur the kinetic energy of colliding molecules must be higher than the activation energy, and that the rate of reactions increases with increasing temperatures), Frank-Kamenetskii developed the thermal explosion theory [3]. The basic principle is that for ignition to occur, within a volume containing a combustible fuel-air mixture, the heat generated, *G(T)*, in the chemical reactions must be greater than the heat lost, *G(L)*, to the surroundings. Since heat generation is proportional to the volume, whereas heat loss is proportional to the surface area, then a larger volume will require a lower temperature before ignition. That means that for any given volume, ignition will occur, if the situation corresponds to (2.7). The basic principle is also illustrated in Figure 2.

$$G(T) = L(T) \tag{2.7}$$

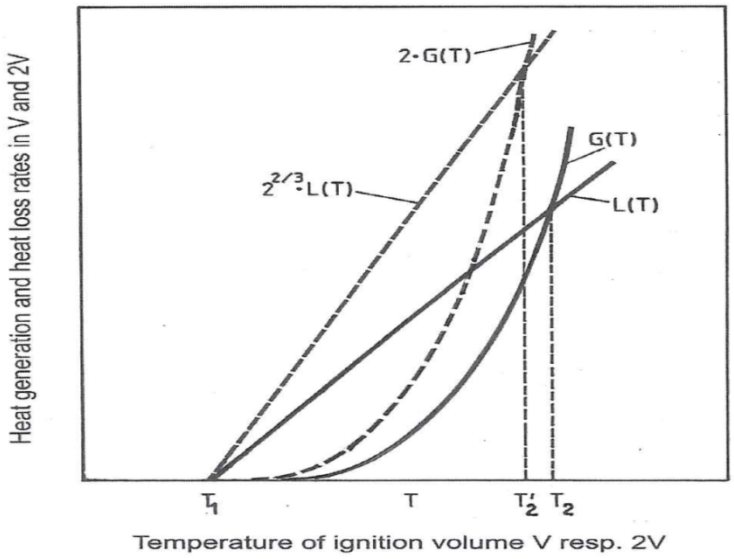

Figure 2: Illustration of the basic principle of the thermal explosion theory. (From Eckhoff, [3]).

2.3 Combustion

A combustion reaction *is a reaction in which a substance reacts with oxygen, usually with the release of heat and light to produce a flame [12]*. Since this thesis concerns the reaction between propane and air, the following example seems suitable;

$$C_3H_8 + 5(O_2 + 3{,}76N_2) \rightarrow 3CO_2 + 4H_2O + 5(3{,}76N_2) + \text{heat} \qquad (2.8)$$

Propane reacts with the oxygen in air to form carbon dioxide, water vapor and heat. Note that although the nitrogen takes no part in the combustion reaction, it is nonetheless important to remember its presence. This is due to the fact that it will function as a heat sink, lowering the post combustion temperature compared to a similar reaction without the presence of nitrogen (for more details see 2.3.2 and 2.4.1). The equation is also balanced. This means that any element present amongst the reactants will be present in an equal amount amongst the products.

Combustion reactions can be further divided into subcategories based on other important parameters. An example of further subdivision is presented in Table 4. Explosions conducted in the 20 liter USBM vessel, belong to the premixed turbulent combustion category.

Table 4: Further subdivision of chemical combustion. (From Warnatz, [13]).

Fuel/Oxidizer Mixing	Fluid Motion	Examples
Premixed	Turbulent	Spark-ignited gasoline engine
		Low NO_x stationary gas turbine
	Laminar	Flat flame
		Bunsen flame (followed by a non-premixed candle for ϕ>1)
Non-premixed	Turbulent	Pulverized coal combustion
		Aircraft turbine
		Diesel engine
		$H_2/0_2$ rocket motor
	Laminar	Wood fire
		Radiant burners for heating
		Candle

2.3.1 Premixed Combustion

An important distinction is made between premixed and non-premixed combustion. The reason for this distinction is that a non-premixed flame is diffusion controlled. This means that the flame zone is limited to a thin layer between the fuel and the surrounding oxygen. The reason for this limitation is that the fuel is only combustible at certain fuel-oxygen ratios. If the fuel concentration is too high or too low, then it will no longer be combustible. This is related to the amount of fuel and oxygen needed for the combustible reactants to oxidize in a chain reaction. If the amount of oxygen present in a fuel-oxygen mixture is exactly equal to the required amount for all the combustible reactants to oxidize, then it is said to be a stoichiometric mixture. The example in equation (2.8) is a stoichiometric reaction. If there is an abundance of fuel, compared to oxygen, the mixture is rich. If the fuel is the limiting factor, it is lean. For calculations on stoichiometry on propane-air mixtures, see Appendix D.

For the premixed combustion there is no such limitation. Instead the flame front moves through the combustible mixture with a burning velocity dependent on the laminar burning velocity and the turbulence intensity. Illustrated examples of a diffusion flame and a premixed propane-air flame are presented in Figure 3 and Figure 4.

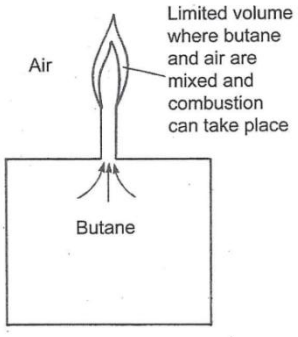

Figure 3: Butane lighter flame. Example of diffusion controlled burning of combustible gas in air. (From Eckhoff, [3])

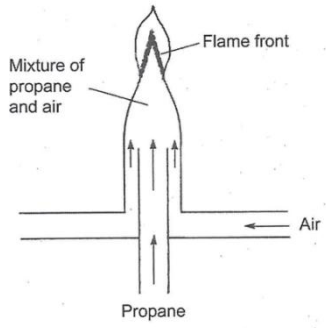

Figure 4: Burning of premixed propane/air in a Bunsen burner. (From Eckhoff, [3])

2.3.1.1 Laminar Burning Velocity

By now it should be clear that several factors influence the burning velocity in a premixed laminar flame. From these factors an ideal laminar burning velocity, denoted S_L, can be defined. It is *the lowest velocity at which a flame front can propagate through a given quiescent gas mixture at a given pressure and temperature* [3].

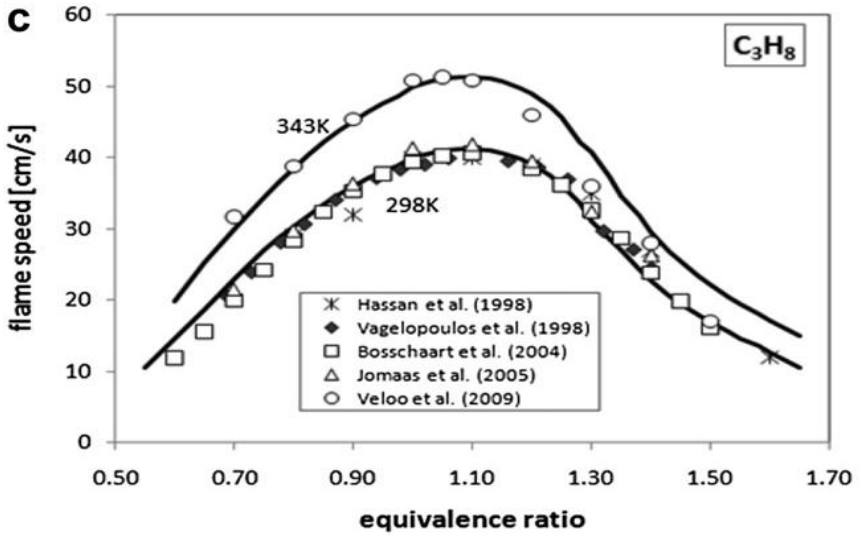

Figure 5: Laminar burning velocities at standard conditions for mixtures propane and air. (From Ranzi, [14])

As illustrated in Figure 5, this velocity peaks at an equivalence ratio slightly above stoichiometry. For propane the laminar burning velocity is approximately 40cm/s at optimal equivalence ratio. Deviations from this equivalence ratio, in either rich or lean direction, will cause a drop in the laminar burning velocity.

If the deviations are large enough to give concentrations outside the flammability range for the mixture in question, it will fail to ignite. The limits of flammability for fuel-oxidizer mixtures are referred to as the lower flammable limit and the upper flammable limit.

The laminar flame front

The width of the flame front is called the flame thickness and is symbolized with δ. The flame thickness for a laminar flame front can be expressed as a ratio between the thermal diffusivity and the laminar burning velocity, as seen in equation (2.9).

$$\delta_L = \frac{\alpha}{S_L} \tag{2.9}$$

Another important characteristic of the flame front is the chemical time scale, τ_c. It can be defined as *the time a laminar flame requires to propagate over a distance equal to its flame thickness*, seen in equation (2.10).

$$\tau_c = \frac{\delta_L}{S_L} \tag{2.10}$$

2.3.1.2 Turbulent Combustion

As mentioned in section 1.4, obstructions can have a severe impact on the pressure in a combustion process. This is clearly illustrated in [15] where experiments were done with an explosive mixture of methane-air in a horizontal cylinder. Inside the cylinder it was possible to mount up to six circular obstructions to generate different levels of turbulence. In the experiments they found that the pressure varied from 0.15bar(g), when using no obstructions, to 8bar(g), when using six. The reason for this is the development of turbulence as the fluid interacts with the obstructions. Shear stress causes the formation of eddies which in turn cause the flame zone to bend and break. An illustration of a typical turbulent flame front can be seen in Figure 6. The much larger reaction zone than that of a laminar flame front, is due to the tearing of the flame front and the following mixing of unburned gas and combustion products.

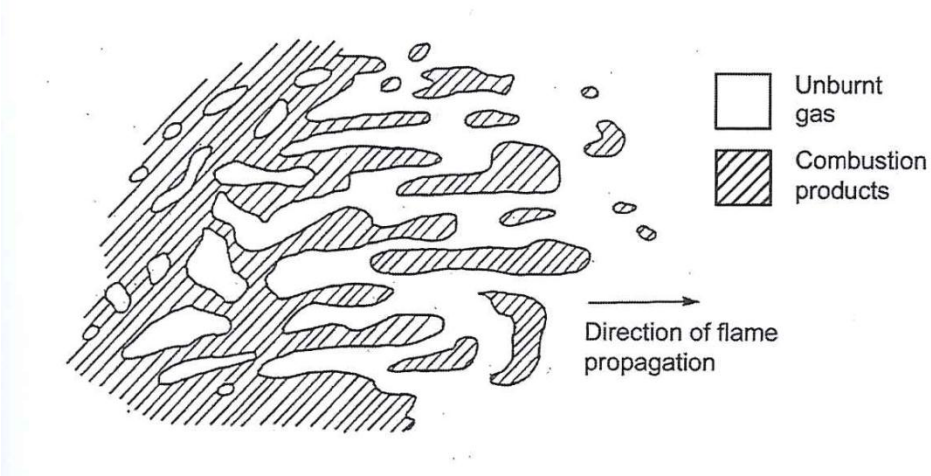

Figure 6: Illustration of flame front structure in turbulent premixed gas. (From Eckhoff, [3])

As turbulence cannot exist without the presence of eddies, an analogy of the behavior of eddies and their influence on the flow, is in order. In general there are three parameters that are used to describe eddies. These are the length scale, the velocity and the time scale. As all of these are rather comprehensive, they are covered in turn.

Turbulent length scales

An energy spectrum describing the dependency of the turbulent kinetic energy, $k(\lambda)$, on the wave number, $\lambda=1/l$, is shown in Figure 7. As is evident, the larger eddies contain the major part of the kinetic energy.

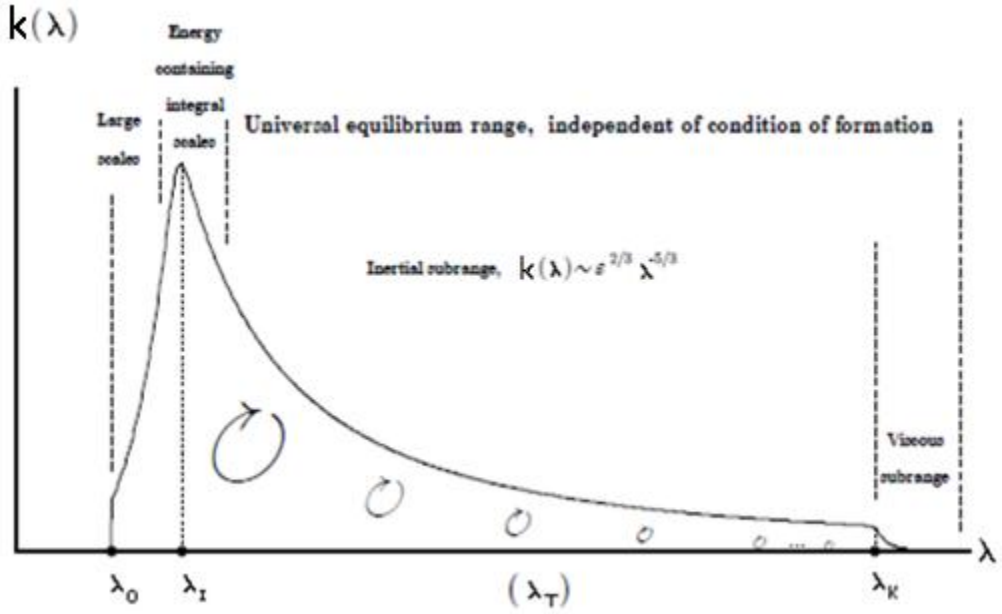

Figure 7: Turbulent energy spectrum, showing the energy cascade (modified from Skjold, [11])

The dotted lines in Figure 7, all correspond to a length scale frequently used in characterization of turbulent flows. These are;

1. The maximum spatial length scale, l_0: The largest length scale possible due to geometrical limitations.
2. The integral length scale, l_I: The mean size of the large eddies in a turbulent flow. Contributes to the greater part of the turbulent kinetic energy [16]. Slightly smaller than the geometrical limitations.
3. The Taylor micro scale, l_T: An intermediate scale between the integral length scale and the Kolmogorov scale [11].
4. The Kolmogorov-length scale, l_K: The length scale where the time for an eddy to rotate half a revolution is equal to the diffusion time across a distance the same as its diameter. Below this length scale diffusion is faster than the turbulence and hence turbulence ceases [13].

Turbulent velocity

Eddies also have an effect the fluid flow, causing the velocity to fluctuate in any given point. Larger eddies have a greater impact on velocity fluctuations. This is due to the variation in kinetic energy discussed in the previous section. Figure 8, illustrates the effect of eddies on the velocity profile as a dye trace passes from laminar to turbulent region.

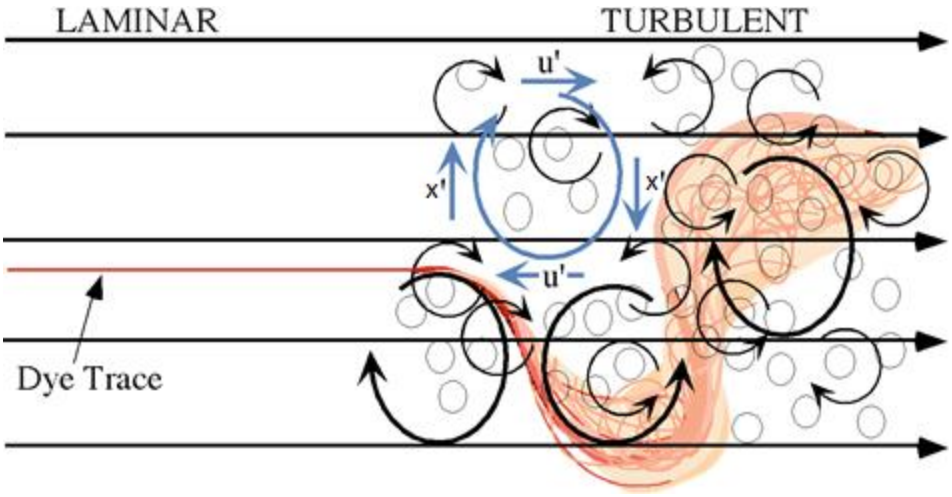

Figure 8: The impact of eddies on a dye tracer as it moves from a laminar to a turbulent region of a fluid flow.

Since the velocity in any fixed position of a turbulent flow fluctuates, it can be decomposed into an average velocity and a velocity fluctuation. For the two directions in Figure 8 this would give the velocity at a time, *t*, for any point in the flow, as

$$u(t) = \bar{u} + u'(t) \tag{2.11}$$

$$x(t) = \bar{x} + x'(t) \tag{2.12}$$

The fluctuation of the velocity is used as a measure of turbulence. However, since the average velocity fluctuation will always be equal to zero, it is necessary to apply statistical methods to quantify the turbulence level. One such method is to calculate the rms of the velocity fluctuation, referred to as the intensity of the turbulence [2], as illustrated in equation (2.13).

$$u_{rms} = \sqrt{\overline{u'(t)^2}} \tag{2.13}$$

Turbulent time scale

Vortex stretching, from the circulation of the eddies, cause eddy break-up until the eddies eventually dissipate due to viscosity [11]. The amount of time this process takes, called the turbulent time scale or the eddy lifetime, can be calculated. It is found by dividing the length scale by the rms of the velocity fluctuation. Equations for calculating the integral time scale and the Taylor time scale are given in equation (2.14) and equation (2.15). For eddies at the integral length scale, this value is also approximately equal to the turbulent kinetic energy divided by the turbulent energy dissipation rate [11].

$$\tau_0 = \frac{l_I}{u_{rms}} \approx \frac{k}{\varepsilon} \tag{2.14}$$

$$\tau_T = \frac{l_T}{u_{rms}} \tag{2.15}$$

Structure of the flame front in turbulent combustion

There are correlations between the length scale, the time scale, the velocity and the structure of the flame front in a turbulent combustion. Presented in a diagram, these are useful for analyzing the type of flame front present in a given turbulent combustion. The diagram, seen in Figure 6, was developed by Borghi, and shares his name. It provides a visual representation of the effect of the correlating parameters and is divided into five distinctly different regions of flame behavior. These regions are separated through the use of three defined dimensionless numbers, namely the turbulent Reynolds number, the turbulent Damköhler number and the turbulent Karlovitz number.

The turbulent Reynolds is defined by the length scale, the rms velocity and the kinematic viscosity [13, 17]. For the integral length scale, it can be calculated with equation (2.16). For any other length scale it is just a matter of switching to the appropriate length scale. In flows with turbulent Reynolds number less than one, the flame front will always be laminar.

$$Re_T = \frac{\rho u_{rms} l_I}{\mu} = \frac{u_{rms} l_I}{\nu} \tag{2.16}$$

The turbulent Damköhler number, Da, is the ratio between the integral time scales and the chemical time scale, see equation (2.17) [13]. For high Damköhler numbers (Da>1) the turbulence tears the flame front apart resulting in many small burning sheets which move through the reactant. Thus you have many thin flame fronts.

For low Damköhler values (Da<1) the turbulence is so high that the chemistry is the only limiting factor of the combustion. As a result the flame front covers the entire mixture.

$$Da = \frac{\tau_I}{\tau_c} = \frac{l_I S_L}{u_{rms}\delta_L} \tag{2.17}$$

The turbulent Karlovitz number, Ka, is the ratio between the time scale of a laminar flame and the smallest turbulent time scale, usually the Kolmogorov time scale (2.18). If the flame thickness is less than the Kolmogorov scale, the time for an eddy to rotate is longer than the time for diffusion over the same distance. This means the flame front will act as a laminar flame front caught in a turbulent flow[13]. If the turbulent Karlovitz number is higher than one the turbulent eddies will bend the flame front enough for it to collide with itself in other areas. This causes the formation of pockets of reactants inside the product dominated area.

$$Ka = \frac{\tau_c}{\tau_K} \tag{2.18}$$

The regions of the Borghi diagram are called a variety of different names [13, 16, 18]. Nonetheless the characteristics of the regimes in the diagram remain the same. Their characteristics are can be summarized as:

1. Weakly wrinkled flames: Large turbulent structures are incapable of wrinkling the flame front to the extent needed to cause flame front interactions. Thus the flame front behaves as a laminar flame.
2. Strongly wrinkled flames: The turbulence is intense enough to cause flame front interactions. This causes formation of product- and flame pockets.
3. Thin reaction sheets: In this region the turbulence is at such a high level compared to the chemistry that the flame front is torn into many small flames. This gives a wide area of combustion.
4. Flamelets in eddies: In this region the turbulence is so intense that there is a perfect mix between reactant, products and flames.

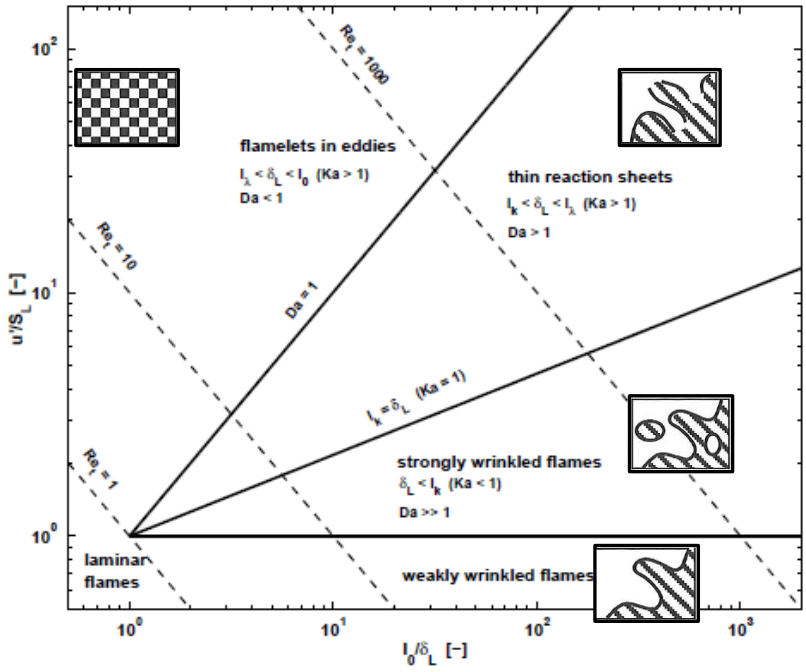

Figure 9: The Borghi diagram. A loglog graph of the relative intensity of turbulence ($u_{rms}/S_{L)}$ vs. the relative large-eddy size of turbulence (l_0/δ_L). (Modified diagram from Vanoverberghe, [16])

2.3.2 Calculating Combustion Temperature

As mentioned in 2.3 a combustion reaction will usually involve the release of heat. For any combustion, it is possible to calculate the heat released by comparing the enthalpy[1] of the reactants with the enthalpy of the products. Standard enthalpies of formation are readily available for many compounds. Those relevant to calculate the heat released in equation (2.8), are presented in Table 5.

Table 5: Standard enthalpies of formation for selected compounds.

Compound		$\Delta H^0_{f,298}$ [kJ/mol]
Propane	C_3H_8 (gas)	-103.85
Oxygen	O_2 (gas)	0
Nitrogen	N_2 (gas)	0
Carbon dioxide	CO_2 (gas)	-393.5
Water vapour	H_2O (gas)	-241.81

[1] Enthalpy is a thermodynamic quantity used to describe heat changes taking place at constant pressure. It is defined by H=E+PV, thus for any process the change in enthalpy can be calculated by $\Delta H=\Delta E+\Delta(PV)$. [12]

By replacing the compounds with their respective standard enthalpies a quick calculation reveals that the total energy released is 2043.89kJ for each mole of propane that reacts with air. This energy then causes a temperature increase amongst the products of the reaction. The size of this increase depends on their specific heat capacity. Thus if all compounds involved in a reaction are known, the standard enthalpies could be used to calculate a theoretical temperature after all compounds have reacted. This can be achieved by assuming adiabatic[2] temperature rise. At constant volume the temperature change can then be calculated, by dividing the energy liberated through the combustion, by the average specific heat capacity for the products, see equation (2.19) [3]. However, since not all compounds in combustion reactions react fully, particularly true for a dust cloud (more on this in section 3.2.2), any calculated temperature will be higher than for a real situation.

$$T_2 - T_1 = \frac{\Delta E}{\overline{C_v}} \tag{2.19}$$

2.4 Automatic Suppression Systems

The first automatic fire suppression system was developed in 1912. Since then, three basic principles have been central in the design of automatic suppression systems [3].

1. The extinguishing agent is kept permanently pressurized.
2. The discharge orifice has a large diameter to allow for quick discharge.
3. The opening valve is triggered by means of an explosive charge to secure quick delivery of the suppressant.

In addition to the suppression system itself, it is also important to have fast-response detection systems. This ensures quick discharge of the extinguishing agent if needed. An example of a design for an automatic suppression system based on pressure increase detection, with corresponding pressure curves, is shown in Figure 10.

[2] i.e. no heat leaves the system.

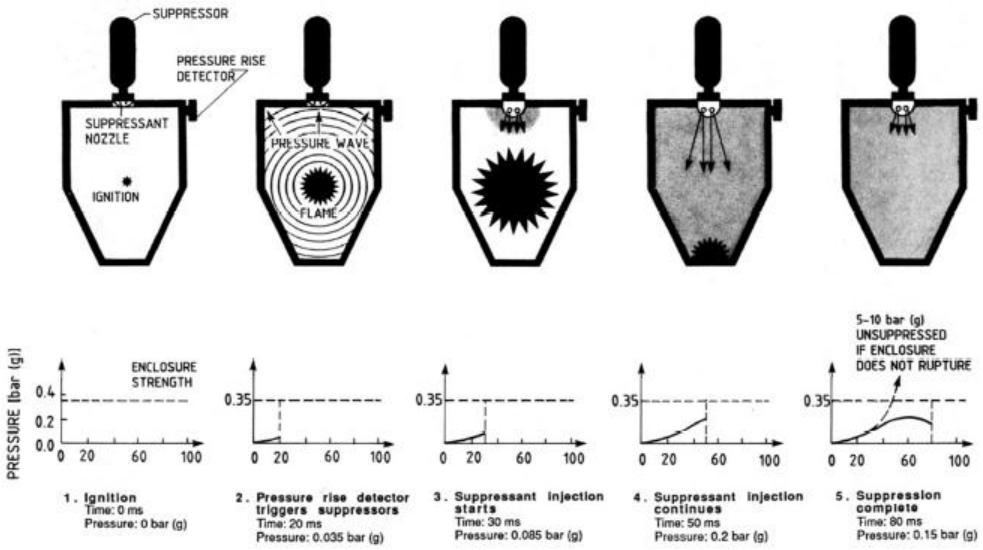

Figure 10: Automatic suppression system designed to activate when the pressure rises above a given lower limit (From Eckhoff, [2])

In the 1980s, Moore and Cooke [19] conducted research into combining automatic suppression with venting. They found that combining these two mitigating measures could further reduce the pressure from explosions by 30-40%, compared to explosions conducted where venting was the only mitigating measure.

2.4.1 Suppressants

The effect of the suppressant depends on the type of suppressant used. For powder suppressants, three basic mechanisms account for the fire suppression performance [20]. (More details on the chemistry involved in the mechanisms, is presented in section 3.1)

1. Cooling by cold mass injected into the flame followed by endothermic reactions forming carbon dioxide and water vapor.
2. Recombination reactions of radicals on the surface of the particles.
3. Diluting of the combustible mixture by the water vapor and carbon dioxide formed from the decomposition of the particles.

Traditionally, compounds containing halogens were used as suppressants. However, in the 1970s, these were discovered to have a depleting effect on the ozone layer. Since then, several alternatives have been found. Amongst the most effective were alkali compounds containing sodium or potassium [21]. These also pose little danger to the environment compared to other compounds of similar suppressive efficiency.

2.4.1.1 Importance of particle size

All three basic mechanisms of suppressors are influenced by the surface area of the particles. This is where the gas and the particles are in direct contact and thus where there is recombination of radicals. This is also where heat is transferred from the combustion to the particles, leading to initial cooling of gas-air mixture, and eventual particle decomposition.

It would therefore seem natural that smaller particles would give better suppression. As illustrated by [22] however, for propane-air counter-flow diffusion flames, little is gained in effectiveness when decreasing particle size below 40µm. A possible explanation for this phenomenon could be the formation of agglomerates, due to the tendency of small particles to combine to form larger particles. This phenomenon is illustrated in Figure 11.

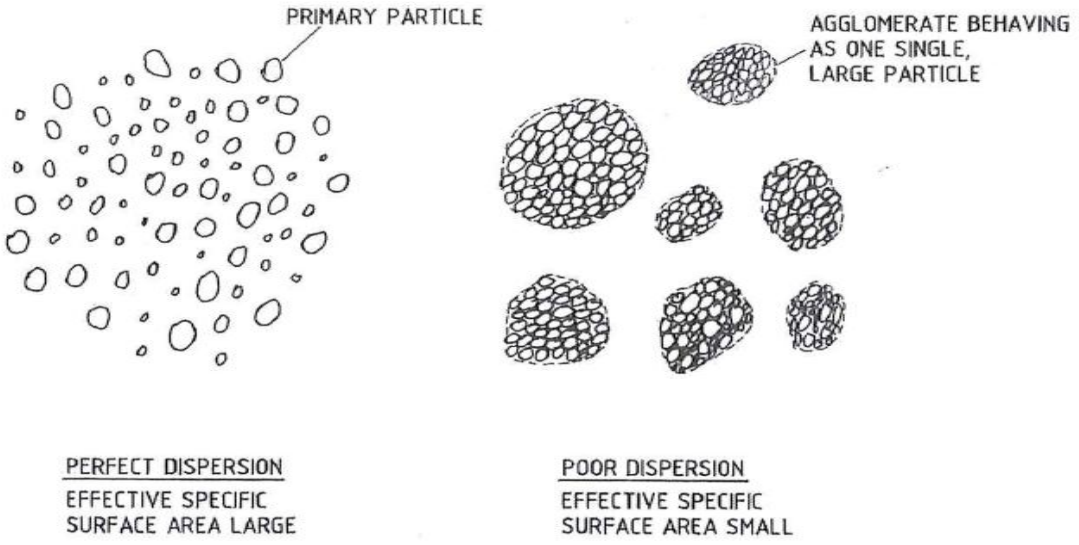

Figure 11: Illustration of perfectly dispersed dust cloud and a cloud consisting of agglomerates (from Eckhoff, [3])

3. Relevant Literature

In this section the findings from recent scientific work which is central to the experimental work of this thesis is reviewed.

3.1 Burning Velocity Sensitivity Analysis

3.1.1 Hoorelbeke and Wingerden

In connection with work on his doctorate thesis, Hoorelbeke did extensive research on the possibility of using inhibitors as a mitigating measure against accidental gas leaks. Much of the experimental work was done in cooperation with GexCon AS and a presentation of the experimental results were held at the 7th Global Congress on Process Safety [23] by Kees van Wingerden.

The experimental research was conducted in both small and large scale experiments.

The small scale experiments were conducted with a 20 liter Siwek sphere. In these experiments, inhibitors of different chemical composition were tested on several hydrocarbon-air mixtures. As illustrated in Figure 12, potassium carbonate was significantly more efficient at lowering the laminar burning velocity of propane-air mixtures than the tested alternatives at low concentrations.

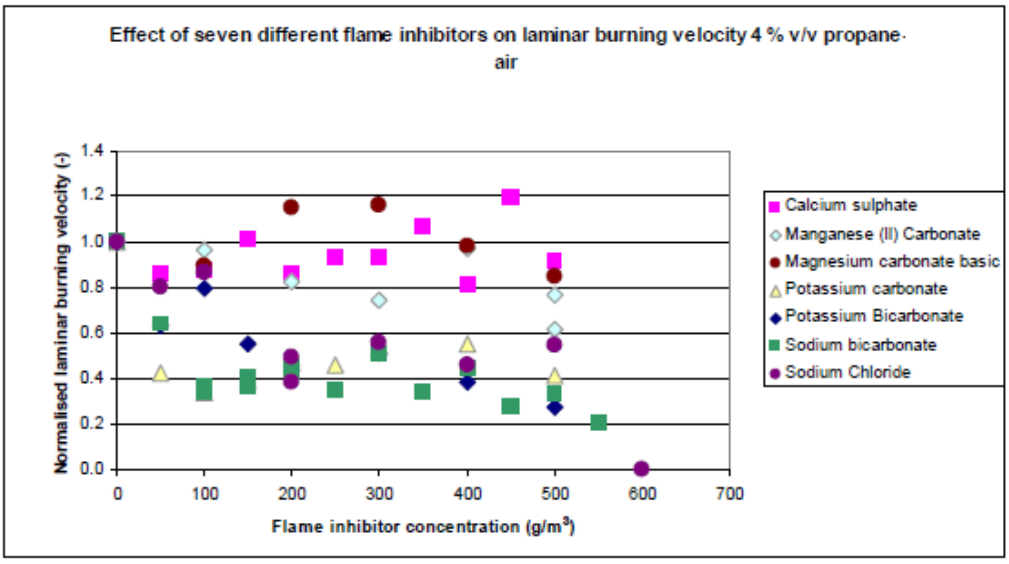

Figure 12: Effect of flame inhibitors on normalized laminar burning velocity, when added to a stoichiometric propane-air mixture. (From Wingerden, [23])

Small scale tests were then conducted with potassium carbonate as inhibitor in other hydrocarbon-air combustible mixtures. As illustrated in Figure 13 potassium carbonate had a negative effect on the laminar burning velocity on all combustions conducted, except for the hydrogen-air mixture.

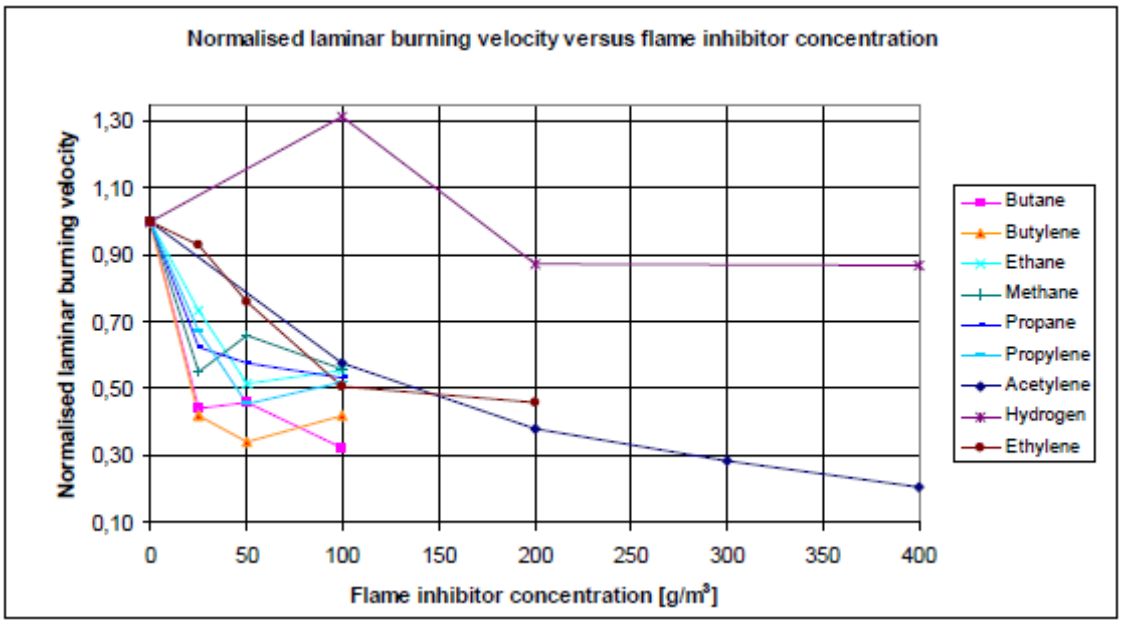

Figure 13: Effect of potassium carbonate on normalized laminar burning velocity when added to several stoichiometric hydrocarbon-air combustible mixtures.

To investigate if the results would be similar for a practical industrial situation, large scale tests were conducted. These experiments were performed in a 50m^3 cuboid explosion test module, with open ends. The dimensions of the module were 8m in length, 2.5m in height, 2.5m in width. The inner volume of the vessel was congested with obstructions representing realistic processing equipment. The results from these experiments were similar to those seen in the 20 liter Siwek sphere. Concentrations of 100g/m^3 potassium carbonate gave both a laminar burning velocity decrease and a reduction in the maximum pressure measured in the explosions. Dispersion of inhibitor both before and after ignition was tested. The inhibitor proved most effective when added before ignition of the combustible mixture.

3.1.2 Babushok and Tsang

In 2000 Babushok and Tsang presented a journal [21] on an investigation they had done on the reaction mechanisms in hydrocarbon fires. Their aim was to present an explanation for the similarity of suppressant effectiveness, independent of the type of hydrocarbon fire. To achieve this they conducted a sensitivity analysis on the kinetics of combustion in C_1-C_4 hydrocarbons. This was done through simulations using the Chemkin suite of programs. They incorporated models from previously published work for the kinetics of both the hydrocarbons and the inhibitors. A quality-assuring of their model was then done by comparing results from simulations with previous results. Through simulations of hydrocarbon fires they found that the burning velocity was largely dependent on only a few chemical reactions, most which were independent of which hydrocarbon they currently simulated. The independent chemical reactions with high influence on the burning velocity were:

1. $H + O_2 = OH + O$
2. $CO + OH = CO_2 + H$
3. $HCO + M = CO + H + M$
4. $H + O_2 + M = HO_2 + M$

where the first reaction is the main chain-branching reaction, of the combustion process. These findings are similar to those reported by [13, 24].

A series of simulations were then conducted to examine whether the reactions with seemingly lower effect on the burning velocity might have a cooperative effect that could cause a higher cumulative contribution then the above reactions. This was found not to be the case. Furthermore simulations with an inhibitor present reveal that the same four reactions still remain as the most important, but that the inhibitor contributes with several new reactions that have a negative contribution to the burning velocity.

3.1.3 Williams and Fleming

In 1999 Williams and Fleming [25] presented the results from a study they had done on alkali metals as inhibitors. Their aim was to discover properties that influence the ability of chemical elements to function as inhibitors. This was done by calculation of the thermal effect of addition of alkali metal compounds to flames, as well as using kinetic modeling to investigate the chemical reactions occurring during combustion. They found that the inhibitor effect of potassium was higher than that of sodium or lithium. This was true even when added as mass fractions instead of mole fractions.

The reaction mechanism, by which alkali metals inhibit combustion, is by scavenging on free radicals and thus preventing them from participating in the combustion process. The chemical reactions are as follows:

1. $K + OH + M = KOH + M$
2. $KOH + H = K + H_2O$

The simulations revealed that the peak amount of radicals was higher when using potassium as an inhibitor, then when using sodium. However, the peak took longer to form. Thus potassium was more effective at scavenging free radicals during the early stages of combustion. A possible explanation for this effectiveness is the larger size of the potassium element. This could contribute with two effects which could give potassium a slight advantage over sodium. Firstly there is a greater cross section for collision which will result in a stable collision complex. Secondly the collision occurs more slowly due to the increase in mass.

3.2 Dispersion of Powders in the 20 Liter Vessel

3.2.1 Kalejaiye et al.

In 2010 a study was presented by Kalejaiye et al. on the effectiveness of dust dispersion in the 20 liter Siwek chamber [26]. Both the rebound nozzle and the perforated annular nozzle were tested. Tests were performed on three different powder samples, namely coal, Gilsonite (trademarked name for a form of natural asphalt) and purple K (dry powder chemical fire suppressant), at five different dust concentrations. An optical dust probe was used to measure the transmittance through the dust cloud at different locations in the 20 liter vessel.

It was found that the degree of dispersion was similar for both nozzles. Size analysis before and after the dispersions showed that each dust had a similar, but constant size reduction from the dispersion process. In other words, the dust concentration had no effect on the final particle size. The size reduction was mainly attributed to the design of the outlet valve with the nozzles having a minor impact. This is in agreement with the warnings in the 20 liter Siwek manual, where both the nozzle and the outlet valve are highlighted as sources of particle reduction size.

3.2.2 Dahoe et al.

In 2001 Dahoe et al. presented a study on the sensitivity of the maximum explosion pressure, of a dust deflagration, to turbulence [27]. A 20 liter Siwek sphere was used for the experiments. The object of the study was to explain why the maximum pressure in dust explosions seemed to be dependent on turbulence, while that of gas explosions were not. This could have one of two explanations. Either the particles influenced the turbulence, or the turbulence influenced the combustion of the particles.

To examine the first possible explanation, laser Doppler anemometry was used to investigate whether the presence of cornstarch in the flow had any impact on the turbulence fluctuations. The concentrations tested ranged from $125g/m^3$-$625g/m^3$. Although the measurements were conducted under conditions that are beyond the range of laser Doppler anemometry, the authors were confident enough in their results to conclude that the turbulent fluctuations of the gas phase, behaved more or less independently of the presence of the solid particles.

Instead it is proposed that the increase in maximum pressure was the result of influence by the turbulence on the combustion of particles. The explanation suggested for this, is that increased turbulence widens the preheat zone and the flame zone. This results in longer residence time for the particles in temperatures high enough to cause release of volatiles.

3.3 Calculating the Laminar Burning Velocity

As mentioned in Appendix D: Calculations, an ideal combustion, in a spherical vessel, should give maximum pressure rise at the wall. As experiments show that $(dP/dt)_{max}$, occurs before the flame front reaches the wall, it is safe to conclude that the flame front is influenced by wall effects. This influence lasts from the point of $(dP/dt)_{max}$ till the flame front reaches the vessel wall. To ensure that wall effects do not influence the results, all calculations are therefore done on the basis of the data in the inflection point, W_p. This is the point in the pressure-time diagram where the rate of pressure rise is at a maximum.

For the same reason, it is necessary to correct the maximum explosion pressure. According to [4] this correction depends on the explosion pressure and the ignition energy delivered by the chemical igniter(s). In experiments where the explosion pressure is below 5.5bar(g) and the chemical igniters discharge an ignition energy of 1000J or more, equation (3.1) should be used to calculate a corrected maximum pressure. In all other experimental situations, equation (3.2) is used to correct the maximum pressure. By correcting the explosion pressure with these equations the results should match those found with experiments using the $1m^3$ standard vessel.

$$P_{max} = 5.5\left(\frac{P_{ex} - P_{ci}}{5.5 - P_{ci}}\right) \tag{3.1}$$

$$P_{max} = 0.775P_{ex}^{1.15} \tag{3.2}$$

3.3.1 Bray

In 1990 Bray presented the results of a study on the turbulent burning velocity of combustion in premixed gas-air mixtures [28]. He had conducted a theoretical analysis of the relationship between turbulent and laminar burning velocity, which he then compared with empirical data gathered by Abel-Gayed et al [29]. He suggested that the relationship found by [29], seen in equation (3.3), could be simplified by an approximation of S_T/S_L as in equation (3.4).

Note that the Karlovitz number used in the calculations is based on the Taylor time scale instead of the Kolmogorov time scale (see section 2.3.1.2). For this reason the term Karlovitz stretch factor, denoted *K*, is used when referring to the Karlovitz number in their work. The approximation is argued to be acceptable due to the large scatter found in the experimental data. The constant *C*, in equation (3.4), is then defined as being roughly similar to u_{rms}/S_L. Thereby reducing the complexity of the problem. This allowed for various values of the Karlovitz stretch factor to be tested to evaluate *B(K)*. The resulting relationship, equation (3.5), was then compared to the original data collected by Abdel-Gayed et al. The agreement between the empirical data and the equation was considered satisfactory for the relationship to be valid.

$$\frac{S_T}{S_L} = f\left(\frac{u_{rms}}{S_L}, K\right) \tag{3.3}$$

$$\frac{S_T}{S_L} = C\left(\frac{u_{rms}}{S_L}\right) \times B(K) \tag{3.4}$$

$$\frac{S_T}{S_L} = 0.875K^{-0.392}\left(\frac{u_{rms}}{S_L}\right) \tag{3.5}$$

3.3.2 Arntzen

In his 1998 doctorate on modeling of turbulence and combustion for simulation of gas explosions in complex geometries [17], Arntzen reformulated the equation developed by Bray for the relationship between turbulent and laminar burning velocity.

This was done by replacing the Karlovitz stretch factor, in equation (3.5) with an expression in terms of the laminar burning velocity, the rms velocity fluctuation, the integral length scale and the kinematic viscosity. A full derivation based on the work of Arntzen is found in Appendix D: Calculations. The resulting equation for the calculation of the turbulent burning velocity is

$$S_T = 1.8{S_L}^{0.784}{u_{rms}}^{0.412}{l_I}^{0.196}\nu^{-0.196} \tag{3.6}$$

This was further simplified by Popat, [30] by defining the kinematic viscosity as $0.00002 m^2/s$. Thus the turbulent burning velocity can be expressed as a function of the laminar burning velocity, the rms turbulence velocity and the integral length scale, as seen in equation (3.7). This can be rewritten to express the laminar burning velocity as a function of the turbulent burning velocity, the rms velocity fluctuations and the integral length scale, as in equation (3.8).

$$S_T = 15.1{S_L}^{0.784}{u_{rms}}^{0.412}{l_I}^{0.196} \tag{3.7}$$

$$S_L = 0.00315{S_T}^{1.276}{u_{rms}}^{-0.526}{l_I}^{-0.250} \tag{3.8}$$

3.3.3 Dahoe et al.

To calculate the laminar burning velocity from equation (3.8) the required variables must be found. Means of calculating all of these have been found through work lead by Dahoe.

In a 1996 paper on dust explosions in spherical vessels [31], Dahoe et al. derive equation (3.9) for calculating the pressure rise of an explosion in a closed spherical vessel, based on the initial and final pressure of the vessel and the turbulent burning velocity.

$$\frac{dP}{dt} = \frac{3(P_f - P_i)}{R_{Vessel}} \left[1 - \left(\frac{P_i}{P}\right)^{\frac{1}{\gamma}} \frac{P_f - P}{P_f - P_i} \right]^{\frac{2}{3}} \left(\frac{P}{P_i}\right)^{\frac{1}{\gamma}} S_T \tag{3.9}$$

Equation (3.9) is valid if the following assumptions are made:

1. The content of the vessel is assumed to consist of an inner region of completely burned mixture and an outer region of completely unburned mixture.
2. The regions are separated by an infinitely thin spherical flame front.
3. The unburned and burnt mixtures behave as ideal gases.
4. The specific heats of the unburned and burnt mixture are equal and constant for the duration of the explosion.
5. The transition from unburned to burnt mixture occurs through a single-step, irreversible chemical reaction.
6. The temperature of the unburned mixture increases continually as a consequence of the, assumed adiabatic, compression.
7. The burning velocity remains constant throughout the course of the explosion.
8. There is point ignition at the center of the dust cloud with negligible ignition energy.

The derivation itself can be found in Appendix D: Calculations, but as is apparent in equation (3.9), this can easily be rewritten as an expression for finding the turbulent burning velocity based on the pressure profile of an explosion. This was done by Skjold [11] giving equation (3.10).

$$S_T = \frac{1}{3(P_f - P_i)} \left(\frac{dP}{dt}\right) \left(\frac{3V_{vessel}}{4\pi}\right)^{\frac{1}{3}} \left(\frac{P}{P_i}\right)^{-\frac{1}{\gamma}} \left[1 - \frac{P_f - P}{P_f - P_i} \left(\frac{P}{P_i}\right)^{-\frac{1}{\gamma}} \right]^{-\frac{2}{3}} \tag{3.10}$$

In 2001 another research group led by Dahoe presented the results of a study of the effect of turbulence on the pressure developed from dust explosions [27]. As part of this study, the turbulence generated in the 20 liter spheres, by the injection process from the high-pressure reservoir, was examined.

This was achieved by building a plastic replica of the 20 liter Siwek sphere and fitting it with large glass windows, 178mm in diameter, through which measurements were taken using laser Doppler anemometry. The velocity was measured in both the horizontal and the vertical direction.

This made it possible to calculate mean velocity, velocity fluctuation and turbulence macro length scales, from the start of turbulence generation till the turbulence dissipated. By plotting the rms velocity fluctuation they found, from correlations shown in Figure 14 and Figure 15, that they could formulate a generalized set of equations. The equations are valid for the decay of turbulence in the 20 liter Siwek sphere, in the time interval from 60-200ms after dispersion. For spheres fitted with the rebound nozzle the appropriate equations are equations (3.11) and (3.12).

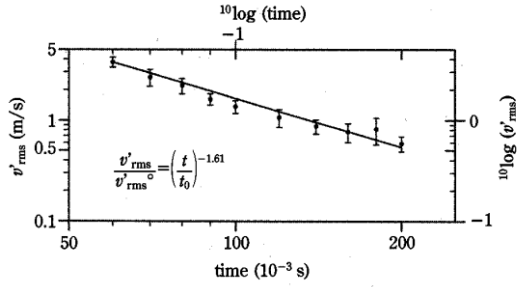

Figure 14: Decay of the rms velocity in the 20-liter sphere fitted with a rebound nozzle. t_0 = 60ms and $u_{rms,0}$ = 3.75ms^{-1} (From Dahoe, [27])

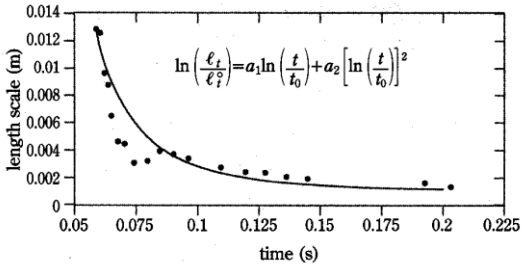

Figure 15: The behavior of the length scales of the macro structure in the 20-liter sphere fitted with a rebound nozzle for the time period of 60 to 200 milliseconds. $l_{I,0}$ = 12.845*10^{-3}m, a_1 = -3.542, a_2 = 1.321 and t_0 = 58.8*10^{-3}s. (From Dahoe, [27])

$$u_{rms} = 3.75\left(\frac{t}{60}\right)^{-1.61} \tag{3.11}$$

$$l_I = 0.012845 \times e^{\left(-3.542\, ln\left(\frac{t}{0.0588}\right)+1.321\left[ln\left(\frac{t}{0.0588}\right)\right]^2\right)} \tag{3.12}$$

4. Experimental

A full description of the sample preparation, experimental setup and the experimental procedures will be presented in this chapter. The experimental apparatus used for the explosions is presented in section 4.3.1.

4.1 Chemical Substances

Two chemical substances were used for the experiments conducted. These were maize starch (simplified chemical formula, $C_6H_{10}O_5$) and potassium carbonate (K_2CO_3). The maize starch had initially been ordered for experiments conducted in 2008, from the Central Mining Institute in Katowice, Poland. However these experiments did not require the use of all the ordered maize starch and much was stored for later use at the University of Bergen. The potassium carbonate consisted of two bulk samples, one shipped from Total Petrochemicals in France to be used in studies by GexCon on inhibitor effect. The other bulk was from earlier experiments conducted at GexCon AS. The potassium carbonate from Total Petrochemicals was micronized, while the other consisted of coarse particles with a diameter above 250μm. The size distribution of the micronized potassium carbonate can be seen in Table 6.

Table 6: Size distribution of the micronized potassium carbonate.

Particle Diameter [μm]	Quantity of Bulk
<45,21	0,900
<18,84	0,500
<6,2	0,100

4.2 Sample Preparation

Several measures were taken to assure the samples were as intended before the experiments were conducted. The preparation was thoroughly documented whenever possible.

4.2.1 Crushing

As mentioned in 4.1 there were two different samples of potassium carbonate available at GexCon AS. The micronized sample was too small for the planed experiments and the coarse sample was too coarse.

The coarse sample had therefore been crushed to obtain particles of the desired particle size. This was done last year during a study on the general effect, of different types of inhibitors, on laminar burning velocity. The crushing was conducted with a cement mixer filled with metal spheres of two different sizes. The size distribution of the pre-crushed potassium carbonate can be seen in Table 7.

A misunderstanding led to the belief that all the coarse potassium carbonate had been pre-crushed. This was first clarified after all the pre-crushed potassium carbonate had been sieved. As crushing with the metal spheres had caused too fine a grind for practical purposes, the second crushing was done with plastic bocce balls in the cement mixer. A third crushing was later conducted by placing the bocce balls in the receiver of the sieve shaker and running the shaker on medium intensity for thirty minutes. The second and third crushing produced far more useful size distributions than the initial had.

Table 7: Size distribution of pre-crushed potassium carbonate

Particle Diameter [µm]	Quantity of Bulk
<125µm	0,976
<100µm	0,950
<75µm	0,922
<50µm	0,880
<32µm	0,420

4.2.2 Moisture Tests & Drying

Preliminary moisture tests were conducted at GexCon, to ensure that moisture would not influence the test results. These were conducted using a Mettler Toledo HG53 Halogen Moisture Analyzer. Unfortunately the analyzer was not connected to a computer for logging, but of all the samples tested, only one had moisture content higher than one percent (1.29%).

Nevertheless, to ensure that moisture would not influence the results, all potassium carbonate was dried prior to sieving. To achieve this, the potassium carbonate was placed in a laboratory drying oven (Termaks, type TS 8024) at ninety degrees Celsius overnight. It was then kept in an eksikator while cooling. After having been sieved to desired size distributions, the potassium carbonate was stored in plastic containers. Containers containing particles with a diameter less than 100µm were kept inside the eksikator when not in use, to prevent absorption of moisture. The two remaining containers were sealed with rubber, when not in use, to keep moisture from entering the containers.

4.2.3 Separation of Samples to the Desired Particle Size Distribution

Initially the potassium carbonate was sieved using the sieve shaker (Cedacería Industrial, type RP-09) at the dust explosion laboratory of the university. However, close examination of samples from this sieving, by means of the electron microscope (for more information on the electron microscope, see Appendix B: The Scanning Electron Microscope), revealed that the sieving had not resulted in separation into desired particle groups. In fact, the pictures taken (Figure 18 in section 5.1) revealed that most samples contained a much larger fraction of particles with a diameter smaller than 32µm, than of the intended diameter.

Attempts were made to use an air classifier instead of the sieve shaker to separate the particles. This effort was abandoned after it became clear that the desired, uniform particle-size distribution would be unobtainable, using this method.

As wet sieving was not an available option, further attempts were made to get the desired particle size separation by means of dry sieving. Samples analyzed with the electron-microscope revealed that far better separation could be achieved by modifying the sieving process. Instead of using many sieves at the same time, the sieving was conducted with one sieve at a time. A brush was used to spread the sample being sieved and to prevent clogging of the sieve-mesh from particles partially through the mesh. Finally the intensity of the sieving was varied according to the grid size of the mesh. The last proved most effective when done in two steps as illustrated in Table 8.

Table 8: Intensity and duration of sieving with respects to grid size

Gridsize Mesh [µm]	First Step		Second Step	
	Intensity	Duration [min]	Intensity	Duration [min]
150	12	10	10	5
125	12	10	10	5
100	11	15	9	7,5
75	11	15	9	7,5
50	10	30	8	15
32	10	40	8	20

Thus the sieving separated the bulk of crushed potassium carbonate to six[3] different particle size sample groups for use in the experiments:

[3] Particles that did not pass through the 150µm mesh were crushed a second time.

Table 9: Particle diameter of the sieved inhibitor samples.

Group	Particle Diameter [μm]
1	125-150
2	100-125
3	75-100
4	50-75
5	32-50
6	<32

4.2.4 Preparation of Individual Test Samples

A digital scale (Sartorius GE412) was used to ensure the desired amount of inhibitor for each experiment. This provided adequate accuracy for the amount of inhibitor required for conducting experiments on chosen propane-air mixtures. A disposable weigh boat was used for each sample weighing.

4.3 Experimental Setup

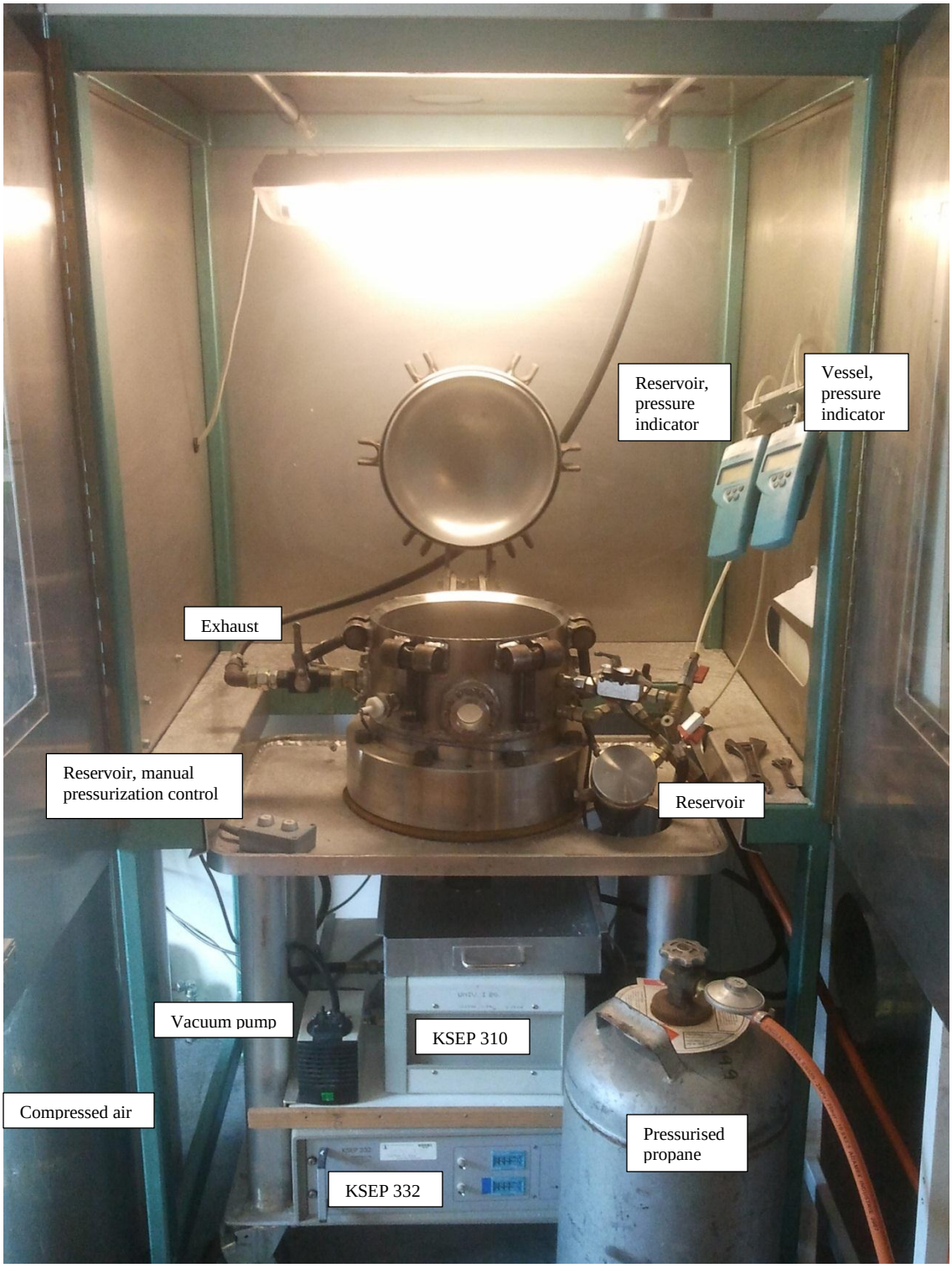

Figure 16: Overview of 20 liter explosion vessel and connected hardware.

4.3.1 Apparatus

The explosion vessel used for the experiments is a modified 20 liter USBM vessel. It was constructed during the establishment of the current dust explosion laboratory at the University of Bergen in 2001. The vessel design was decided by Trygve Skjold and the following description is therefore based on the description given in [11].

The vessel is made of 304 liters of stainless steel and has an inner volume of 20.5±0.02liters. It can mount any nozzle with ¾" NPSM threads. It currently features only pressure sensors, but was designed for addition of optical dust probes, oxygen sensors and infrared pyrometers. It should also be possible to add water cooling, though this requires some modifications. It is certified to a working pressure of 27bar(g) by the Norwegian Directorate for Fire and Electrical Safety.

An overview of the vessel and connected hardware is shown in Figure 16. Schematics of the vessel and of the test facility are shown in Appendix C: Schematics. Note that the electric spark generator is disconnected. Ignition is now initiated with chemical igniters by signals from the KSEP 310 control unit.

4.3.1.1 Measurement and Control System

The measurement and control systems are adapted from the Siwek 20 liter set-up. It consists of two units, a control unit (KSEP 310) and a measurement and control system (KSEP 332). The KSEP 332 receives signals from piezoelectric pressure sensors which measure the pressure as a function of time. There are two independent measuring channels to add extra security to the measured results. The KSEP 332 also controls the valves and the ignition system in the 20 liter vessel. It is connected to the computer software through an RS232 cable and relays signals between the computer software, the KSEP 310 unit, and the explosion vessel.

4.3.1.2 Ignition

As mentioned in 4.3.1, ignition is conducted with chemical igniters. Each of these deliver an ignition energy of 100J. The igniters were ordered from Fr. Sobbe GmbH in Dortmund. For each experiment a single igniter was mounted in the center of the vessel. By aligning the cap of the igniter in the center of the former spark gap (from the old ignition system), it should be possible to ignite from a reasonably stable position for each experiment.

4.3.1.3 Computer Software

The KSEP software was developed by Kühner AG, with the aid of Christoph Cesana and Richard Siwek, for use with the 20 liter Siwek sphere. Although designed for the Siwek sphere, it can be incorporated into the design of any experimental setup consisting of a 20 liter sphere as long as the necessary KSEP-hardware is included in the setup. Cesana and Siwek also authored the instructions manual which, if followed, ensures that experiments using the 20 liter spheres are conducted according to international standards.

The KSEP-software communicates with the KSEP measurement and control unit. It is used to initiate experiments and presents a pressure-time graph of the explosion, as illustrated in Figure 1, shortly after an experiment has been conducted.

4.4 Experimental Procedures

The experimental procedures were similar for all the conducted experiments. For this reason only the standard procedure for experiments with inhibitor is described in detail.

For experiments on the effect of the nozzle on the inhibitor, the inhibitor was placed either in the reservoir, before pressurizing it, or between the pneumatic valve and the nozzle. Additionally, in those experiments, no igniter was used and no propane was injected into the vessel. In the propane-air reference experiments, no inhibitor was placed inside the vessel.

The numbers in section 4.4.1 refer to the numbered units in the schematic (Figure 47 in Appendix C: Schematics).

4.4.1 Standard Experimental Procedure

Before conducting experiments the ventilation is started and the valves for the pressurized air and the propane container are opened. A chemical igniter is then mounted inside the 20 liter vessel and the desired amount of inhibitor is placed on top of the nozzle, as seen in Figure 17. The lid is then shut and bolted.

The exhaust valve [1] from the vessel is closed and the vacuum pump is activated. The vessel is evacuated until the absolute pressure reaches below 0.4 bar. The exact pressure varies depending on the desired equivalence ratio. The ball valve [5] is closed, and if necessary, the air inlet valve [6] is used to fine tune the pressure.

Figure 17: Placement of inhibitor for the standard experiments with inhibitor.

With the pressure inside the vessel at the desired value, the gas inlet valve [8] is opened and the desired vol% of gas is transferred into the vessel. When the reservoir pressure indicator [4], reads 0.4 bar, the 3-way valve [1] and the safety switch [3] are closed. The manual control is then used to fill the reservoir with pressurized air until the reservoir digital pressure indicator [2] reads approximately 20 bar(g).

The experiment is software controlled from this point onwards. After inserting the inhibitor concentration, the propane gas concentration, the ignition energy and the ignition delay time in the KSEP 6.0f control window, it is possible to activate the experiments. Since the pressure in the reservoir drops after manual pressurizing is stopped, the ignition sequence starts with the KSEP 310 unit opening a valve to the reservoir, re-pressurizing it to 20 bar(g). After a few seconds this valve is shut and a pneumatic outlet valve, leading from the reservoir into the vessel, is opened. The pressurized air flows through the outlet valve and the dispersion nozzle, consequently creating a turbulent dust cloud inside the vessel. The outlet valve shuts, and after the preset ignition delay of 60ms, the chemical igniter discharges the 100J of energy.

The two pressure sensors measure the pressure development inside the vessel signal the KSEP 6.0 software, via the KSEP 332 unit. A pressure-time graph, as illustrated in Figure 1, is presented along with the data listed in Table 2. The pressure at, and the time interval to the inflection point are also noted in the worksheet. All the data is stored on the computer and is available for later use. The pressure remaining in the reservoir is also noted in the worksheet. This is subtracted from the pressure added to the vessel from the reservoir, when calculating the laminar burning velocity.

After the experiment, the exhaust valve is opened. Then the lid is opened and the igniter removed. A wet piece of cloth is used to clean the inside of the vessel. To dry the vessel and help cool the vessel walls pressurized air is applied to the inside of the vessel for several minutes.

5. Experimental Results

The experimental results are separated into two sections. In the first section, images produced with the electron microscope will be shown along with comments on the findings. In the second section, graphs illustrating the results from the experimental work with the 20 liter vessel will be presented. A more comprehensive explanation of the results, is presented in the discussion of the results in chapter 6.

5.1 Electron Microscope Images

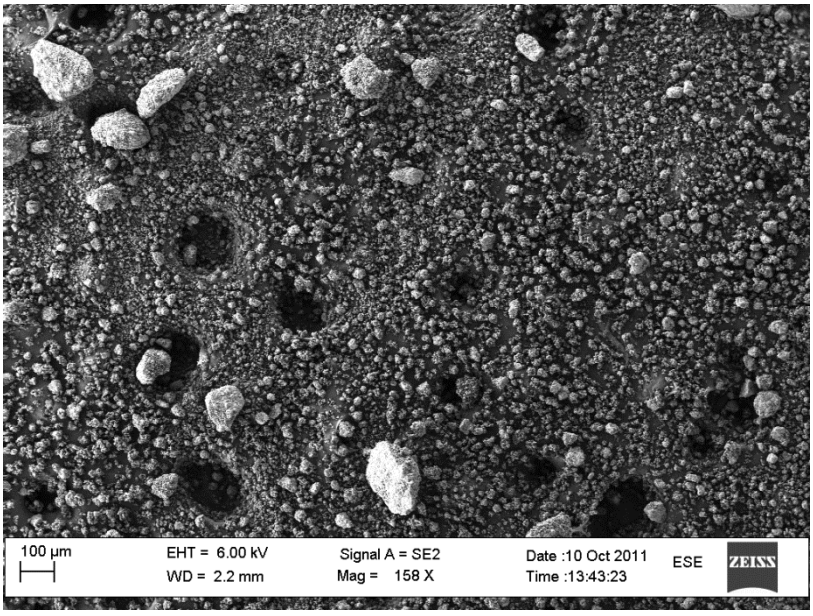

Figure 18: Electron microscope image of sample one, which should contain particles with a diameter between 125µm and 150µm.

Figure 18 shows the result of the first attempt at separating the particles, according to size, with the sieve shaker. Settings used on the sieve shaker were the same as those used in the last study on inhibitor effect.

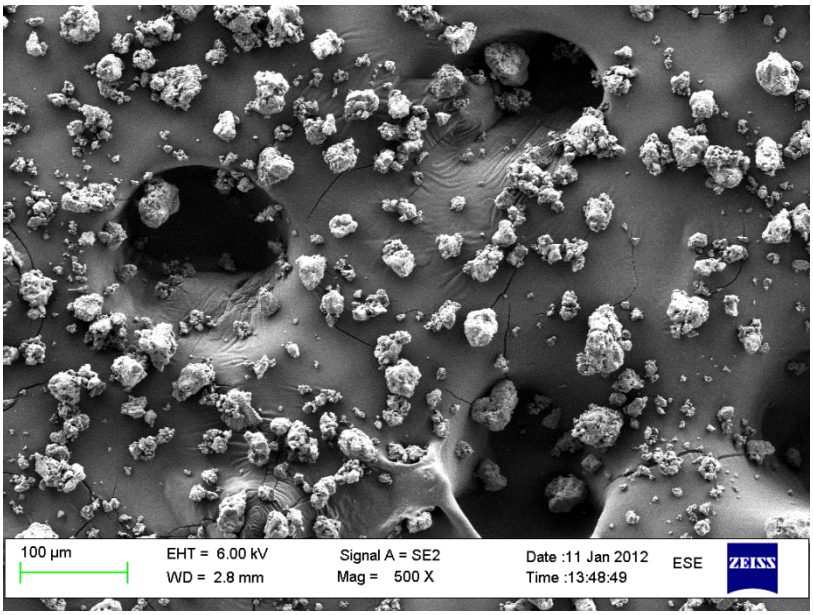

Figure 19: Electron microscope image of sample five, which should contain particles with a diameter between 32 µm and 50 µm. Prepared at with low intensity on the sieve shaker.

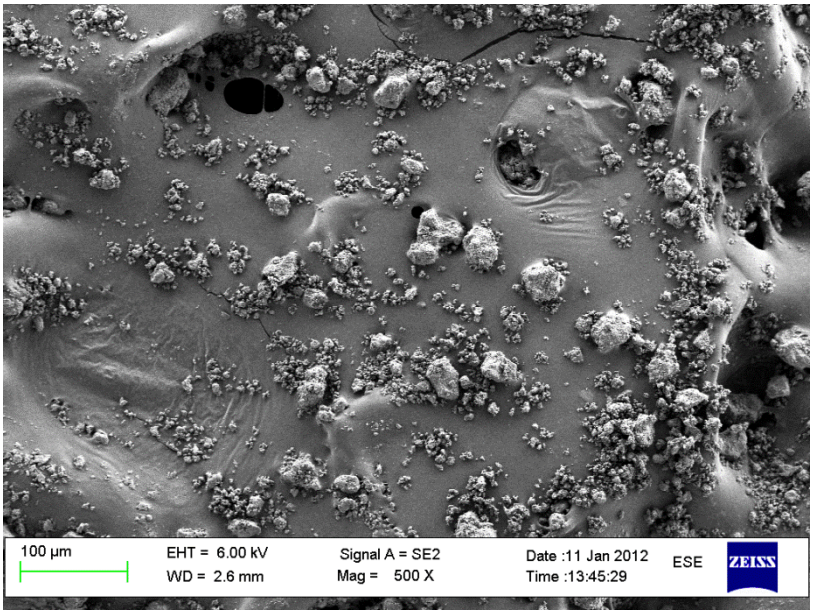

Figure 20: Electron microscope image of sample five, which should contain particles with a diameter between 32 µm and 50 µm. Prepared with high intensity on the sieve shaker.

Figure 19 and Figure 20 show samples prepared with the same duration of sieving, but at different intensities. Figure 19 was prepared at a lower intensity on the sieve shaker.

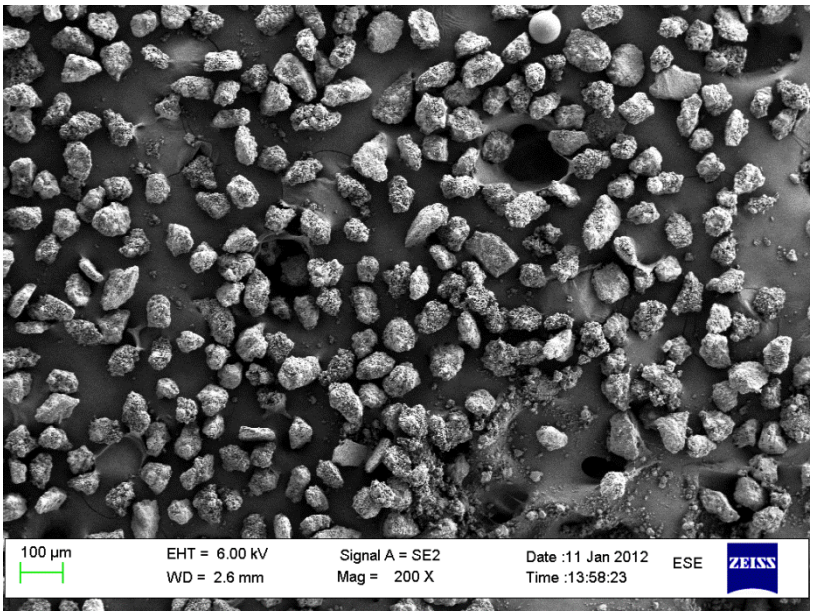

Figure 21: Electron microscope image of sample four, which should contain particles with a diameter between 50µm and 75µm.

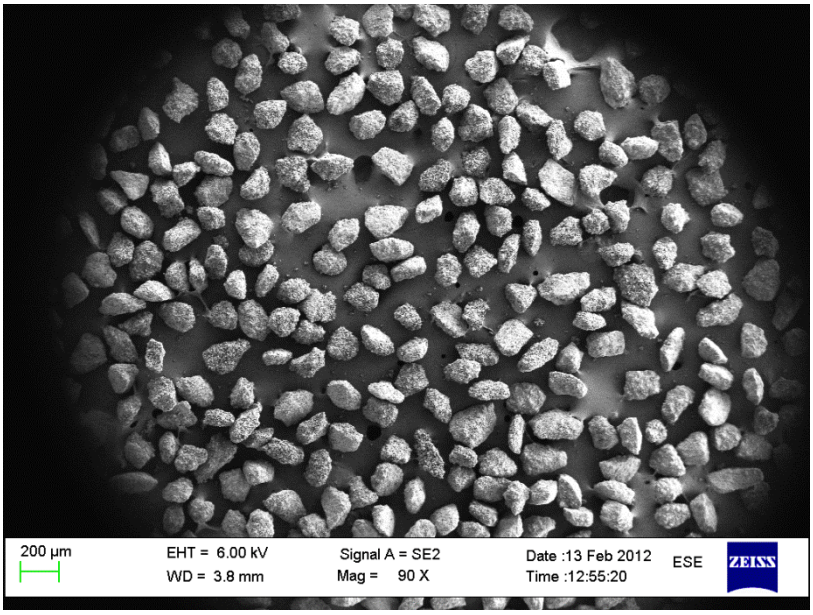

Figure 22: Electron microscope image of sample one, which should contain particles with a diameter between 125µm and 150µm.

Figure 21 and Figure 22 show samples prepared by the new sieving method described in 4.2.3.

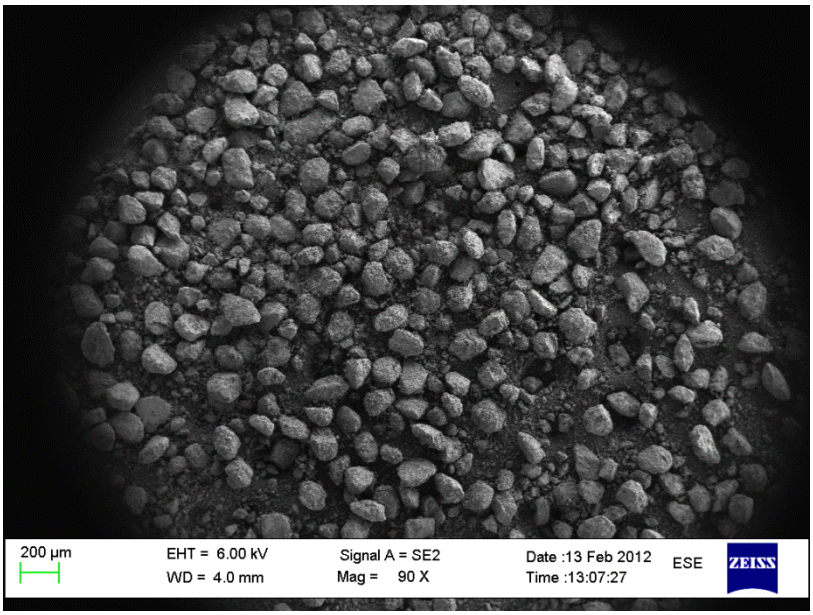

Figure 23: Electron microscope image of sample one, which initially contained particles with a diameter between 125µm and 150µm, after having been injected into the main vessel from the high-pressure reservoir, at a concentration of 200g/m^3.

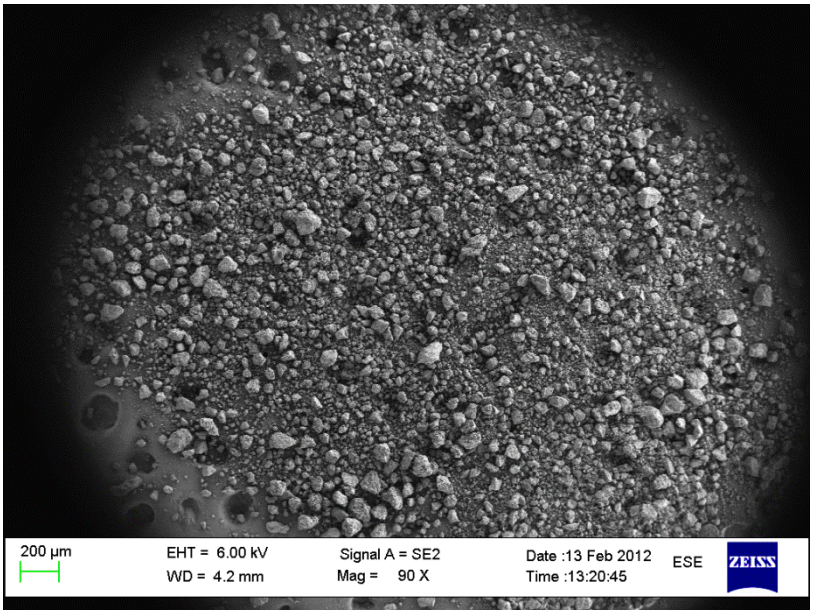

Figure 24: Electron microscope image of sample one, which initially contained particles with a diameter between 125µm and 150µm, after having been injected into the main vessel from the high-pressure reservoir, at a concentration of 25g/m^3.

Figure 23 and Figure 24 show the impact of sample concentration on the particle size as the sample is injected from the high-pressure reservoir into the main vessel. For a reference comparison, see Figure 22.

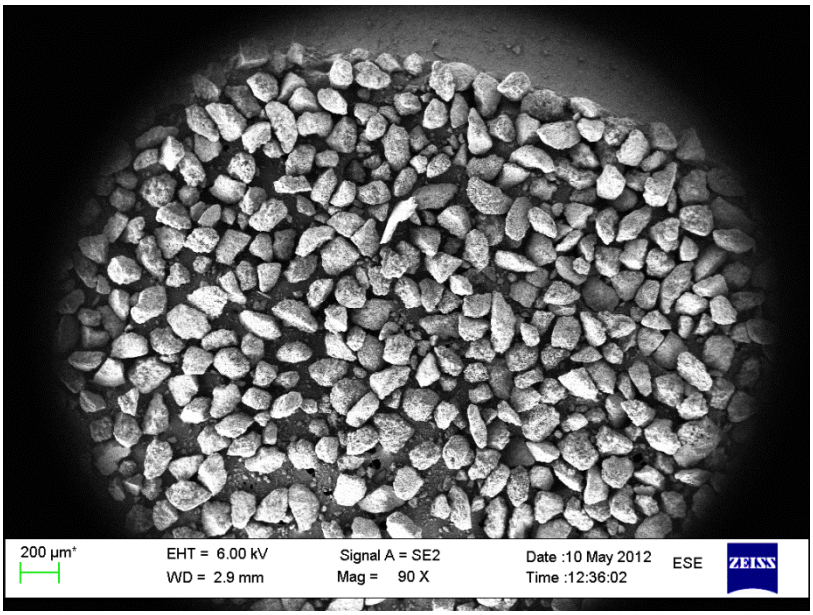

Figure 25: Electron microscope image of sample one, which initially contained particles with a diameter between 125µm and 150µm, after having been dispersed in the main vessel by the impact of the pressure wave from the reservoir, at a concentration of 200g/m^3.

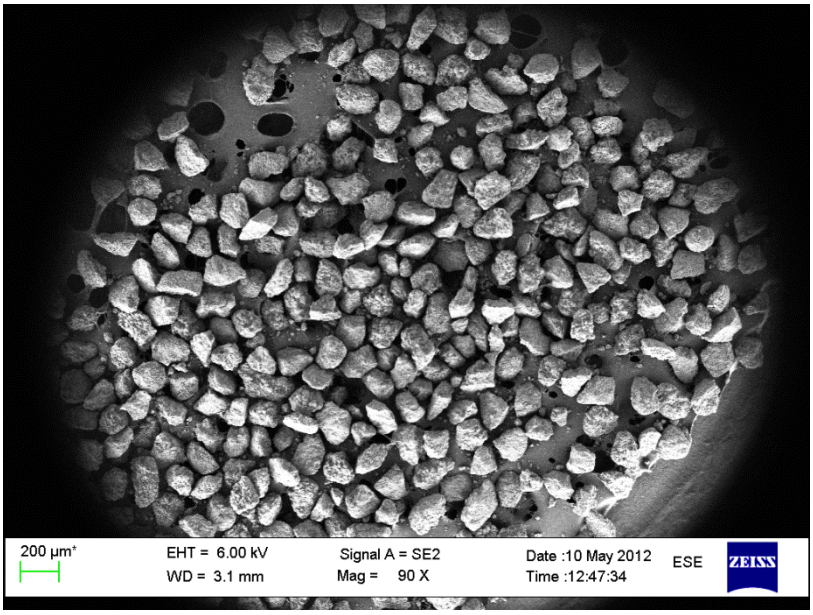

Figure 26: Electron microscope image of sample one, which initially contained particles with a diameter between 125µm and 150µm, after having been dispersed in the main vessel by the impact of the pressure wave from the reservoir, at a concentration of 12.5g/m^3.

Figure 25 and Figure 26 show the impact of sample concentration, on the particle size, as the sample is dispersed in the main vessel by a pressure wave from the reservoir (reference seen in Figure 22). The sample was placed on the nozzle, as illustrated in Figure 17.

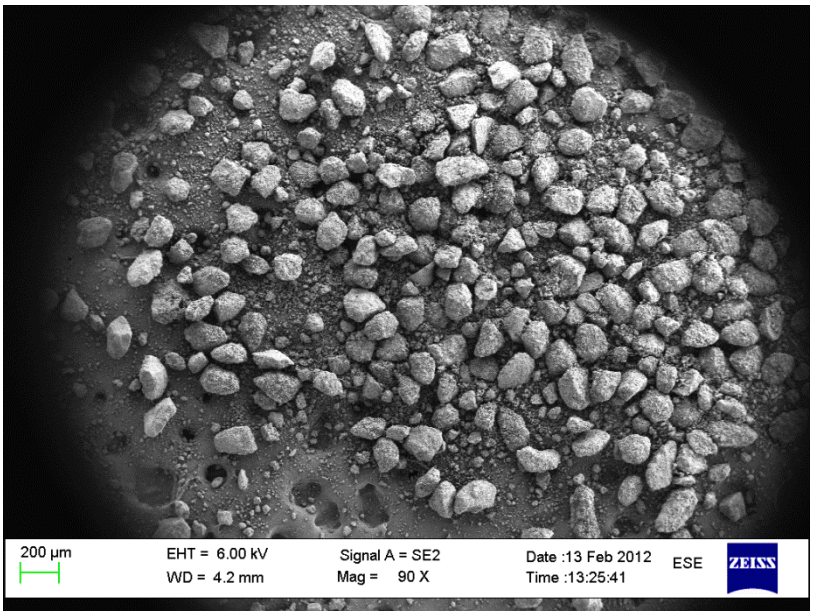

Figure 27: Electron microscope image of sample one, which initially contained particles with a diameter between 125µm and 150µm, after having been dispersed in the main vessel from underneath the nozzle, at a concentration of 25g/m^3.

Figure 27 shows the effect on the particle size from passing through the nozzle in the dispersion process.

5.2 Results from the Experiments with the 20 Liter Explosion Vessel

The experimental results are presented with graphs depicting the impact of the average particle diameter and the inhibitor concentration on parameters describing the explosion violence. They are separated into two subsections. The first section contains graphs summarizing the impact of average particle diameter, for all concentrations, on the explosion parameters. The second section contains graphs depicting the impact of average particle size, for a given concentration, on normalized explosion parameters. The graphs in the second section also show the experimental standard deviation for each of the parameters. The propane-air mixtures contain 4.2 and 5.25vol% propane.

For graphs depicting the impact of average particle size diameter for each of the explosion parameters measured, refer to Appendix E: Graphs Depicting the Impact of Particle Size on Individual Explosion Parameters.

Graphs depicting the results from the experiments are presented in pairs. The first graph depicts the effect for the 4.2vol% mixture, the second the 5.25vol% mixture. Other factors are the same for the paired graphs.

5.2.1 Average Inhibitor Effect on Explosion Parameters

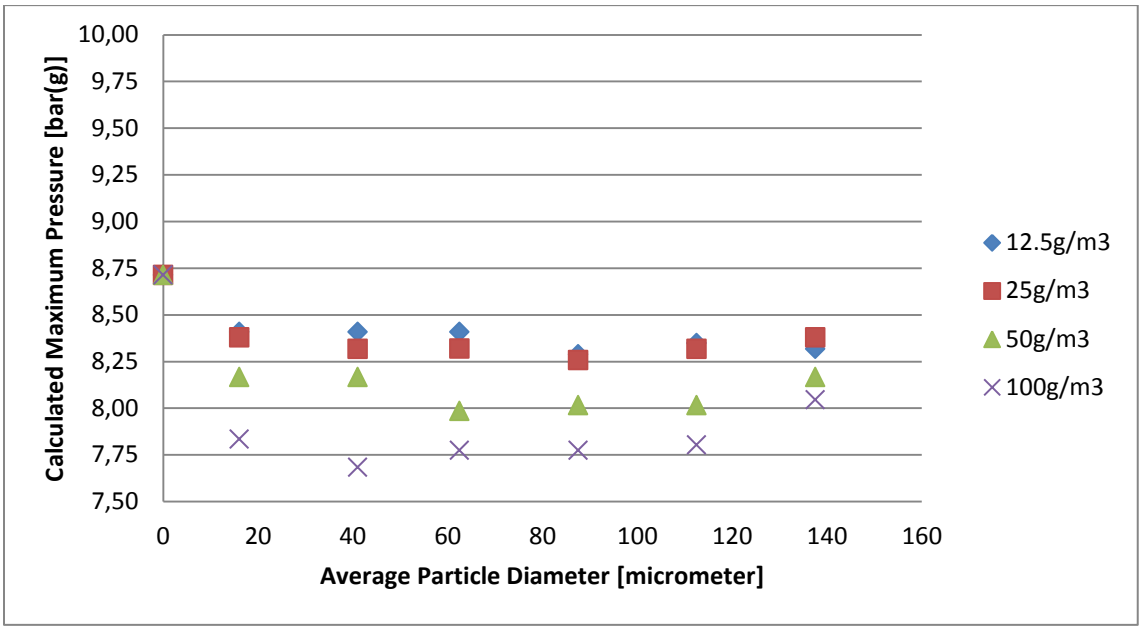

Figure 28: Relationship between average particle diameter and explosion pressure for experiments done with a propane-air mixture with 4.2vol% propane.

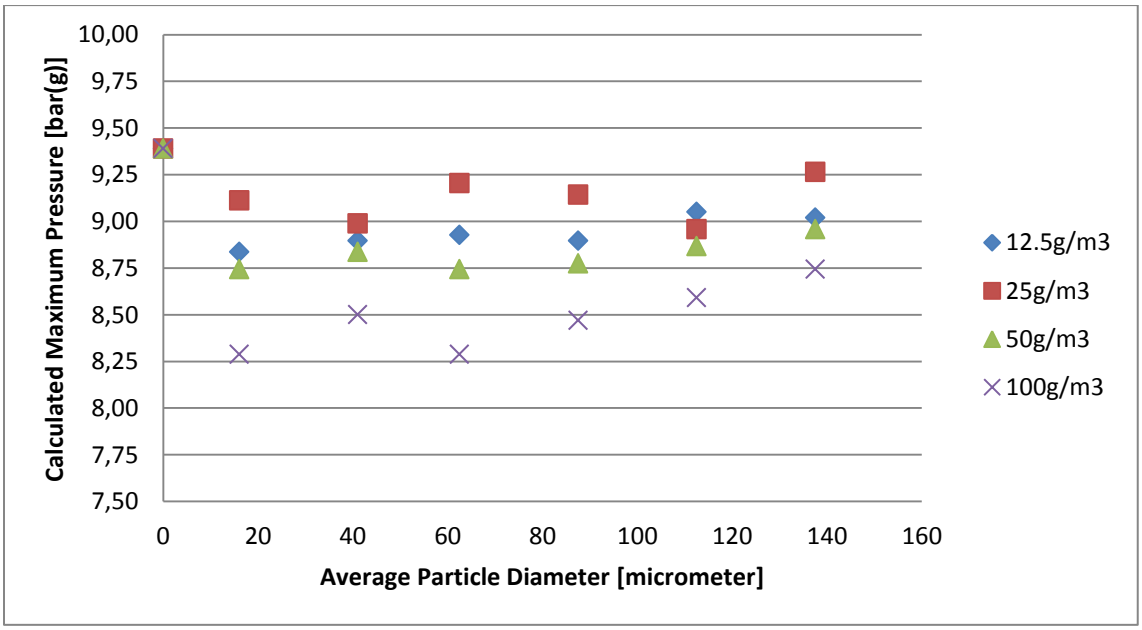

Figure 29: Relationship between average particle diameter and explosion pressure for experiments done with a propane-air mixture with 5.25vol% propane.

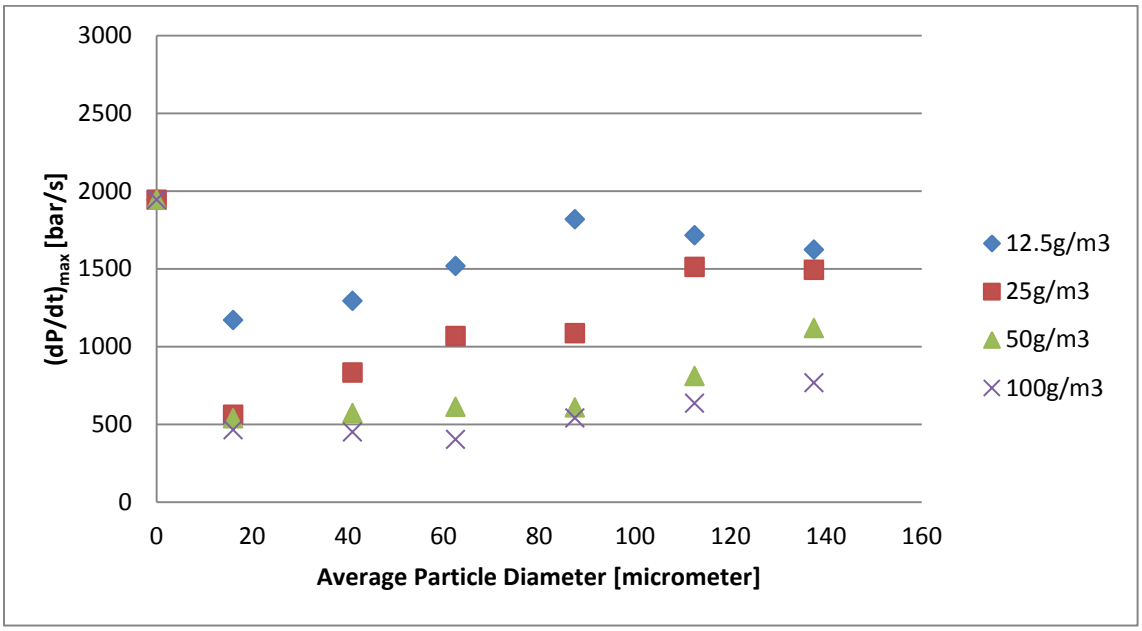

Figure 30: Relationship between average particle diameter and the maximum rate of pressure rise for experiments done with a propane-air mixture with 4.2vol% propane.

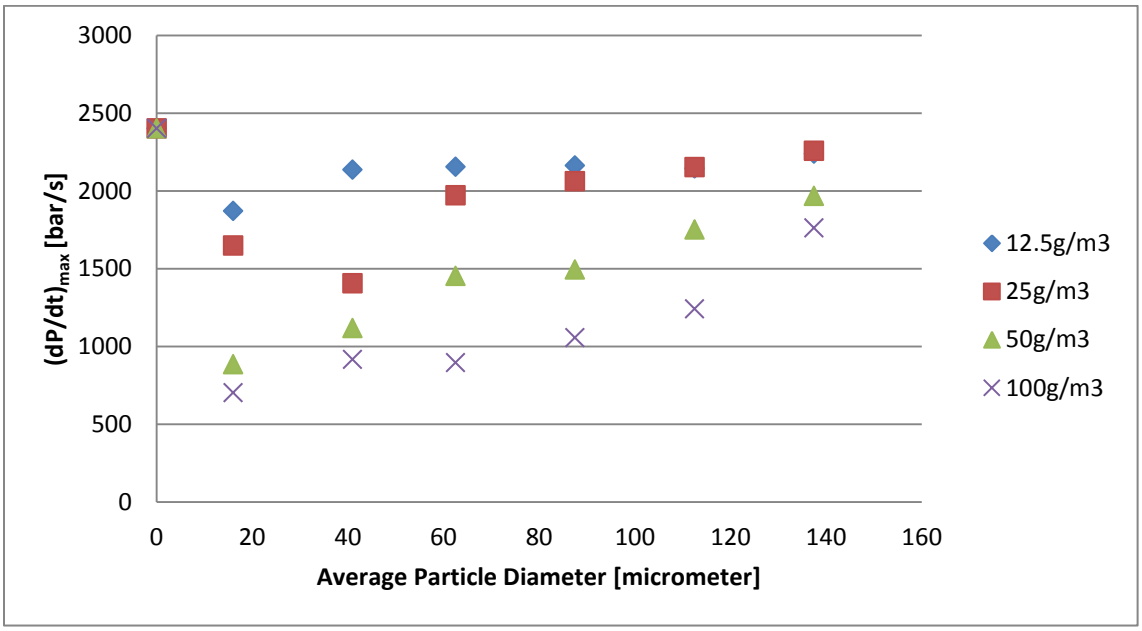

Figure 31: Relationship between average particle diameter and maximum rate of pressure rise for experiments done with a propane-air mixture with 5.25vol% propane.

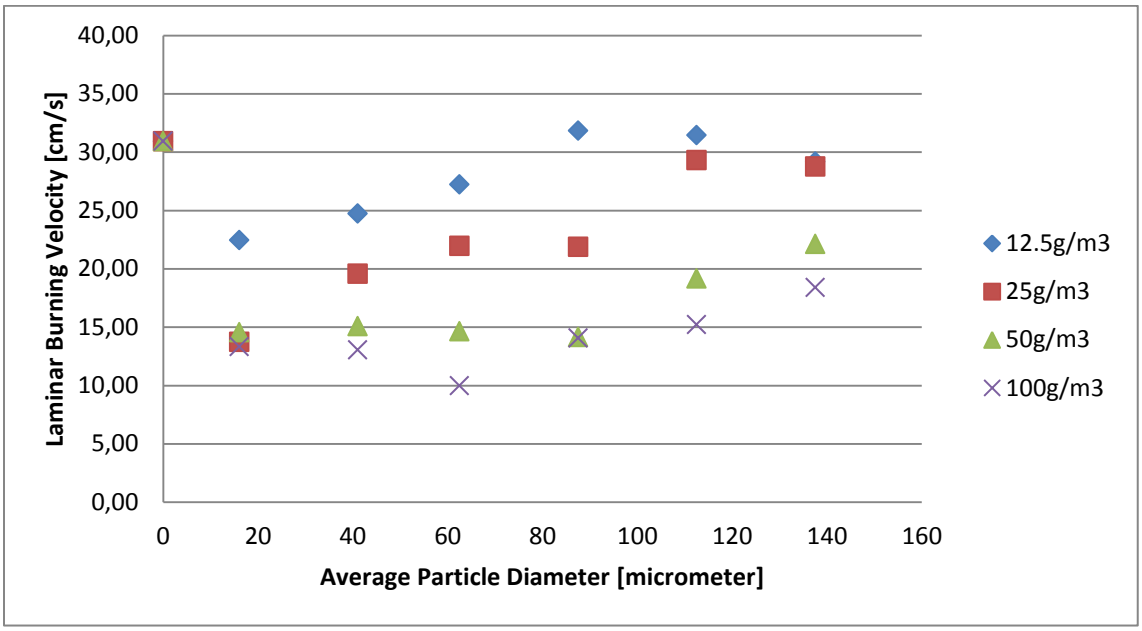

Figure 32: Relationship between average particle diameter and calculated laminar burning velocity for experiments done with a propane-air mixture with 4.2vol% propane.

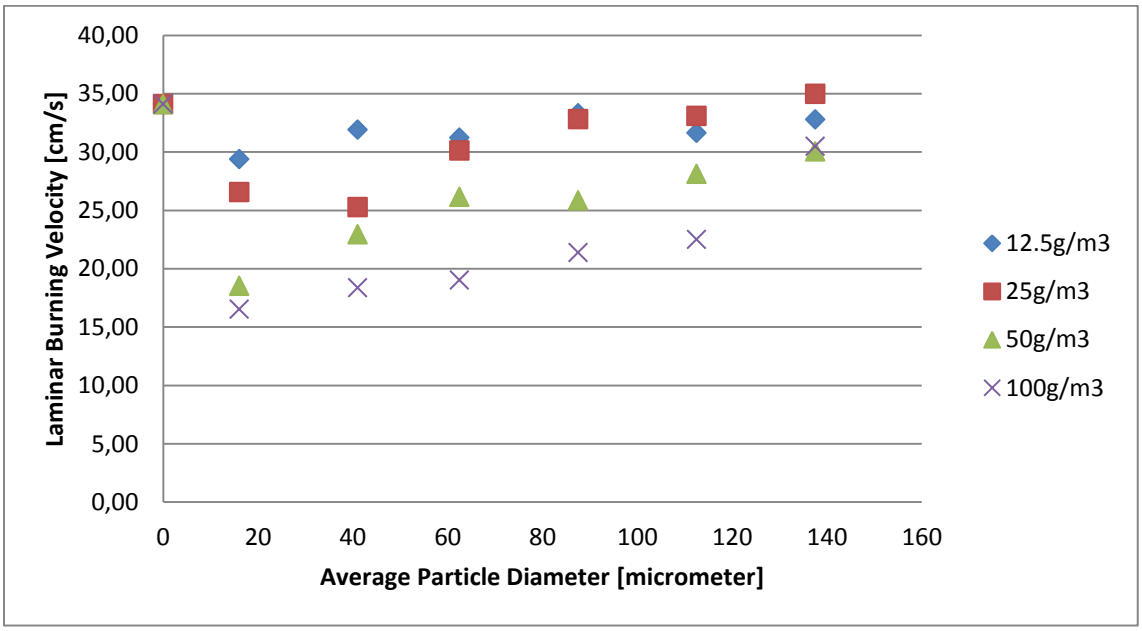

Figure 33: Relationship between average particle diameter and calculated laminar burning velocity for experiments done with a propane-air mixture with 5.25vol% propane.

5.2.2 Normalized Average Inhibitor Effect on Explosion Parameters

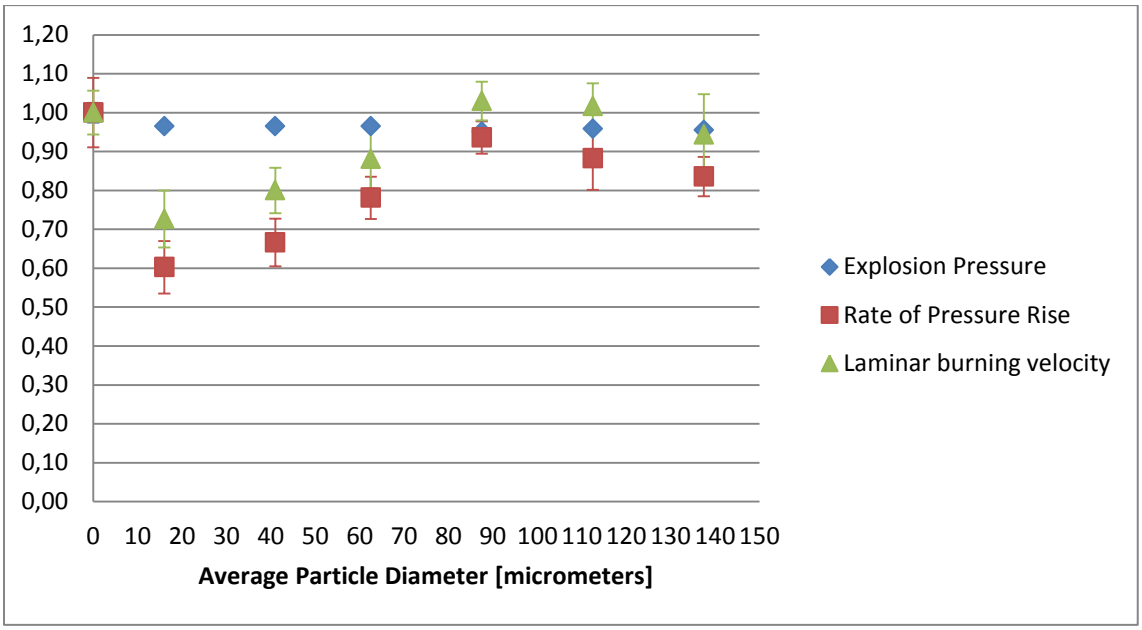

Figure 34: Relationship between average particle diameter and normalized explosion parameters for experiments done with an inhibitor concentration of 12.5g/m^3 and a propane-air mixture with 4.2vol% propane.

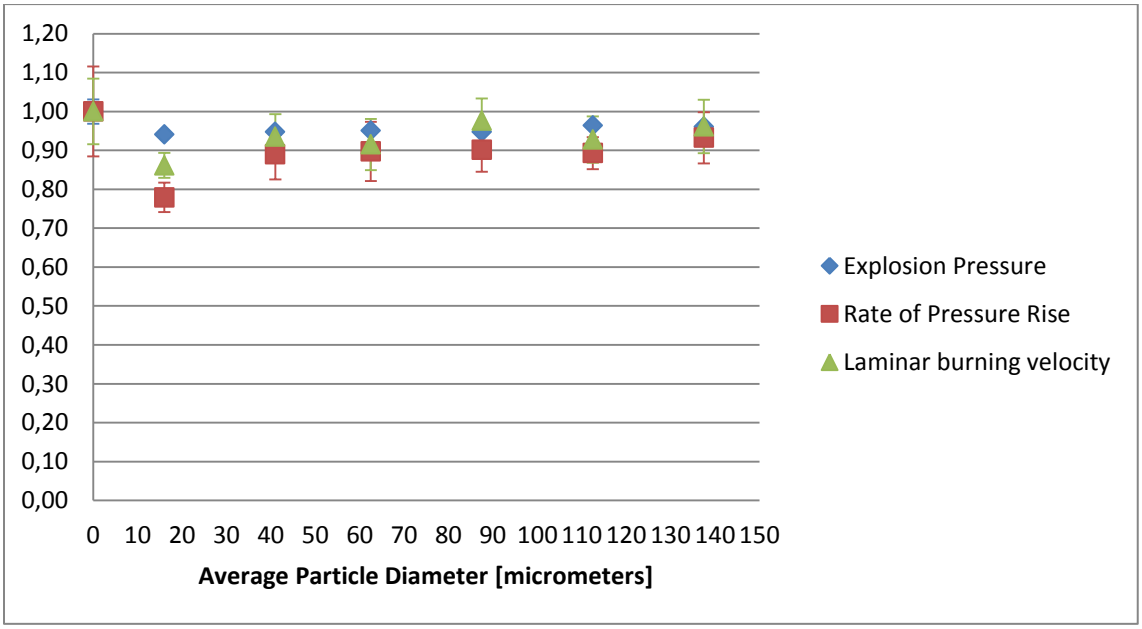

Figure 35: Relationship between average particle diameter and normalized explosion parameters for experiments done with an inhibitor concentration of 12.5g/m^3 and a propane-air mixture with 5.25vol% propane.

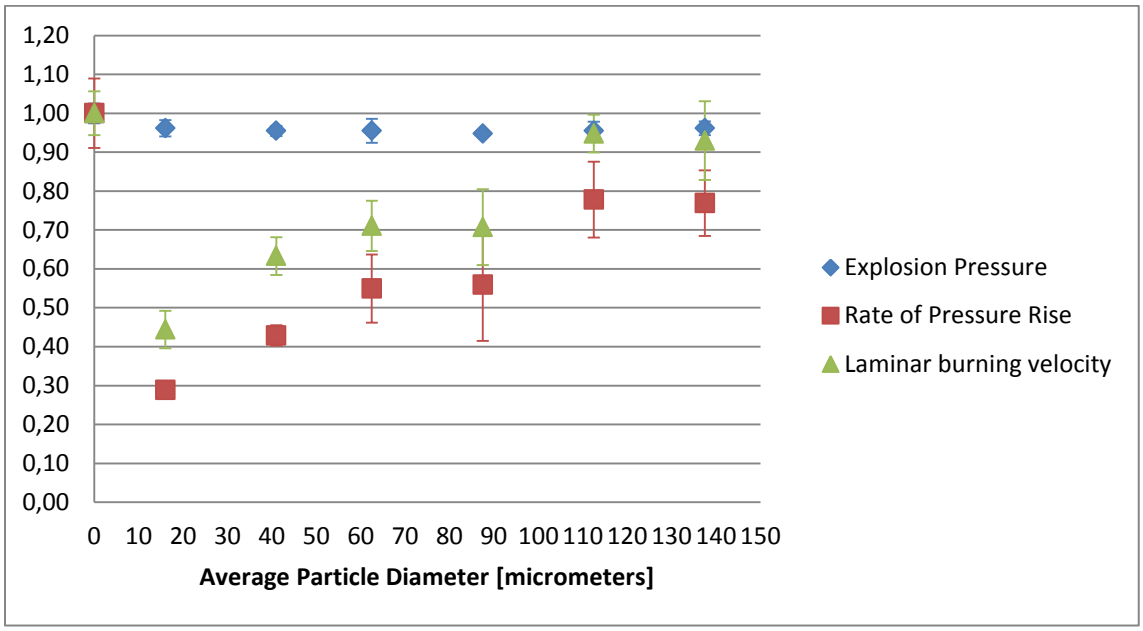

Figure 36: Relationship between average particle diameter and normalized explosion parameters for experiments done with an inhibitor concentration of 25g/m^3 and a propane-air mixture with 4.2vol% propane.

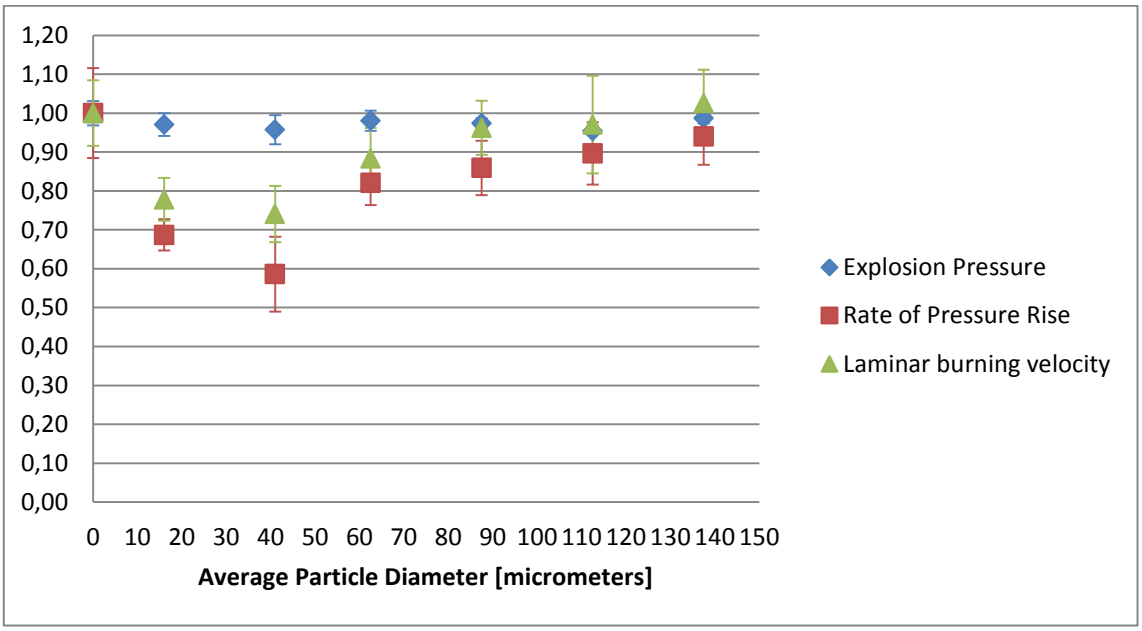

Figure 37: Relationship between average particle diameter and normalized explosion parameters for experiments done with an inhibitor concentration of 25g/m^3 and a propane-air mixture with 5.25vol% propane.

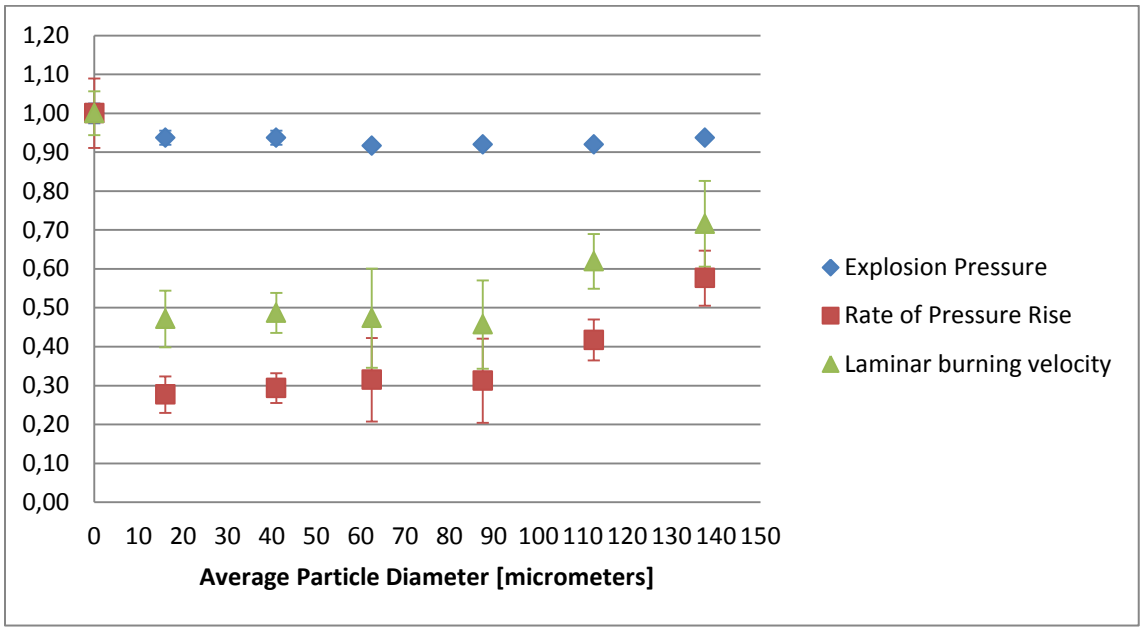

Figure 38: Relationship between average particle diameter and normalized explosion parameters for experiments done with an inhibitor concentration of 50g/m^3 and a propane-air mixture with 4.2vol% propane.

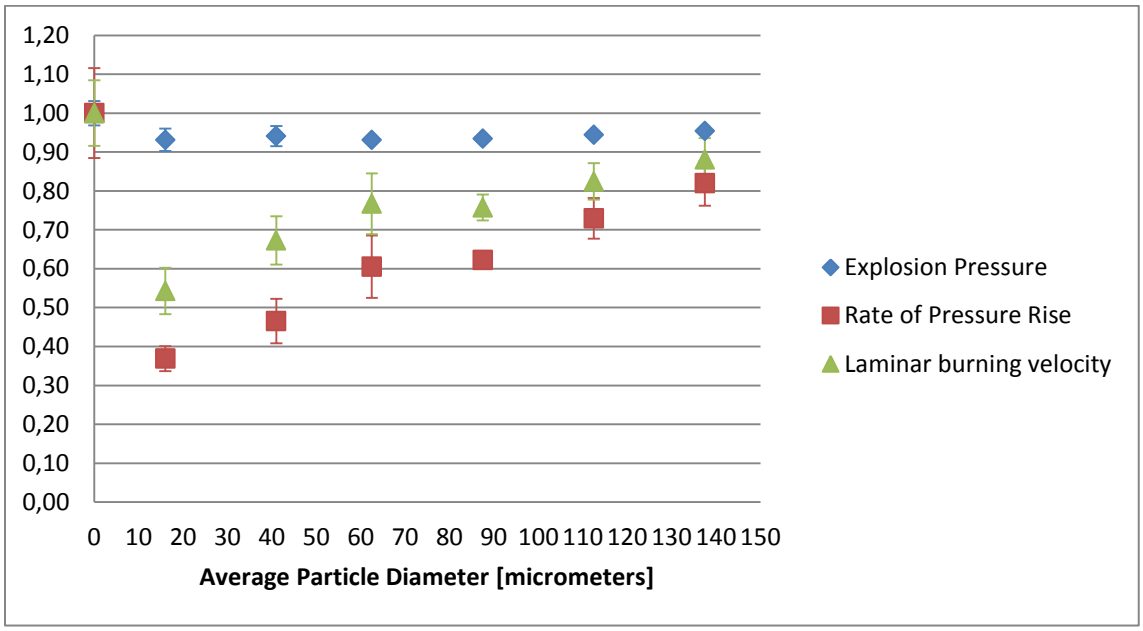

Figure 39: Relationship between average particle diameter and normalized explosion parameters for experiments done with an inhibitor concentration of 50g/m^3 and a propane-air mixture with 5.25vol% propane.

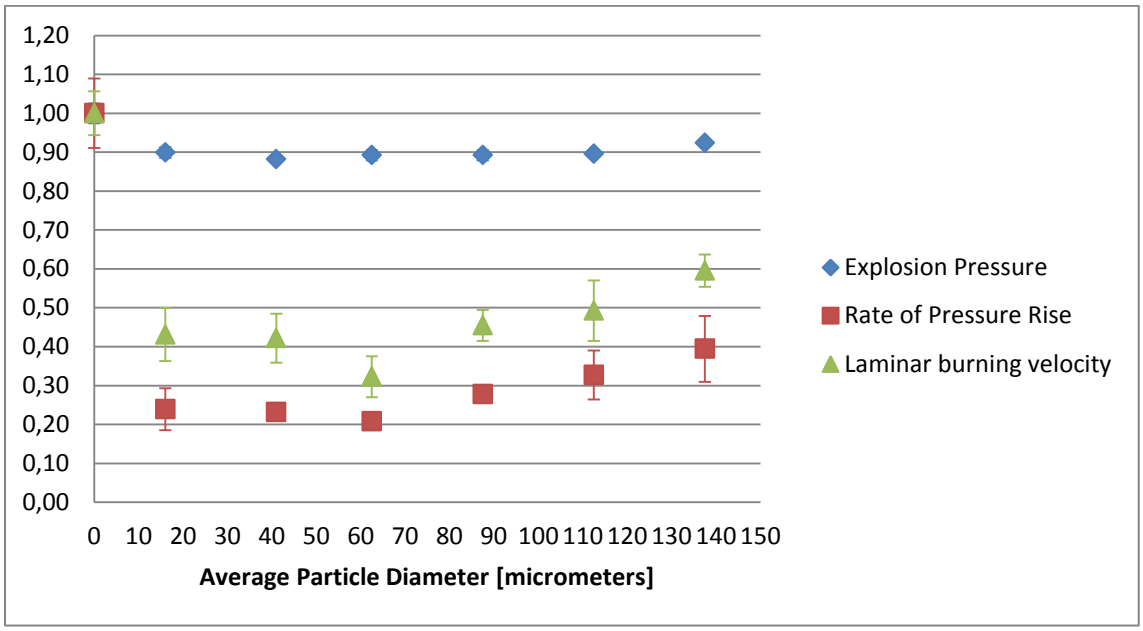

Figure 40: Relationship between average particle diameter and normalized explosion parameters for experiments done with an inhibitor concentration of 100g/m^3 and a propane-air mixture with 4.2vol% propane.

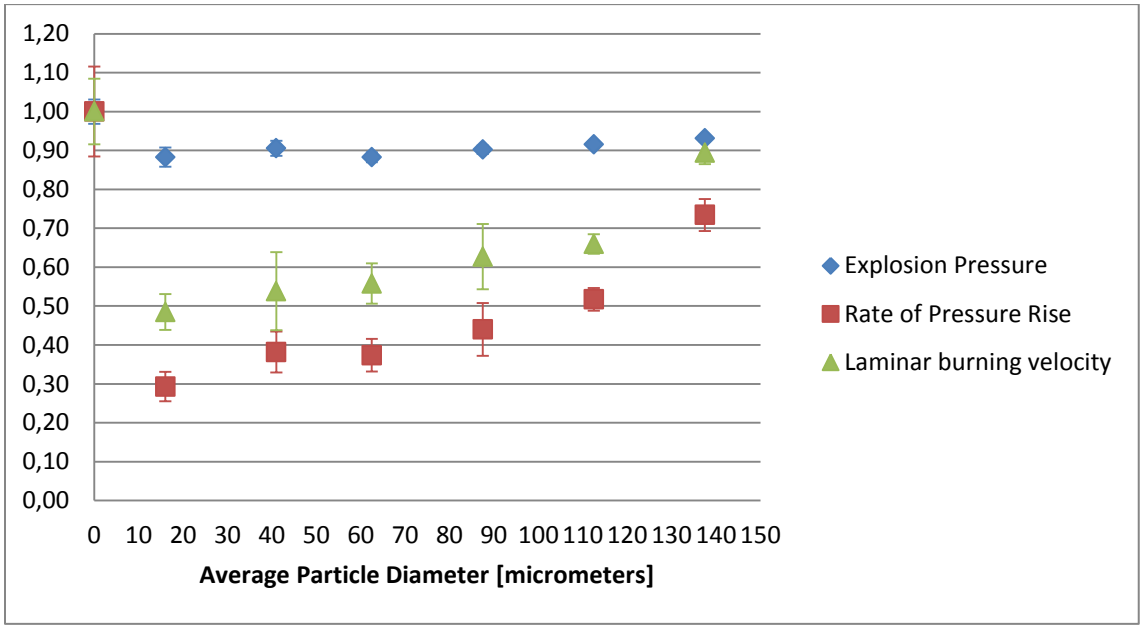

Figure 41: Relationship between average particle diameter and normalized explosion parameters for experiments done with an inhibitor concentration of 100g/m^3 and a propane-air mixture with 5.25vol% propane.

6. Discussion

In the following chapter, the results presented in the previous chapter will be discussed. The chapter is divided into sections. These are to a large extent based on the sections in the results, but with the addition of a short introductory comment on the calculations used.

6.1 Calculation of the Laminar Burning Velocity

The equations used to calculate the laminar burning velocity are the same equations that are used in the CFD code FLACS. This software has been tested thoroughly for many years. The testing has been done both by assessing the development of accidental explosions after the fact, and by simulating large scale experiments for comparison of measured experimental data and simulated results. The comparisons between simulated scenarios and real explosions show that FLACS has a slight tendency to exaggerate the dimensions of explosions [17]. Thus it would seem safe to assess that the theoretical assumptions made to simplify the problem of calculating a laminar burning velocity from turbulent combustion, if it should have a significant impact on the calculated laminar burning velocity, probably slightly exaggerates the predicted laminar burning velocity. However, as illustrated in the standard deviations from the experiments in the 20 liter vessel, experimental explosions have variations, even when attempts are made to create the exact same conditions. Thus the slight exaggeration could be considered a safety margin. Any further consideration on the validity of the assumptions done when deriving the equations, used to calculate the laminar burning velocity, is beyond the scope of this thesis.

6.2 Inhibitor Particle Size Separation

The sample seen in Figure 18 was prepared by the instructions used in the last study on inhibitors at the UoB. It is evident that the sample contains a wide range of particle sizes and that the vast majority have a diameter below 50µm. The sample seen is from the top sieve in the sieve shaker (125-150µm), but the same size distribution could be seen in the samples from sieves located beneath it. This would explain the lack of structure in the results of the former study at the UoB, as all the samples probably contained a similar ratio of large to small particles.

The difficulty of sieving the bulk sample is due to the presence of extremely small particles. According to ASTM standards [32] wet sieving should be used to properly sieve samples containing particles with a diameter of less than 75µm. In wet sieving, instead of gravity, the fluid leads the smaller particles through the sieves. Thus the shaking, which causes a large degree of dispersion in dry sieving, would not cause the same problems. Unfortunately, no wet sieve is available at the UoB.

It was therefore necessary to develop a new sieving method. Instead of placing a stack of sieves on the sieve shaker, one sieve was used at a time. For large particles, high intensity on the sieve and continual brushing, gave good uniformity on the samples collected. This can be seen in Figure 21 and Figure 22. For smaller particles a lower intensity worked better, as seen in Figure 19 and Figure 20.

Although the new method gave relatively uniform particle size, there are still particles with a diameter of less than 32µm on all the electron microscope pictures (though more frequent, on pictures from samples with a small particle diameter). This could have two causes. It could be that the new method is not thorough enough for separation when the grid size of the mesh is reduced below 50µm. It could also be that the small particles seen in the pictures are remnants of larger particle pieces that were torn, as the samples were prepared for the electron microscope. The sample preparation involved using pressurized air to remove excess inhibitor powder from the double sided carbon adhesive tape. This could tear weak particle structures apart, leaving only a small piece attached to the tape.

6.3 The Dispersion Grinding Effect

In the instruction manual for the Siwek 20 liter apparatus [4], Cesana and Siwek warn that the particle size on dust samples tested could be reduced in the dispersion process. This is due to a grinding effect as the dust flows through the outlet valve and through the dispersion device. However in [26] this reduction is concluded to be a constant factor, independent of concentration. As seen in Figure 23 and Figure 24, a size reduction by a constant factor was not seen in the conducted experiments. The higher concentration resulted in reduced average grinding of each sample particle, from the dispersion process, compared to the lower concentration.

This indicates that the particles dispersed at higher concentrations shield each other from some of the grinding effect, probably due to less mobility of the particles in the flow. At lower concentrations there is more room for particle movement in the flow. This could lead to more grinding, both from stationary surface areas and from other particles, as the flow evacuates from the reservoir into the vessel. This finding has not been described in other scientific journals. The reason for this is probably that the 20 liter vessels were originally designed to find maximum explosive parameters. As combustible dusts react more violently the smaller the particle size, it makes perfect sense to design the apparatus with smaller particles in mind. In fact, in the instruction manual for testing with the Siwek sphere [4], it is specified that particles should have a median size no larger than 63 µm. This, due to the drop in explosiveness found with solid particles as their size increases beyond this.

Although the concentrations were found to have an impact on the dispersed particle size, the source of this grinding could be either the outlet valve or the rebound nozzle, or a combination of both. In [4] both are listed as possible causes, but in [26], the nozzle impact on the grinding effect is concluded to be minimal.

Tests were therefore conducted where the inhibitor sample was placed between the outlet valve of the reservoir and the dispersion nozzle. As seen in Figure 27, this resulted in less particle size reduction, but the grinding effect was still considerable.

Thus the only way to remove the grinding effect from the dispersion process, while still using the rebound nozzle, was to place the sample inside the vessel. This approach is illustrated in Figure 17. Figure 25 and Figure 26 illustrate that this resulted in negligible particle size reduction, at both high and low inhibitor concentration.

To ensure that the dispersions were adequate with the inhibitor placed inside the vessel, a few explosion experiments were conducted with combustible maize starch-air mixtures. As mentioned in 3.2.2, the maximum pressure in dust explosions is turbulence dependent. Since the maize starch used has a particle diameter in the region of 10-20μm and high concentrations are needed for a combustible dust cloud, it is unlikely that there will be a major particle size reduction when dispersing it from the reservoir. The maximum pressures found in experiments with 1.5 and 2 times the stoichiometric maize starch concentration, were similar for the dispersions from the reservoir and inside the vessel. The largest average deviation was 0.2bar and was found for the experiments at the lowest concentration, 500g/m^3.

6.4 The Inhibitor Effect

Three parameters commonly used to describe the violence of explosions were examined. The effect of the inhibitor on these parameters will be discussed in turn.

6.4.1 Effect on Maximum Pressure

From Figure 28 and Figure 29 it can be seen that an increase in the concentration of potassium carbonate has a tendency to lead to a drop in the maximum pressure. This effect is seen for almost all the tested particle sizes. The exception is for 12.5 and 25g/m^3 in the mixture with 4.2vol% propane. This is probably due to experimental inaccuracy, as the 25g/m^3 inhibitor tests have large standard deviations for the maximum pressure, as seen in Figure 36. In addition, the impact of inhibitor concentration on the maximum pressure is very small, leading only to an approximate drop of the maximum pressure by ten percent, or less, in all the experiments.

This can be explained by the chemical effect of the inhibitor. As mentioned in 3.1.3, alkali metals inhibit flames by scavenging on free radicals. All inhibiting chemical reactions will however, at some point, reach chemical equilibrium. From that point on, the combustion will proceed with the remaining radicals. That means that the maximum pressure will depend not on the amount of free radicals scavenged throughout the combustion, but on the end displacement of the chemical equilibrium due to the addition of more inhibitor.

In addition, the extra inhibitor mass will also have a diluting effect and it also functions as a heat sink (as discussed in section 2.3). These two factors also contribute to the drop in the final pressure. The experimental findings thus differ from those of [23], where a large pressure drop was found. This can however, be explained by the fact that the explosions in [23] were conducted in a vented module. The impact of which will be clarified in section 6.4.2.

It is also evident that decreasing the particle size of the inhibitor has very little or no impact on the maximum pressure. Again, this can be explained by the effect of the inhibitor. Extra surface area and better dispersion, due to smaller particles, will increase the chances of surface reactions (see sections 2.4.1 and 2.4.1.1), but as with increasing concentrations of inhibitor, the chemical equilibrium will limit its effect greatly.

6.4.2 Effect on Maximum Rate of Pressure Rise

As seen in Figure 34 through Figure 41, the potassium carbonate had a much larger impact on the maximum rate of pressure rise, than it had on the maximum pressure generated in the explosions. Again, this can be explained by the chemical effect of the inhibitor. As previously mentioned, the inhibitor works by scavenging on free radicals. At ignition, the amount of free radicals increases dramatically as the combustion starts. However, with a chemically active inhibitor present, it will attack these radicals until a state of chemical equilibrium between the reactants, is reached. This will dramatically slow down the rate of combustion, as the amount of radicals available to participate in combustion reaction mechanisms is limited, due to the reactions involving the inhibitor.

A requirement for chemical reactions to occur is that there are collisions between the reacting molecules. Reactions between potassium and the free radicals are therefore more likely to occur, if the potassium is more evenly divided in the volume. For this reason, it would be expected that an increase in the concentration, or a decrease in the particle size, would both contribute to a lower rate of pressure rise. As seen in Figure 30 and Figure 31 however, this is not entirely the case.

There are four possible explanations for this deviation. The first is the possible formation of agglomerates when the particle diameter of the inhibitor is small. The second is that larger particles could start to settle before ignition. The third possible explanation is the limitation in the potential reactions between inhibitor and radicals, due to chemical equilibrium. The fourth possibility is that larger particles result in less particle decomposition and thus a lower release of potassium for inhibiting reactions.

The first explanation could explain the lack of difference seen for the maximum rate of pressure rise seen in Figure 30, for the inhibitor concentrations of 25, 50 and 100g/m^3 in the 4.2vol% experiments. However, if this was the explanation, the same tendency should also be seen in Figure 31 with the 5.25vol% experiments.

As this is not the case, 50g/m^3 is more efficient at inhibiting than 25g/m^3, it therefore seems very unlikely that a significant formation of agglomerates occurs in the experiments.

The second possible explanation, that larger particles start to settle before ignition, should give a drop in the efficiency of the inhibitor at larger particle diameters. This drop would probably be more marked at higher concentrations as particle collisions are more frequent, both with each other and with the nozzle. Such a marked drop in efficiency is seen in Figure 31 for the 100g/m^3 inhibitor concentration and in Figure 30 for the 50g/m^3 inhibitor concentration, but to state that this is a tendency in all experiments would be a gross exaggeration. Thus is seems unlikely that the settling of larger particles is a major contributor to the results.

By comparing the curvature in Figure 30 and Figure 31 it is possible to determine if there is a chemical limitation to the inhibitor effect. It can be seen that the curvature for the 50g/m^3 inhibitor concentration is more particle size dependent in the richer of the two mixtures. This is also true for the concentration of 100g/m^3 of inhibitor, though to a lesser degree. This is a strong indication that the 4.2vol% propane explosion is near saturated with inhibitor, when the concentration is higher than 50g/m^3, up to an average particle size between 85 and 115μm. The saturation effect when adding a large amount of inhibitor is consistent with findings in other work [21, 25].

A lower rate of particle decomposition for larger particles, due to the increase in the particle volume requiring to be heated for decomposition to occur, should be possible to see in the results by a slow decrease in inhibitor effect in the non-saturated curvature. This can be seen for 12.5 and 25g/m^3 in the 4.2vol% mixture and for 50 and 100g/m^3 in the 5.25vol% mixture. Considering the arguments for saturation in the previous paragraph, it seems very likely that this is the explanation for the difference in inhibition effect on the rate of pressure rise, when the average particle diameter is varied.

6.4.3 Effect on the Laminar Burning Velocity

The laminar burning velocity is calculated from measured values in the inflection point of the pressure-time graph. These values are; the pressure in the inflection point, the rate of pressure rise, and the time from the onset of dispersion till the inflection point (used to calculate the turbulence levels with the equations found in 3.3.3). Since the inhibitor has little impact on the pressure, and the time-delays from dispersion till the inflection point, are relatively stable (74-130ms, with 71.5%, in the region 75-100ms), the laminar burning velocity will largely depend on the measured rate of pressure rise. This means that the influence from the average particle diameter of the inhibitor, on the laminar burning velocity will, to a large extent, be the same as its impact on the rate of pressure rise. Thus the effect of the average particle size will be much the same as for the maximum rate of pressure rise.

The normalized burning velocities obtained in the current experiments can be compared with the results from [23]. Those experiments were conducted with a Siwek sphere and on a stoichiometric propane-air mixture, but should still largely resemble the results obtained in this thesis. Comparing Figure 13 with Figure 36, Figure 38 and Figure 40, it can be seen that the normalized laminar burning velocities obtained in this thesis are in reasonable agreement with those findings. A more exact comparison is not possible without knowing the particle sizes used for those tests.

The calculated laminar burning velocity from the conducted experiments can also be compared to the experimental laminar burning velocities seen in Figure 5. The graph in this figure shows the results from five independent experimental investigations, involving four different approaches (spherical flame, stagnation flow, flat burner and counterflow), to finding the laminar flame speed. The high degree of correlation seen in those results, indicate that they are near a definitive answer. If nothing else, they give the best comparison currently available.

According to Figure 5, the equivalence ratios used for the conducted experiments should result in laminar burning velocities of approximately 38 and 33cm/s for the 4.2 and 5.25vol% propane-air mixtures, respectively. In the conducted experiments the calculated laminar burning velocities were 30.92 ± 1.73 and 34.11 ± 2.88cm/s respectively.

There are two possible explanations for this deviation. It could be caused by a leak in the air inlet valve. This would cause air to flow into the vessel during the filling of propane. If this were the case however, both equivalence ratios should be displaced an equal amount in Figure 5. As this is not the case, there must be at least one other cause.

The second possible explanation is that the cleaning of the vessel was not thorough enough. That would result in the presence of small amounts of potassium in every experiment conducted. The inhibitive effect of potassium diminishes as a combustible mixture gets richer. Therefore any unwanted presence of potassium would affect the mixture with the lowest volume percentage of propane, more than the other. It therefore seems reasonable to conclude that this explanation, or a combination between this and the previous, are the cause of the deviation from the laminar burning velocities seen in Figure 5.

6.5 Sources of Error

Although great care was taken to avoid error in the experimental work, there are several factors that could influence the results and should be mentioned.

Crushing of Powder

As mentioned in 4.2.1, the crushing of the potassium carbonate was conducted using several different methods. Common for all the methods is the danger of foreign elements being mixed with the sample. Steps were taken to prevent this, by washing the equipment used and throwing the first bulk that was crushed, but residue from earlier crushing could still get mixed with the samples. However, as the experiments focus on the different effect when varying the particle size with inhibitor and the crushing led to particles of all sizes, any pollution should probably affect the results in the same fashion for every experiment. Thus it could affect the efficiency seen, but would likely have extremely little effect in regards to the comparisons. The spectroscopy analysis conducted also failed to find any pollutants.

Sieving

As mentioned in the discussion, sieving of samples containing particles smaller than 75μm, should according to ASTM recommendations be done through wet sieving. Pictures taken with the electron microscope shoved that the samples <32μm and 32-50μm had an overwhelming majority of smaller particles. Stating that these have an average diameter of 16μm and 41μm is therefore an approximation.

Moisture

Due to the handling of the inhibitor in its crushed state over a time period of several months, and the fact that it, as a deliquescent material, absorbs moisture from the air. The probability of it absorbing some water is not unlikely. For that reason, storage precautions were taken (see section 4.2.2). Combined those precautions should limit the extent of any absorption. The moisture tests taken before drying also showed that potassium carbonate could be stored over long periods of time without being compromised by high moisture content. The necessary storing of the crushed inhibitor, should therefore not compromise the ten weight-percent limit advised by [4] to avoid moisture influencing the results.

Weighing

The weight used had a good accuracy for the initial concentrations tested, but as the need was seen for tests on lower concentrations, its accuracy became an issue. This was particularly so for the lean concentration tested. The high efficiency of the inhibitor however, led to the cancellation of further testing on lean equivalence ratios thus removing most of the tests where this posed a problem.

It should be stated however, that the experiments containing a concentration of 12.5g/m^3 has potential error from the accuracy of the weight of approximately 1.6wt%.

Propane Gas

The propane gas used was of industrial standard. That means that there is probably a higher presence of heavier hydrocarbons than in specially refined propane gas. This could influence the stoichiometry. This is however, a larger problem as the propane cylinder starts to empty. As the propane cylinder used, still contained large quantities of pressurized gas, it is unlikely that this had any large influence on the results.

Temperature and Moisture in the Air

As previously mentioned, the experiments were conducted over a period of several months. This naturally caused variations in the moisture content of the air and in the temperature. Fortunately the city of Bergen has a relatively stable climate, so most of the experiments were conducted with high moisture content and indoor temperatures around eighteen degrees Celsius.

Temperature of Apparatus

The modified USBM-vessel used for the experiments did not have a cooling system fitted. Each experiment therefore led to an increase in the apparatus temperature. To counter this heating the apparatus was washed, after each experiment, with a wet cloth and then dried with compressed air.

The Dispersion of Sample

Although moving the sample from the reservoir onto the rebound nozzle had no impact on the turbulence level inside the vessel, it is possible that it had an impact on the dispersion of the inhibitor. This could lead to a more uneven spread of inhibitor inside the vessel, than if it had been injected through the nozzle. The relative low deviations achieved in the results indicate that the dispersion is acceptable, but future testing with laser Doppler anemometry should be done to confirm or refute this.

Measured gas accuracy

Although the USBM vessel had received an extensive maintenance, involving the replacement of all valves and flanges, as recent as eighteen months prior to the experiments, a leakage of 0.1mbar per second was witnessed. As the evacuation of the vessel and the injection of propane, were monitored through the use of pressure indicators and controlled with manual valves, this led to some urgency when preparing the mixture. Deviations of $\pm$0.1vol% were therefore considered acceptable with the attitude that such deviations would likely cancel each other out through repetitions.

7. Conclusion

As with the results, the conclusion will be presented in two sections, the first concerning the effect of the apparatus on the inhibitor, the second the effect of the particle size of the inhibitor on the explosive mixture.

Apparatus Effect on Inhibitor

The 20 liter USBM vessel is initially ill-suited for tests where the impact of the particle size of inhibitors is to be evaluated. This is due to the grinding effect from impacts, both as the flow passes through the outlet valve of the reservoir, and as the flow passes through the rebound nozzle.

Previous literature has reported that the rebound nozzle has little grinding effect on particles, compared to the outlet valve. Experiments conducted show that this is true, but also that the grinding effect due to the rebound nozzle is still substantial.

It was discovered that the concentration of the inhibitor had a large impact on the particle size reduction. This correlation has not been found reported in previous literature. The only reference found, concerning variations in dust sample concentration, stated that the particle size reduction was constant, regardless of concentration changes.

It was also found, from experiments on the maximum pressure obtained in maize starch explosions, that the problems regarding particle size reduction could be bypassed by placing the inhibitor inside the vessel. This could however, have slight effects on the measured results, due to the uncertainty concerning the degree of dispersion.

Inhibitor Particle Size

The particle size of the inhibitor had very little effect, if any at all, on the maximum pressures obtained in turbulent constant volume combustion. As the inhibitor itself, has little effect on pressures obtained in turbulent constant volume combustion, this is to be expected.

It did however, have a significant impact on the maximum rate of pressure rise obtained during the course of the explosions, reducing it by as much as seventy-five percent. Considering the reaction mechanisms of inhibitors, the scavenging on free radicals by potassium molecules released due to particle decomposition, this makes perfect sense. It is also consistent with the recent work on inhibitors.

Its impact on the laminar burning velocity was similar as that of the maximum rate of pressure rise. This is also to be expected, as the pressures obtained in inhibited closed vessel explosions are relatively stable, despite the presence of a chemical inhibitor. This leaves the maximum rate of pressure rise as the most important parameter for calculations of the laminar burning velocity.

8. Recommendations for Further Work

The work conducted for this thesis showed that the particle size, of potassium carbonate, had a significant impact on its effectiveness as a chemically active inhibitor. The work was conducted with a modified 20 liter USBM vessel. Due to the grinding effect from the dispersion, the experiments were conducted with the inhibitor placed inside the vessel. This could have an impact on the measured parameters.

The following investigations, concerning the use of the USBM vessel on dispersion of inhibitor dusts, are therefore recommended:

1. A study on the degree of dispersion of larger particles in the USBM vessel using LDA or similar methods. Particularly when dispersed from inside the vessel, which is currently the only way to disperse large particles without a significant size reduction.

2. Development of a new nozzle, that does not cause particle grinding and can be used to bypass the reservoir outlet. This should be combined with a study on the turbulence generated inside the vessel using the new nozzle design.

It should also be pointed out that this is the first study on particle size of inhibitors, in turbulent combustion, that show a significant effect when varying the particle size.

The following investigations, on the effect of inhibitor particle size, are therefore recommenced:

1. Experiments at higher inhibitor concentrations to investigate if the particle size has any consequence for the quenching concentration.

2. Experiments with different combustible mixtures to investigate if the particle size has the same impact in all combustion. It could be particularly interesting to investigate its effect in dust explosions.

3. Experiments with other chemically active inhibitors to investigate if the results are similar for all inhibitors of this type.

References

1. Aven, T., *Pålitelighets- og risikoanalyse*. 1994, Oslo: Universitetsforlaget. VII, 282 s.
2. Eckhoff, R.K. and ScienceDirect (Online service), *Dust explosions in the process industries*. 3rd ed ed. 2003, Amsterdam Boston: Gulf Professional Pub. xxi, 719 s.
3. Eckhoff, R.K., *Explosion hazards in the process industries*. 2005, Houston, TX: Gulf Pub. xi, 439 s.
4. Cesana, C. and R. Siwek, *Operating Instructions 20-l-Apparatus 6.0 Adolf Kühner.* 2001.
5. Eckhoff, R.K., *Use of (dP/dt)max from closed-bomb tests for predicting violence of accidental dust explosions in industrial plants.* Fire Safety Journal, 1985. **8**(2): p. 159-168.
6. Anderson, J.D., *Computational fluid dynamics : the basics with applications*. McGraw-Hill series in mechanical engineering. 1995, New York: McGraw-Hill. XXIV, 547 s.
7. Reed, M.D., et al., *Laboratory Evaluation of Bicarbonate Powders as Fire Suppressants.* Proceedings of the International Conference of Ozone Protection Technologies, Baltimore, MD, 1997.
8. Sheinson, R.S. and J.W. Fleming, *Suppression Effectiveness of Aerosols.* 2003.
9. Chelliah, H.K., et al., *Effect of sodium bicarbonate particle size on the extinction condition of non-premixed counterflow flames.* Combustion and Flame, 2003. **134**(3): p. 261-272.
10. Dodding, R.A., R.F. Simmons, and A. Stephens, *The extinction of methane-air diffusion flames by sodium bicarbonate powders.* Combustion and Flame, 1970. **15**(3): p. 313-315.
11. Skjold, T., *Selected Aspects of Turbulence and Combustion in 20-Litre Explosion Vessels.* Master thesis, 2003.
12. Chang, R., *General chemistry : the essential concepts*. 5th ed. 2008, Boston ,: McGraw-Hill. XXVI, 757, [47] s.
13. Warnatz, J., et al., *Combustion Physical and Chemical Fundamentals, Modeling and Simulation, Experiments, Pollutant Formation*. 4th Edition ed. 2006, Berlin, Heidelberg: Springer Berlin Heidelberg.
14. Ranzi, E., et al., *Hierarchical and comparative kinetic modeling of laminar flame speeds of hydrocarbon and oxygenated fuels.* Progress in Energy and Combustion Science, 2012. **38**(4): p. 468-501.
15. Moen, I.O., et al., *Pressure development due to turbulent flame propagation in large-scale methane ‧ air explosions.* Combustion and Flame, 1982. **47**(0): p. 31-52.
16. Vanoverberghe, K., *Flow, turbulence and combustion of premixed swirling jet flames*. 2004.
17. Arntzen, B.J., *Modelling of Turbulence and Combustion for Simulation of Gas Explosions in Complex Geometries.* 1998.

18. Veynante, D. and L. Vervisch, *Turbulent combustion modeling.* Progress in Energy and Combustion Science, 2002. **28**(3): p. 193-266.
19. Moore, P.E., P.L. Cooke, and N. Gibson, *Report on a Research project on the Suppression of Metal Dust Explosions.* Journal of Loss Prevention in the Process Industries, 1989. **2**(4): p. 242-243.
20. Agafonov, V.V., et al., *The Mechanism of Fire Suppression by Condensed Aerosols.* 2005.
21. Babushok, V. and W. Tsang, *Inhibitor rankings for alkane combustion.* Combustion and Flame, 2000. **123**(4): p. 488-506.
22. Fleming, J.W., et al., *Extinction Studies of Propane/Air Counterflow Diffusion Flames: The Effectiveness of Aerosols.* 1998.
23. Wingerden, K.v. and P. Hoorelbeke, *On the potential of mitigating vapour cloud explosions using flame inhibitors.* 2011.
24. Turányi, T., *Applications of sensitivity analysis to combustion chemistry.* Reliability Engineering & System Safety, 1997. **57**(1): p. 41-48.
25. Williams, B.A. and J.W. Fleming, *Suppression Mechanisms of Alkali Metal Compounds.* 1999.
26. Kalejaiye, O., et al., *Effectiveness of dust dispersion in the 20-L Siwek chamber.* Journal of Loss Prevention in the Process Industries, 2010. **23**(1): p. 46-59.
27. Dahoe, A.E., et al., *On the sensitivity of the maximum explosion pressure of a dust deflagration to turbulence.* KONA - Powder and Particle, 2001. **19**: p. 178-196.
28. Bray, K.N.C., *Studies of the Turbulent Burning Velocity.* Proceedings of the Royal Society of London. Series A: Mathematical and Physical Sciences, 1990. **431**(1882): p. 315-335.
29. Abdel-Gayed, R.G., D. Bradley, and M. Lawes, *Turbulent Burning Velocities: A General Correlation in Terms of Straining Rates.* 1987.
30. Popat, N.R., et al., *Investigations to improve and assess the accuracy of computational fluid dynamic based explosion models.* Journal of Hazardous Materials, 1996. **45**(1): p. 1-25.
31. Dahoe, A.E., et al., *Dust explosions in spherical vessels: The role of flame thickness in the validity of the 'cube-root law'.* Journal of Loss Prevention in the Process Industries, 1996. **9**(1): p. 33-44.
32. 06, A.C.-. *Standard Test Method for Sieve Analysis of Fine and Coarse Aggregates.* 2006.
33. Siwek, R., *Reliable Determination of the Safety Characteristics in 20-L Apparatus.* Proceedings of the Flammable Dust Explosion Conference, St. Louis, Missouri, 1980: p. 529-573.
34. E1226-00, A., *Standard Test Method for Pressure and Rate of Pressure Rise for Combustible Dusts.* Annual Book of ASTM Standards, 2005.
35. Bradley, D., *How fast can we burn?* Symposium (International) on Combustion, 1992. **24**(1): p. 247-262.

Appendix

Appendix A: Historic Development of Standard Apparatus for testing of Explosion Parameters

A-1: The 1.2 Liter Hartmann Bomb

According to [5], the first effort in this direction was probably conducted by Dr. Hartmann and his colleagues at the U.S. Bureau of Mines in 1943. There they developed a 1.2 liter cylindrical apparatus for testing of explosion characteristics of combustible powders. The rate of pressure rise, when igniting a combustible powder, was subsequently adopted as a measure of the powders explosion violence. The Hartmann bomb remained the standard method for assessing the explosion violence for decades. However developments discussed in 1.4, led to the design of new standard apparatus.

A-2: The $1m^3$ Standard ISO Vessel

In 1971 Bartknecht introduced a new and much larger vessel for experimental research. It was spherical and had an inner volume of $1m^3$. The idea was that this would produce results more in line with what could be expected in an industrial situation [5]. This would result in more realistic data, which in turn would result in more realistic design of any mitigating measures.

Another new concept to be introduced was the dispersion system. The vessel contained a semicircular perforated dust dispersion pipe connected to a pressurized container. This type of dispersion resulted in higher turbulence and a more even distribution of any solids involved in the experiments. Unfortunately the $1m^3$ had some severe drawbacks as well. Its size caused a severe increase in the costs of experiments and also in the time needed to perform them.

A-3: The 20 Liter Vessels

The amount of time and funding required for experimental research with the $1m^3$ vessel, led to a search for viable alternatives. In 1980 Siwek conducted a series of experiments to determine the relationship between the volume of spherical apparatus and acquired K_{ST} values in experimental explosions. His findings are presented in Figure 42 [33].

As can be seen in the figure, the experimental apparatus would have to have a volume of 16 liters or more for the experimental results to match the results from experiments with the $1m^3$ vessel. Siwek eventually presented a 20 liter apparatus with the same dispersion system as the $1m^3$ vessel, but scaled down to match the new volume. The ignition delay time was reduced to 60ms, to match the turbulence measured in the $1m^3$-vessel, and a design for continual water cooling of the vessel was introduced. The last measure enables a higher frequency of testing. A new nozzle type, called the rebound nozzle, was introduced in 1988. According to Siwek this nozzle produces pressure and K_{ST} results in reasonable agreement with those of the perforated-ring system [2].

Another 20 liter apparatus in common use is the U.S. Bureau of Mines vessel. This is similar to the Siwek sphere, except it has a larger top opening which gives better access to the inside of the vessel. It also has a slightly more cylindrical shape, as can be seen in Figure 45, Appendix C: Schematics.

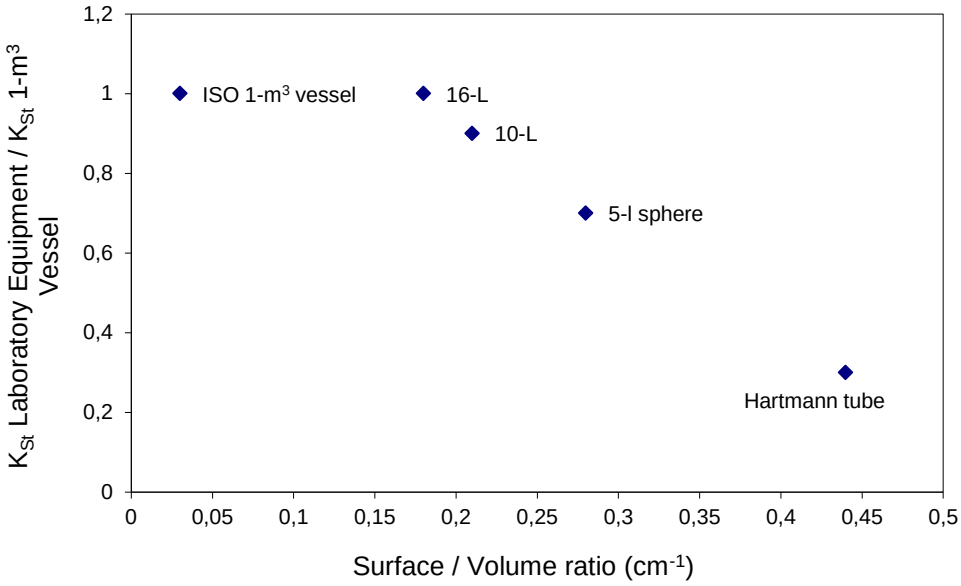

Figure 42: The relationship between surface/volume ratio and KST (Siwek, 1980)

Appendix B: The Scanning Electron Microscope

The electron microscope pictures were taken with the Supra 55VP scanning electron microscope at the *Elektronmikroskopisk Felleslaboratorium* at the University of Bergen. A picture of the microscope can be seen in Figure 43.

Samples were gathered from the 20 liter vessel using specimen stubs with double-sided carbon adhesive tape. These were cleared of excess sample by applying pressurized air across the surface. In order to make the samples electrically conductive, they were coated with a gold/palladium alloy before scanning.

An element analysis was conducted using energy-dispersive X-ray spectroscopy. The results from this analysis confirmed the elemental composition of the sample. An example of a specter produced by the spectroscopy analysis is seen in Figure 44.

Figure 43: Picture of the ZEISS Supra 55VP scanning electron microscope at the University of Bergen. (From www.uib.no, picture by Irene Heggstad)

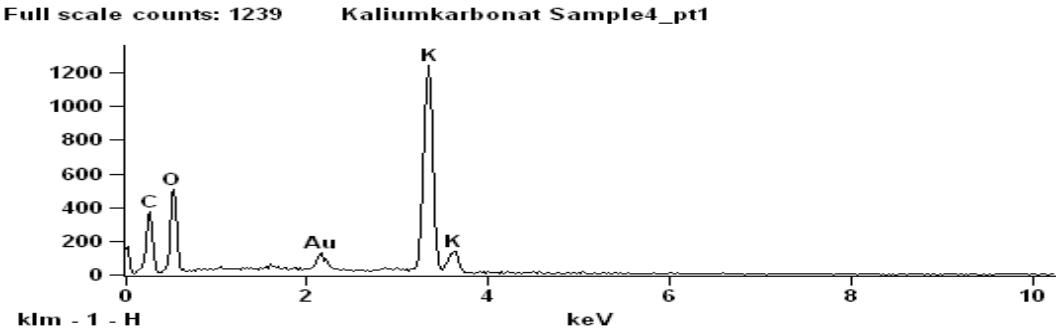

Figure 44: Specter of the inhibitor sample produced using energy-dispersive X-ray spectroscopy.

Appendix C: Schematics

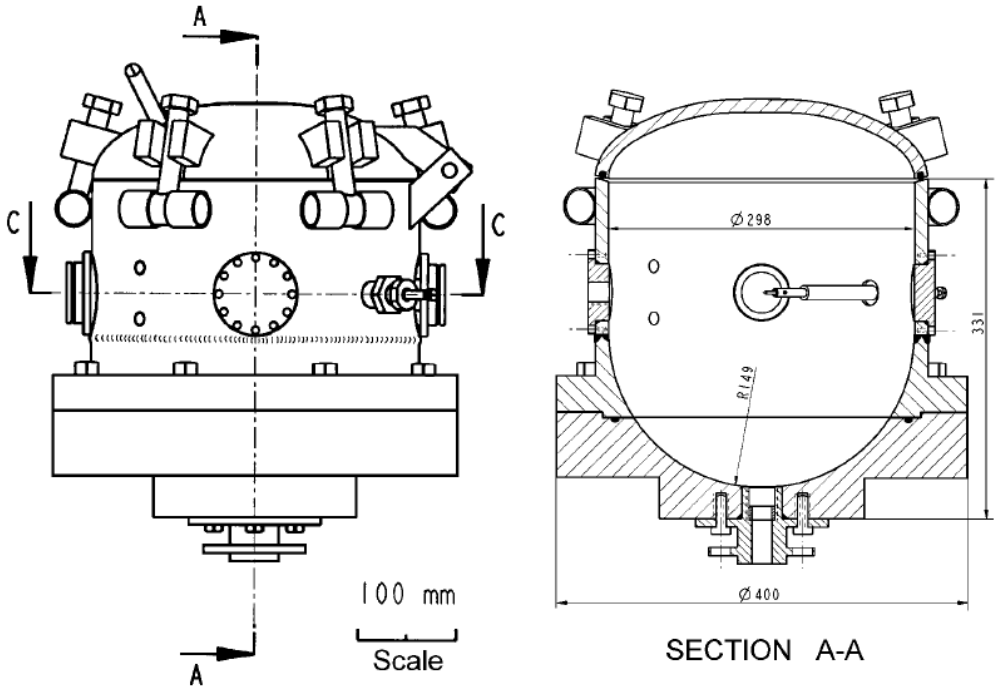

Figure 45: The modified USBM vessel at the University of Bergen (from Skjold, [11])

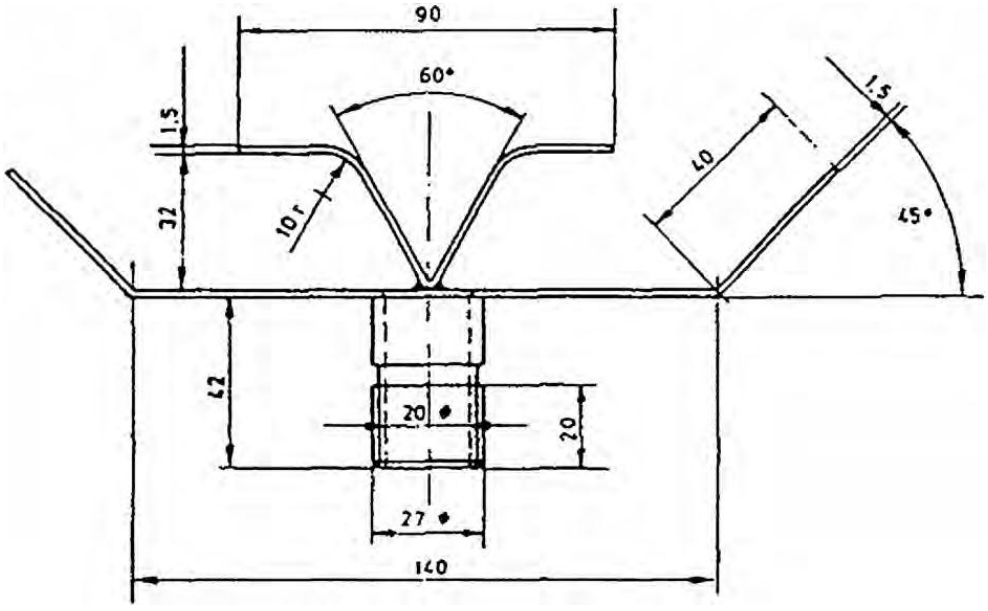

Figure 46: The rebound nozzle (from ASTM standard E1226, [34])

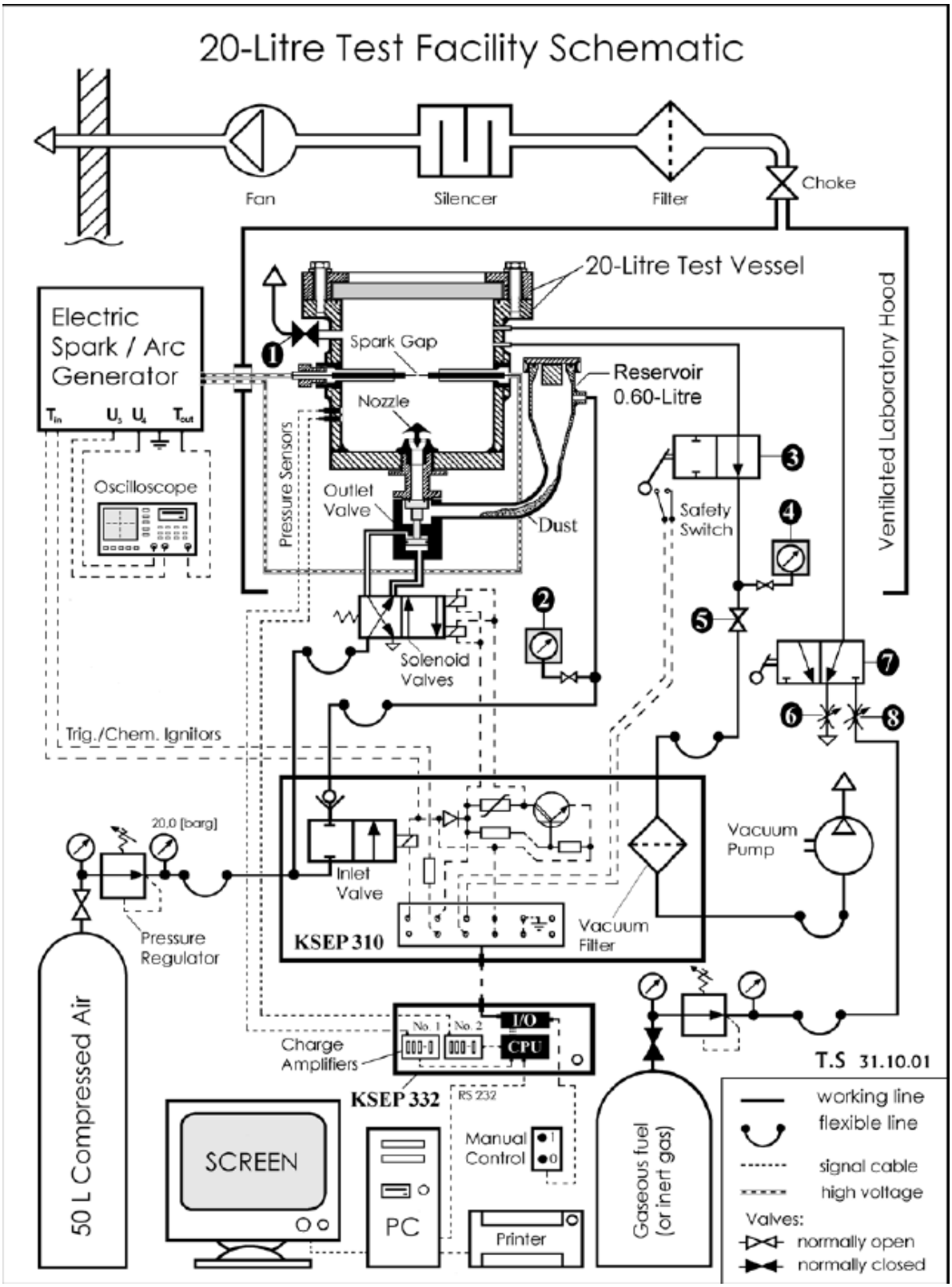

Figure 47: Schematic of apparatus in the 20 liter dust explosion laboratory at UoB. (From Skjold, [11])

1. Exhaust valve
2. Pressure indicator, reservoir (Druck, type DPI 705, pressure range 0 to 20bar(g))
3. Safety switch protecting the pressure indicator (4) from explosion pressure
4. Pressure indicator, vessel (Druck, type DPI 705, pressure range -1 to 1 bar(g))
5. Valve preventing escape of gas from vessel through vacuum pump
6. Air inlet for adjusting vessel pressure
7. 3-way valve
8. Gas inlet for addition of gaseous fuel or inert gas to vessel

Note that the Electric Spark/Arc Generator is no longer in use and has been disconnected. Ignition is currently being initiated with chemical igniters. These are controlled by a signal cable from the KSEP 310 Control Unit.

Appendix D: Calculations

D-1: Stoichiometry for Propane

Balanced reaction, simplified air composition:

$C_3H_8 + 5(O_2 + 3{,}76N_2) \rightarrow 3CO_2 + 4H_2O + 5(3{,}76N_2)$

Stoichiometric Ratio = $(mol_{fuel}) / (mol_{total})$, for a balanced reaction
Stoichiometric Ratio = 1/24.8 = 0.0403 or 4.03vol%

Equivalence ratio of experiments:

$$EQ = \frac{\left(\frac{mole_{fuel}}{mole_{tot}}\right)_{mix}}{\left(\frac{mole_{fuel}}{mole_{tot}}\right)_{stoich}} \quad \text{(A.1)}$$

which gives experimental equivalence ratios of 1.04 and 1.3 for the two propane-air mixtures tested.

D-2: The Cube-Root Law

As mentioned in the introduction, this derivation is based on the explanatory example found in [5].

Several assumptions are needed for the cube-root law to be valid. They are:

1. The vessels are geometrically similar, but of different size. Due to influence from the vessel wall they should be spheres, as this will give the least disturbance of the flame front due to the vessel wall. The vessels should not be too small either, as this could lead to quenching before full development of the flame.
2. The ignition source is located in the center of the vessels and produces an infinitely thin spherical laminar flame front, which subsequently propagates toward the wall of the vessels.
3. Any changes of pressure, temperature or turbulence in the spherical vessels will have the same effect on the burning velocity in both vessels.

As the burning velocity depends on the pressure and temperature of the unburned mixture, the laminar burning velocity will change as the flames propagate toward the vessel walls. At any given time in the combustion where the relationship

$$\frac{r_{f,1}}{r_{v,1}} = \frac{r_{f,2}}{r_{v,2}} \tag{A.2}$$

is satisfied, where $r_{v,1}$ and $r_{v,2}$ are the vessel radius' and $r_{f,1}$ and $r_{f,2}$ are the flame radius', the burning velocity in the vessels will be the same.

This is due to the fact that at this point the relationship between burned and unburned gas in the two vessels will be the same. It follows that for the pressure to increase at the same rate in the larger vessel as in the smaller vessel, the flame propagation must travel a longer distance from the center of the vessel. This difference in distance is the same as the relationship between the two radii. Since this argument can be extended the entire length of the vessel radius, it follows that the pressure growth as a function of time is highest as the flame front reaches the vessel wall. Since

$$\frac{r_{v,2}}{r_{v,1}} = \left(\frac{V_2}{V_1}\right)^{\frac{1}{3}} \tag{A.3}$$

it then follows, with the earlier mentioned assumptions, that

$$\left(\frac{dP}{dt}\right)_{max,1} \times {V_1}^{\frac{1}{3}} = \left(\frac{dP}{dt}\right)_{max,2} \times {V_2}^{\frac{1}{3}} = constant \equiv K_{ST} \tag{A.4}$$

D-3: Deriving the Expression for Turbulent Burning Velocity

The derivation is largely based on similar derivations in [17, 35].

Abdel-Gayed et al. define a Karlovitz stretch factor, K, as the ratio of the of flow strain rate to flame gradient. This is expressed as the ratio between the time scale of a laminar flame and the Taylor time scale.

$$K = \frac{\tau_c}{\tau_T} = \frac{\delta_L / S_L}{l_T / u_{rms}} = \frac{\delta_L u_{rms}}{l_T S_L} \tag{A.5}$$

Replacing the flame thickness with (2.9) gives

$$K = \frac{\alpha u_{rms}}{l_T (S_L)^2} \tag{A.6}$$

The Taylor turbulent length scale is related to the dissipation by (from [11])

$$l_T{}^2 = 15\nu \frac{u_{rms}^2}{\varepsilon} \tag{A.7}$$

This can be rewritten as

$$l_T = 15^{\frac{1}{2}} \times u_{rms} \times \varepsilon^{-\frac{1}{2}} \times \nu^{\frac{1}{2}} \tag{A.8}$$

Substituting (A.8) into (A.6) gives

$$K = \frac{\alpha\sqrt{\varepsilon}}{S_L{}^2\sqrt{15} \times \sqrt{\nu}} \tag{A.9}$$

Multiplying with the square-root of the kinematic viscosity in both numerator and denominator and simplifying by assuming that the Prandtl number, Pr=ν /α, is equal to one (for hydrocarbon-air mixtures the Prandtl number is 0.7) gives

$$K = \frac{\sqrt{\varepsilon\nu}}{S_L{}^2\sqrt{15}} \tag{A.10}$$

The integral length scale in homogeneous turbulence is approximately (from [35])

$$l_I = 0.2\frac{k^{\left(\frac{3}{2}\right)}}{\varepsilon} \tag{A.11}$$

This can be rewritten as

$$\varepsilon = 0.2\frac{k^{\left(\frac{3}{2}\right)}}{l_I} \tag{A.12}$$

Furthermore, turbulent kinetic energy is related to the rms velocity fluctuations by (from [11])

$$k = \frac{3}{2}u_{rms}^2 \tag{A.13}$$

Substituting (A.20) into (A.19) gives

$$\varepsilon = 0.2\frac{u_{rms}^3}{l_I}\left(\frac{3}{2}\right)^{\frac{3}{2}} \tag{A.14}$$

Substituting (A.21) into (A.10) gives

$$\frac{1}{S_L^2\sqrt{15}}\sqrt{\frac{0.2\left(\frac{3}{2}\right)^{\frac{3}{2}}\nu u_{rms}^3}{l_I}} \tag{A.15}$$

Multiplying with the rms velocity fluctuations in both the denominator and the numerator then rearranging the equation, yields the Karlovitz stretch factor expressed by the rms velocity fluctuations, the laminar burning velocity and the turbulent Reynolds number

$$K = 0.157\left(\frac{u_{rms}}{S_L}\right)^2 \frac{1}{\sqrt{R_T}} \tag{A.16}$$

Substituting into (3.5) (from [28]) and rearranging yields an expression for the turbulent burning velocity from the laminar burning velocity, the rms velocity fluctuations, the integral length scale and the kinematic viscosity as formulated by [17]

$$S_T = 1.8{S_L}^{0.784}{u_{rms}}^{0.412}{l_I}^{0.196}\nu^{-0.196} \tag{A.17}$$

D-4: Deriving the Expression for the Rate of Pressure Rise in an Explosion

Similar derivations can be found in [11, 31].

Assume that the fractional pressure rise is proportional to the mass fraction burned in a vessel, which can be expressed as

$$\frac{P - P_i}{P_f - P_i} = \frac{m_b}{m_{tot}} = \frac{m_b}{m_{u,i}} \tag{A.18}$$

Differentiation with respect to time and conservation of mass gives

$$\frac{dP}{dt} = -\frac{P_f - P_i}{m_{u,i}}\frac{dm_u}{dt} \tag{A.19}$$

The velocity at which the unburned mixture enters the combustion wave is minus the burning velocity, thus the mass consumption rate of the unburned mixture can be expressed as

$$\frac{dm_u}{dt} = -A_{sphere\ surface}\rho_u S_T = -4\pi r_{flame}^2 \rho_u S_T \tag{A.20}$$

By substituting (A.20) into (A.19) a relationship between the rate of pressure rise and the burning velocity is established as

$$\frac{dP}{dt} = 4\pi \frac{P_f - P_i}{m_{u,i}} r_{flame}^2 \rho_u S_T \tag{A.21}$$

For adiabatic compression of the unburned mixture, $P\rho^{-1} = \text{constant}$, which can be formulated as

$$\frac{\rho_{u,i}}{\rho_u} = \left(\frac{P_i}{P}\right)^{\frac{1}{\gamma}} \tag{A.22}$$

Furthermore the relationship between the volumes of burned, unburned and the vessel ($V_{vessel} = V_{unburned} + V_{burned}$) can be expressed as

$$\frac{4}{3}\pi r_{flame}^3 = V_{vessel} - \frac{m_u R T_u}{P} \tag{A.23}$$

where R denotes the specific gas constant in J kg^{-1} K^{-1}. Since $\rho^{-1} = RT/P$, we can rewrite (A.23) as

$$\frac{4}{3}\pi r_{flame}^3 = V_{vessel} - \frac{m_u}{\rho_u} \tag{A.24}$$

Substituting (A.22) into (A.24) gives

$$V_{vessel} = \frac{4}{3}\pi r_{flame}^3 + m_u \rho_{u,i}^{-1} \left(\frac{P}{P_i}\right)^{-\frac{1}{\gamma}} = \frac{4}{3}\pi r_{flame}^3 + m_u \frac{V_{vessel}}{m_{u,i}} \left(\frac{P}{P_i}\right)^{-\frac{1}{\gamma}} \tag{A.25}$$

An equation for $m_u/m_{u,i}$ can be derived from (A.18) as shown in (A.26) through (A.28)

$$\frac{P - P_i}{P_f - P_i} = \frac{m_b}{m_{u,i}} = \frac{(m_b + m_u) - m_u}{m_{u,i}} = 1 - \frac{m_u}{m_{u,i}} \tag{A.26}$$

$$\frac{m_b}{m_{u,i}} = \frac{P - P_i}{P_f - P_i} = \frac{(P_f - P_i) - (P_f - P)}{P_f - P_i} = 1 - \frac{P_f - P}{P_f - P_i} \tag{A.27}$$

$$\frac{m_u}{m_{u,i}} = \frac{P_f - P}{P_f - P_i} \tag{A.28}$$

Substituting (A.28) into (A.25) and rearranging as an expression of the radius of the flame, gives

$$r_b = \left[\frac{3V_{vessel}}{4\pi}\left(1 - \frac{P_f - P}{P_f - P_i}\left(\frac{P}{P_i}\right)^{-\frac{1}{\gamma}}\right)\right]^{\frac{1}{3}} \tag{A.29}$$

Substituting (A.22) and (A.29) into (A.21) gives

$$\frac{dP}{dt} = 4\pi(P_f - P_i)\frac{\rho_{u,i}}{m_{u,i}}\left(\frac{P}{P_i}\right)^{\frac{1}{\gamma}}\left[\frac{3V_{vessel}}{4\pi}\left(1 - \frac{P_f - P}{P_f - P_i}\left(\frac{P}{P_i}\right)^{-\frac{1}{\gamma}}\right)\right]^{\frac{2}{3}} S_T \tag{A.30}$$

(A.30) can easily be rearranged as an equation for the turbulent burning velocity giving

$$S_T = \frac{1}{3(P_f - P_i)}\left(\frac{dP}{dt}\right)\left(\frac{3V_{vessel}}{4\pi}\right)^{\frac{1}{3}}\left(\frac{P}{P_i}\right)^{-\frac{1}{\gamma}}\left[1 - \frac{P_f - P}{P_f - P_i}\left(\frac{P}{P_i}\right)^{-\frac{1}{\gamma}}\right]^{-\frac{2}{3}} \tag{A.31}$$

Appendix E: Graphs Depicting the Impact of Particle Size on Individual Explosion Parameters

Concentration of 12.5g/m^3

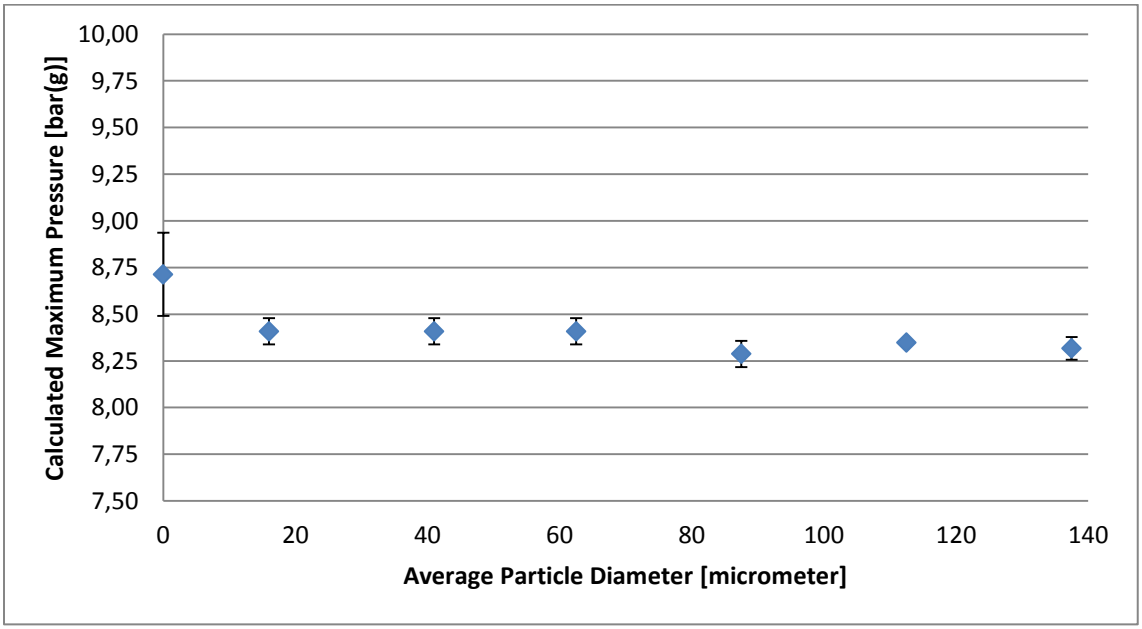

Figure 48: Relationship between average particle diameter and explosion pressure for experiments done with a propane-air mixture with 4.2vol% propane.

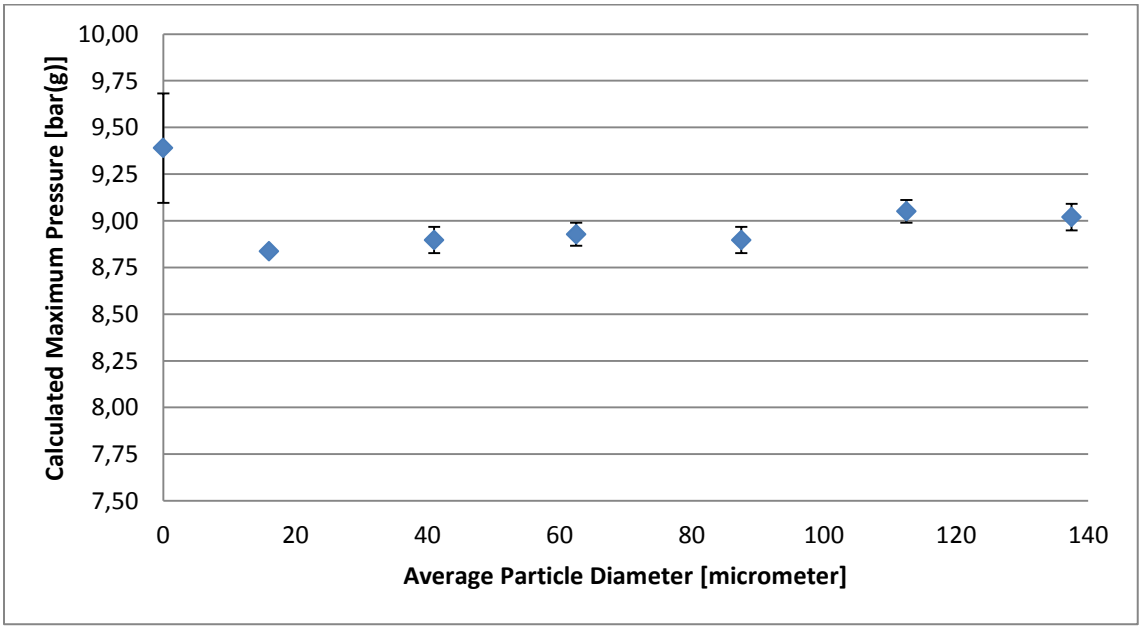

Figure 49: Relationship between average particle diameter and explosion pressure for experiments done with a propane-air mixture with 5.25vol% propane.

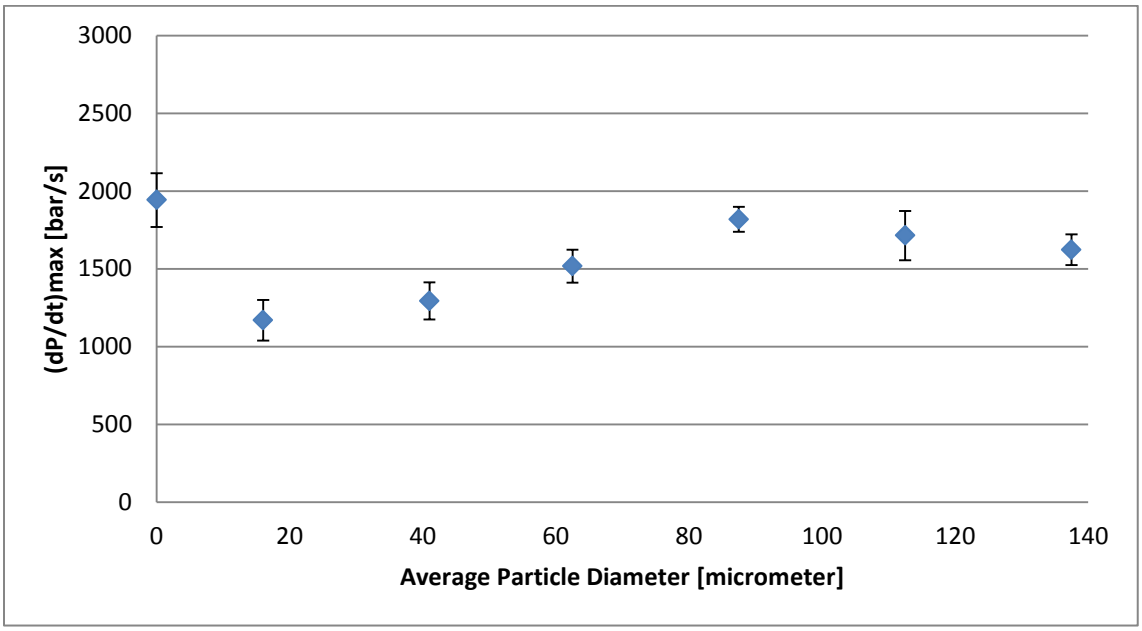

Figure 50: Relationship between average particle diameter and maximum rate of pressure rise for experiments done with a propane-air mixture with 4.2vol% propane.

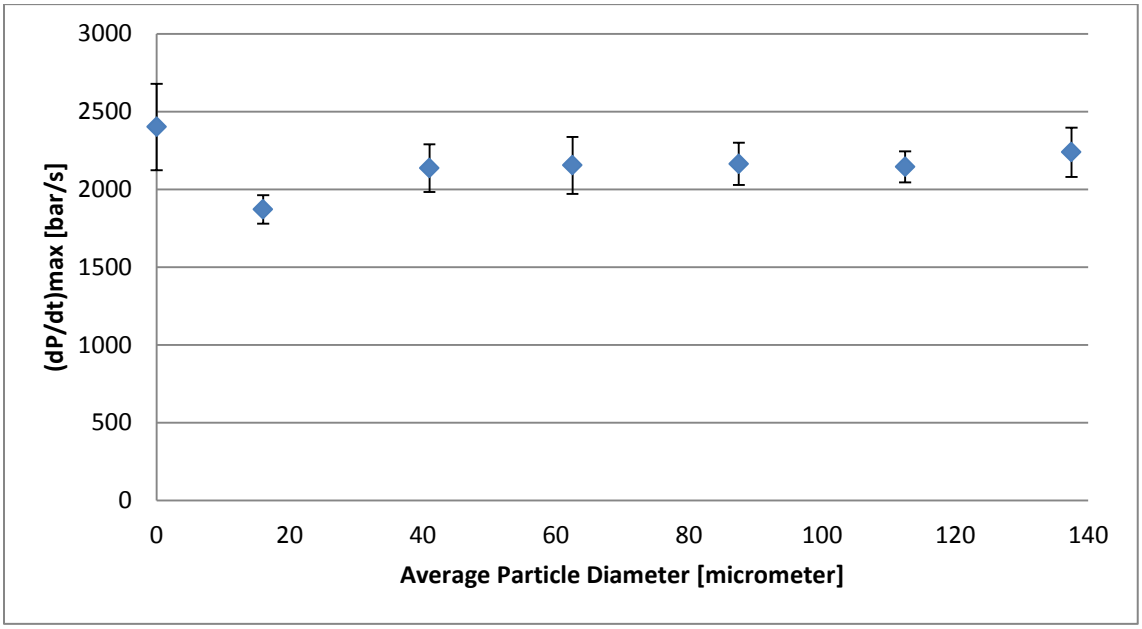

Figure 51: Relationship between average particle diameter and maximum rate of pressure rise for experiments done with a propane-air mixture with 5.25vol% propane.

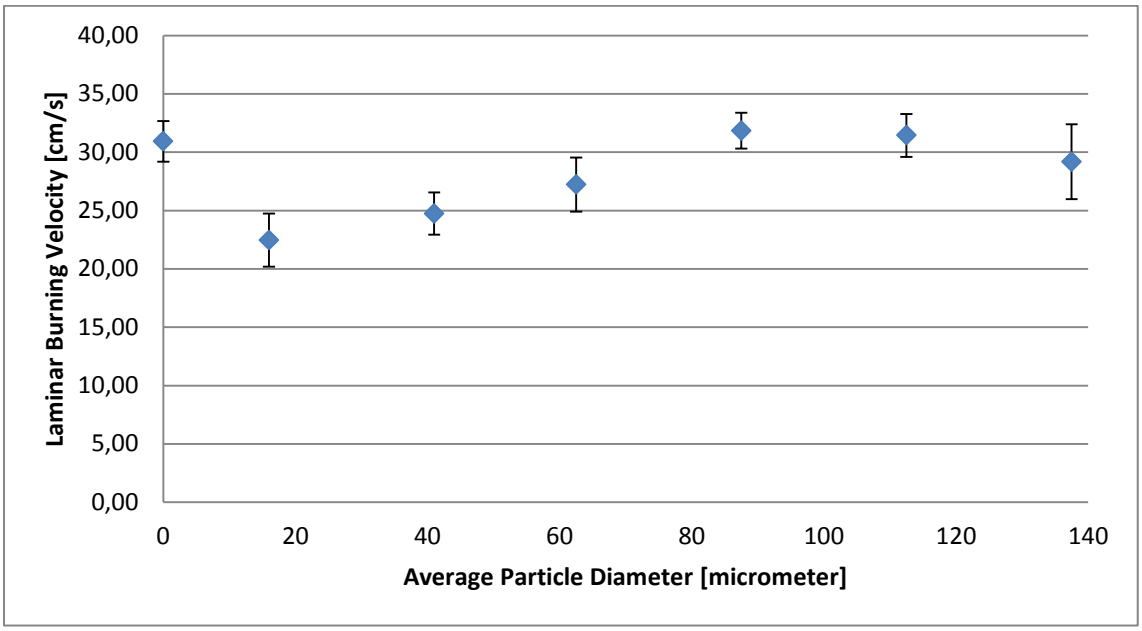

Figure 52: Relationship between average particle diameter and the laminar burning velocity for experiments done with a propane-air mixture with 4.2vol% propane.

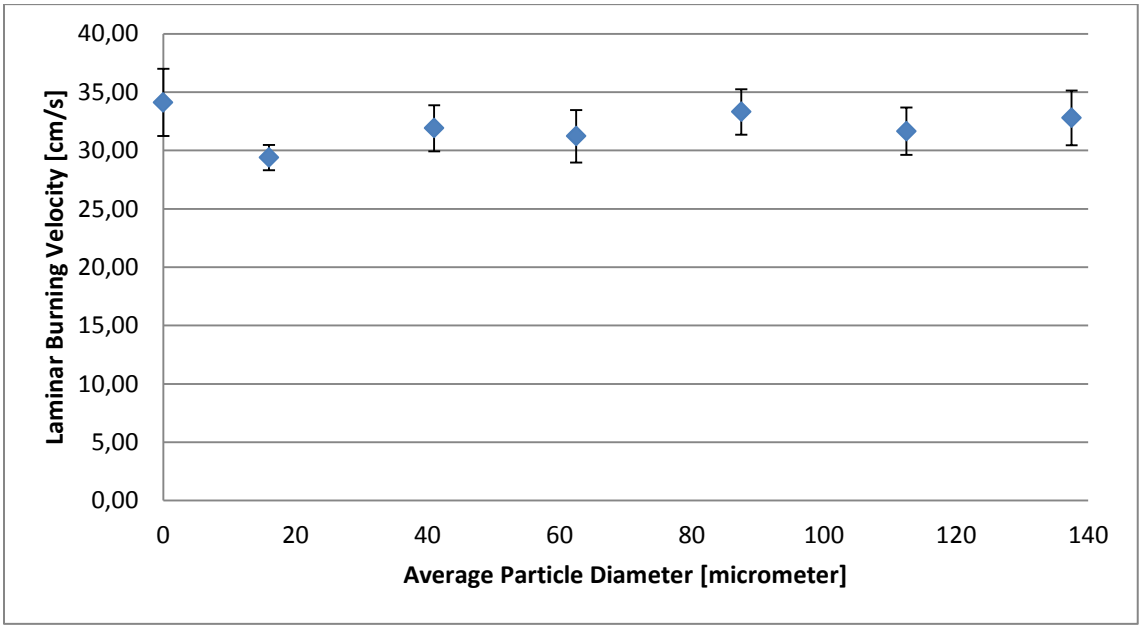

Figure 53: Relationship between average particle diameter and the laminar burning velocity for experiments done with a propane-air mixture with 5.25vol% propane.

Concentration of 25g/m^3

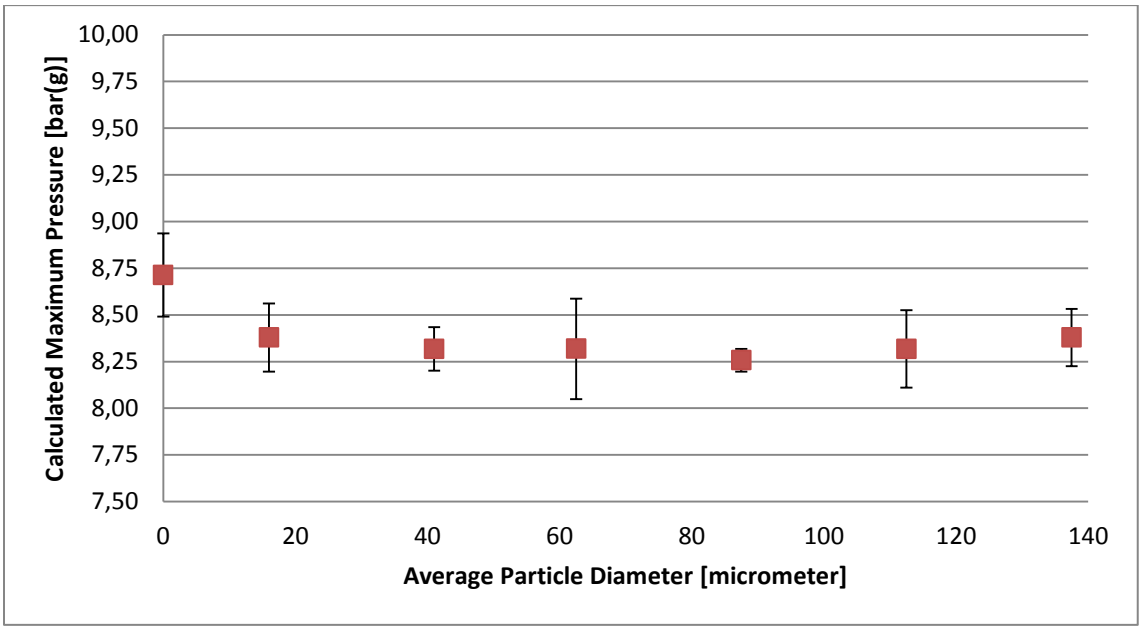

Figure 54: Relationship between average particle diameter and the calculated explosion pressure for experiments done with a propane-air mixture with 4.2vol% propane.

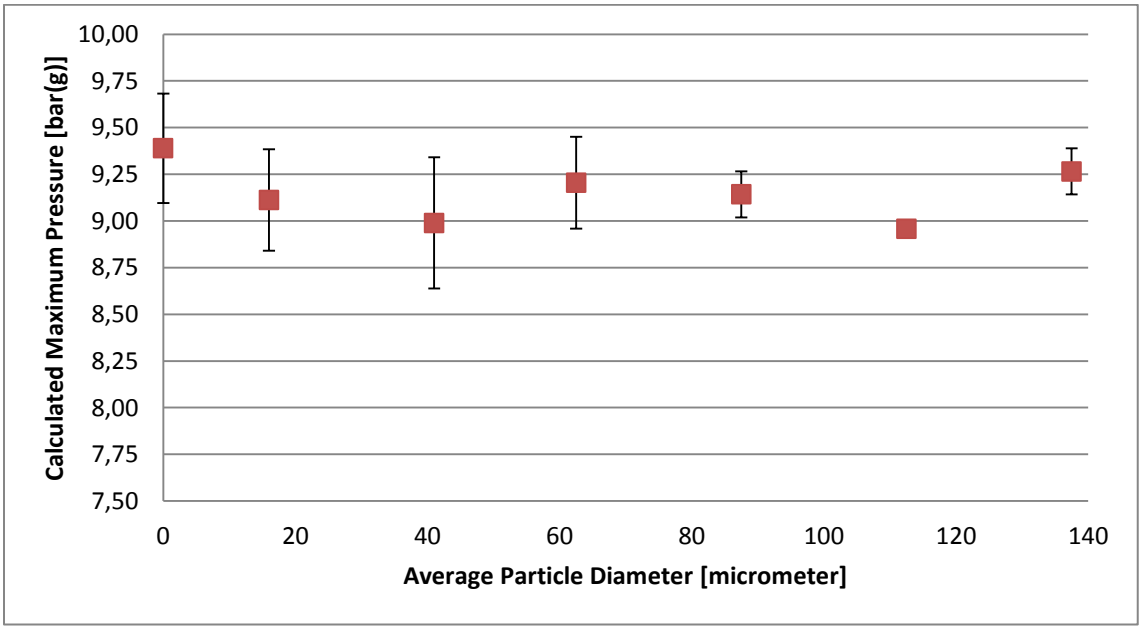

Figure 55: Relationship between average particle diameter and the calculated explosion pressure for experiments done with a propane-air mixture with 5.25vol% propane.

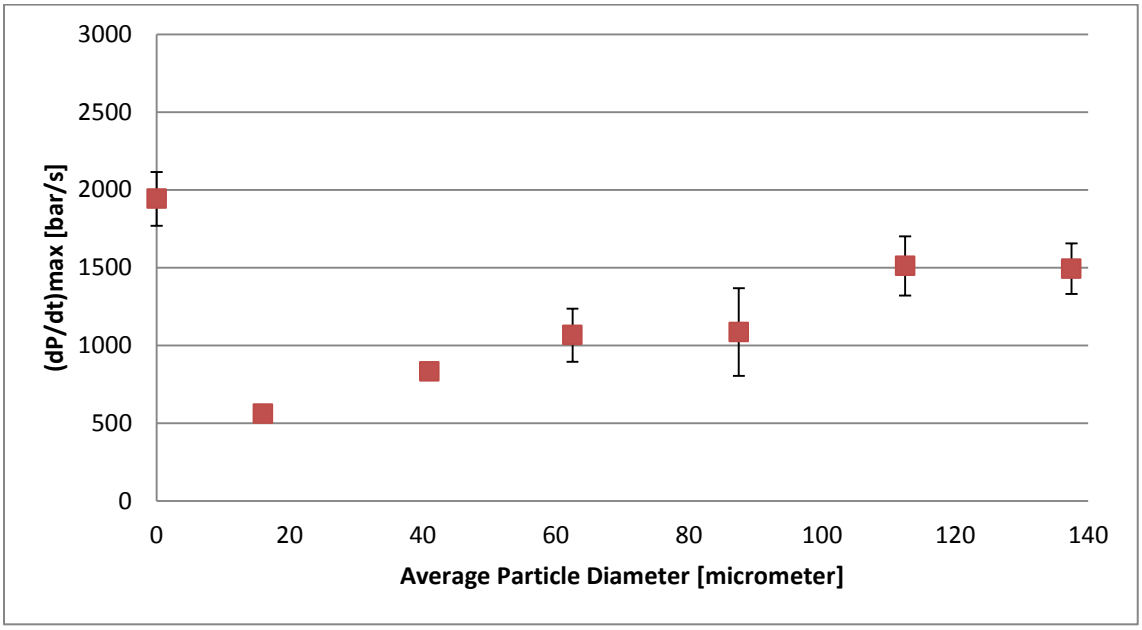

Figure 56: Relationship between average particle diameter and maximum rate of pressure rise for experiments done with a propane-air mixture with 4.2vol% propane.

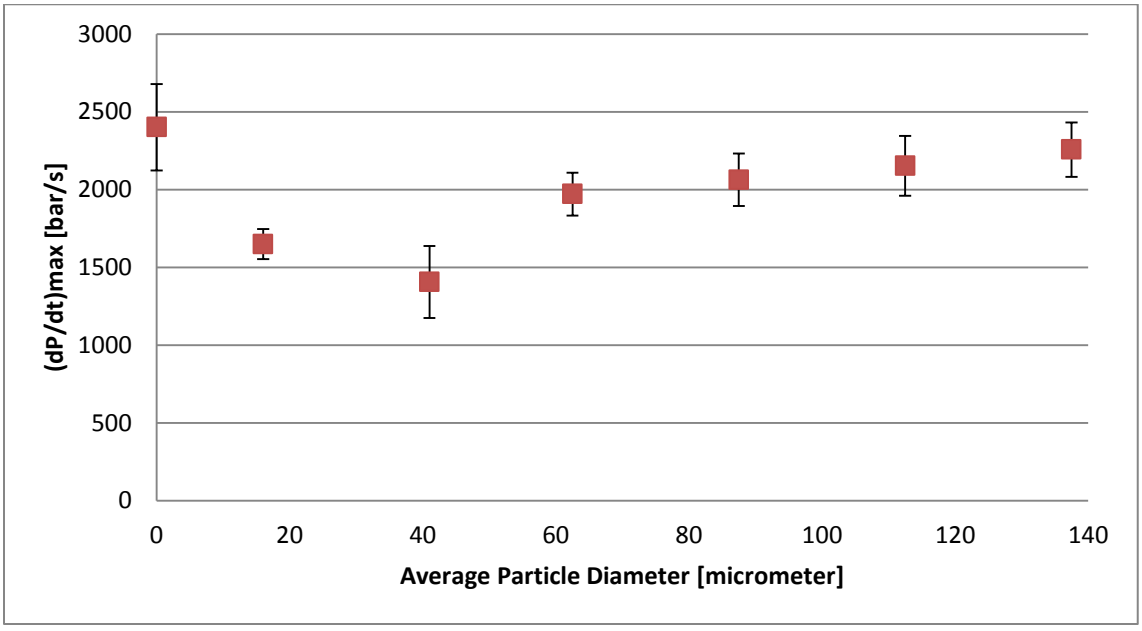

Figure 57: Relationship between average particle diameter and maximum rate of pressure rise for experiments done with a propane-air mixture with 5.25vol% propane.

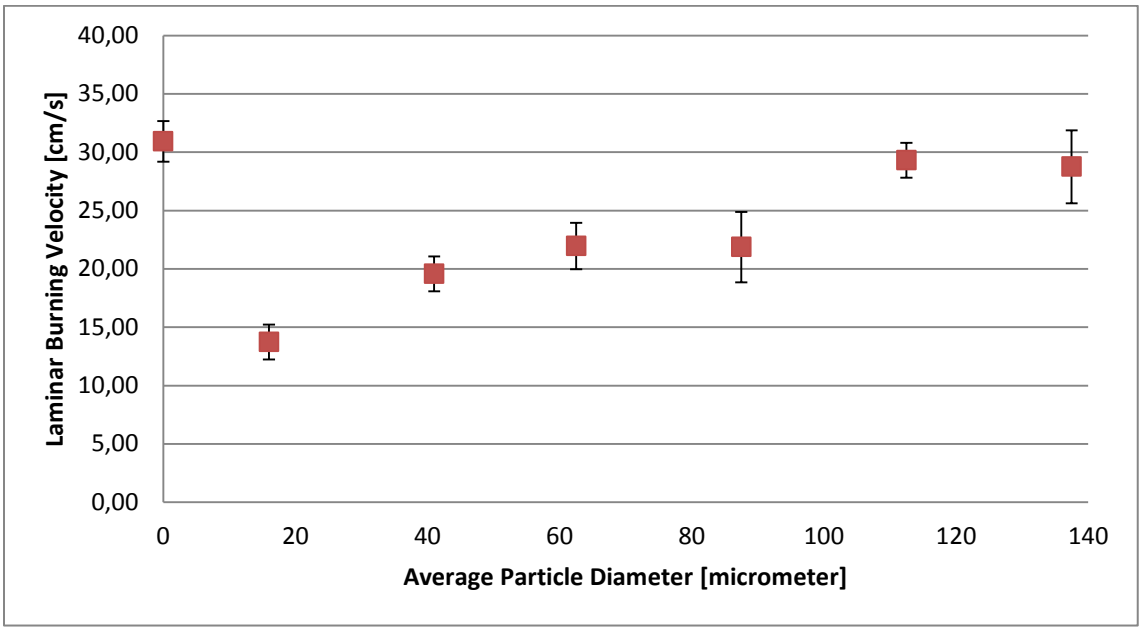

Figure 58: Relationship between average particle diameter and the laminar burning velocity for experiments done with a propane-air mixture with 4.2vol% propane.

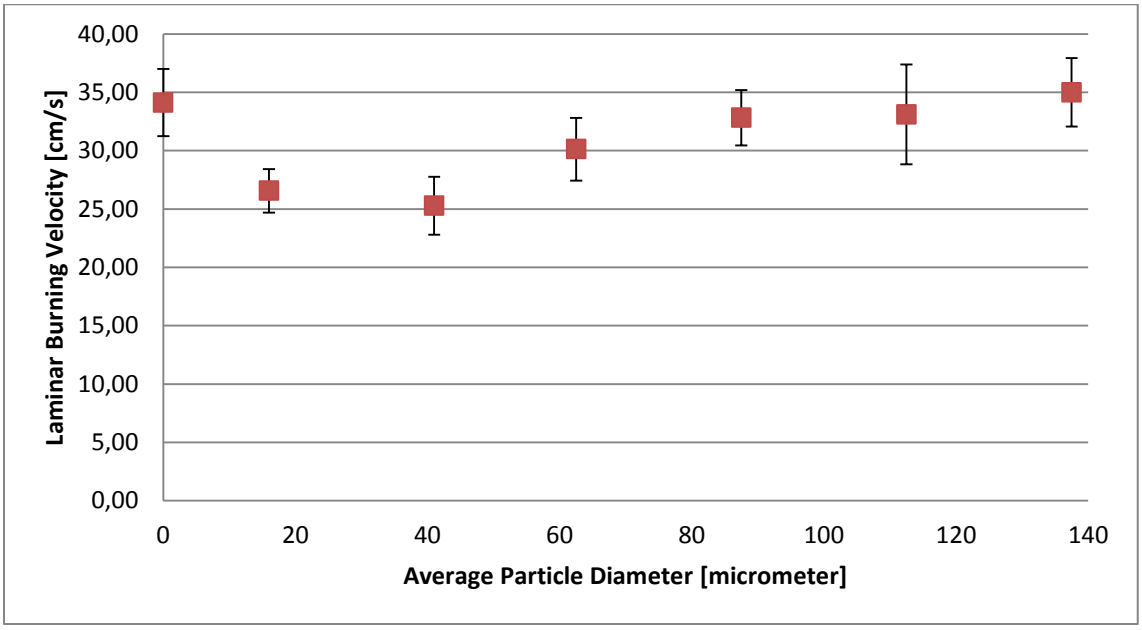

Figure 59: Relationship between average particle diameter and the laminar burning velocity for experiments done with a propane-air mixture with 5.25vol% propane.

Concentration of 50g/m^3

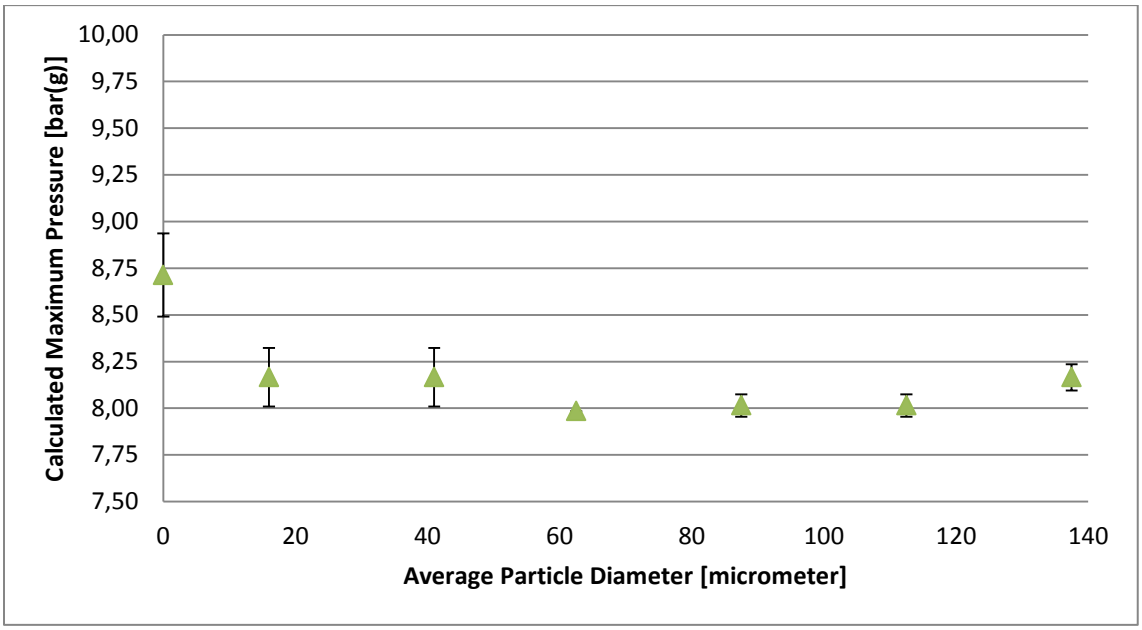

Figure 60: Relationship between average particle diameter and the calculated explosion pressure for experiments done with a propane-air mixture with 4.2vol% propane.

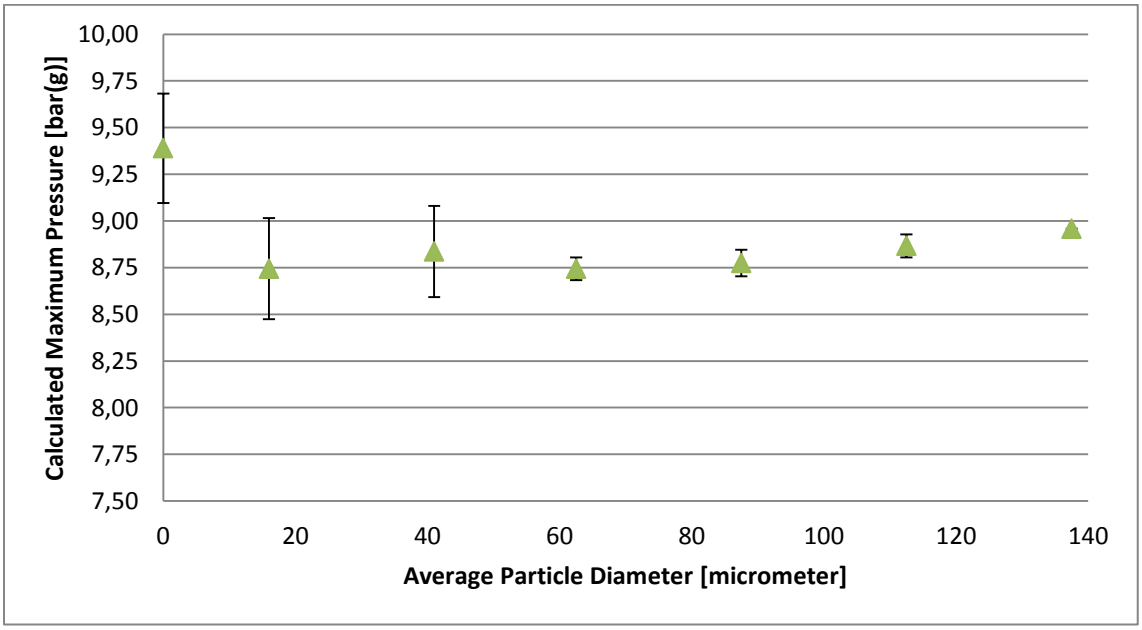

Figure 61: Relationship between average particle diameter and the calculated explosion pressure for experiments done with a propane-air mixture with 5.25vol% propane.

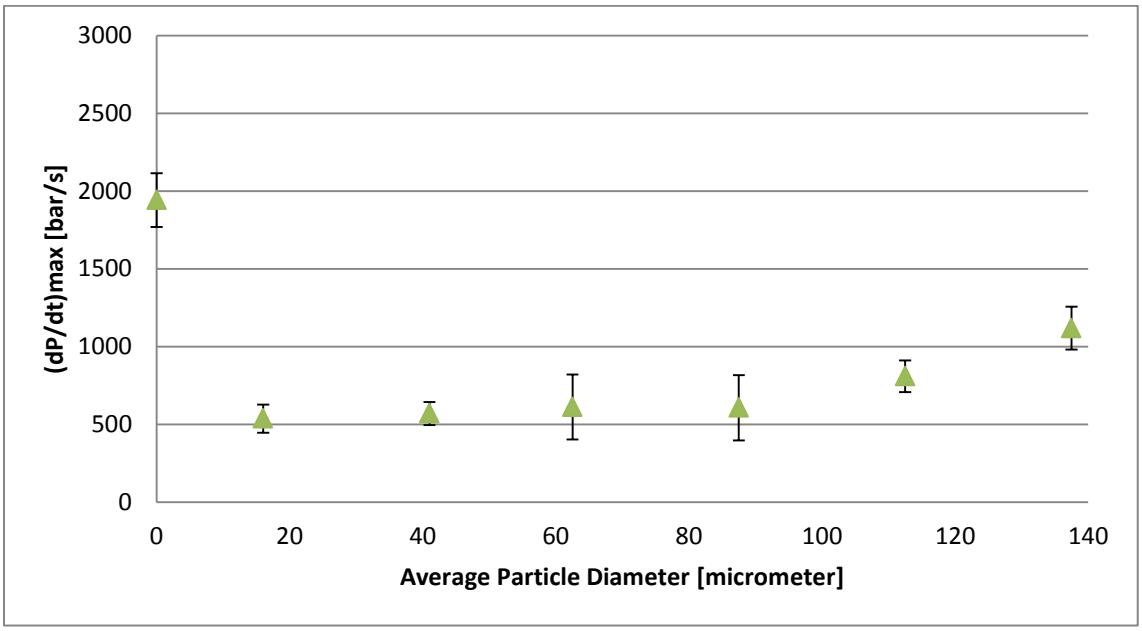

Figure 62: Relationship between average particle diameter and maximum rate of pressure rise for experiments done with a propane-air mixture with 4.2vol% propane.

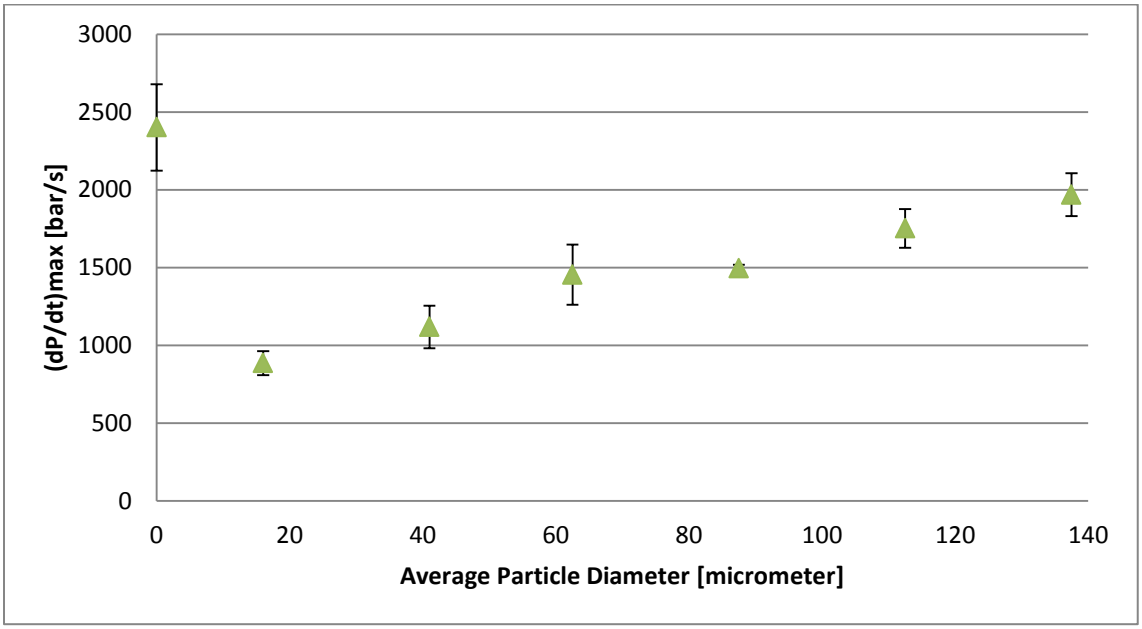

Figure 63: Relationship between average particle diameter and maximum rate of pressure rise for experiments done with a propane-air mixture with 5.25vol% propane.

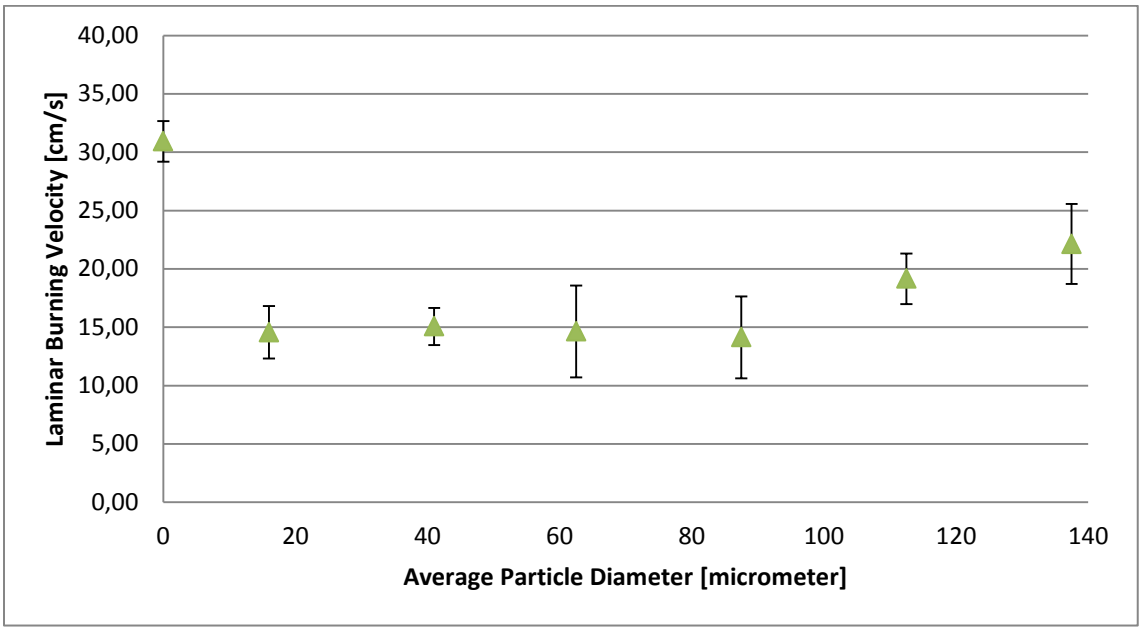

Figure 64: Relationship between average particle diameter and the laminar burning velocity for experiments done with a propane-air mixture with 4.2vol% propane.

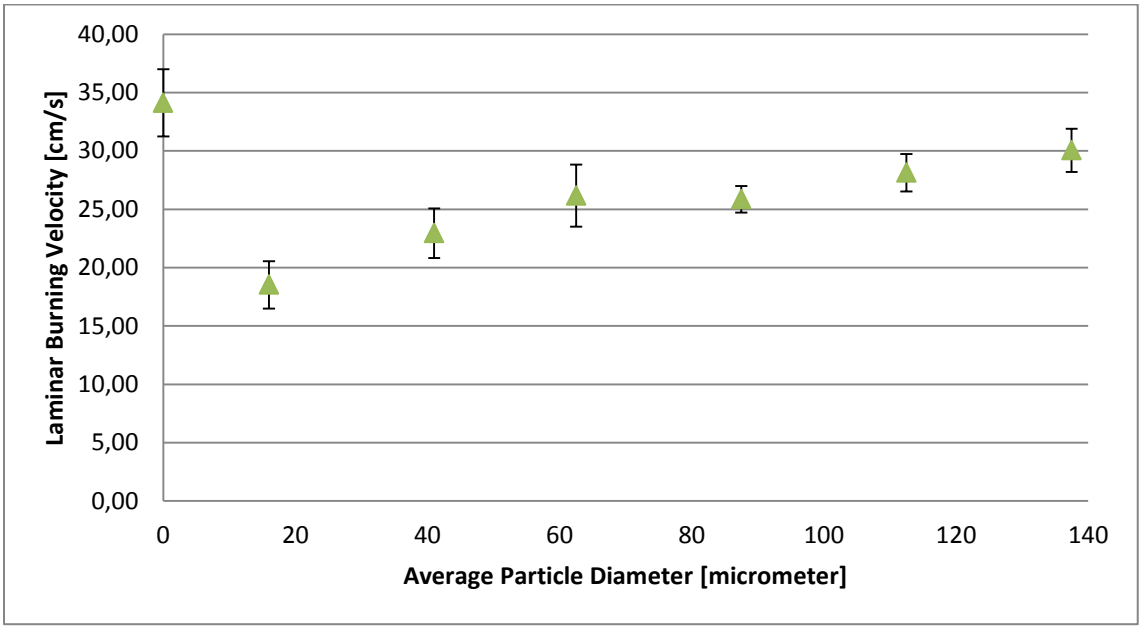

Figure 65: Relationship between average particle diameter and the laminar burning velocity for experiments done with a propane-air mixture with 5.25vol% propane.

Concentration of 100g/m^3

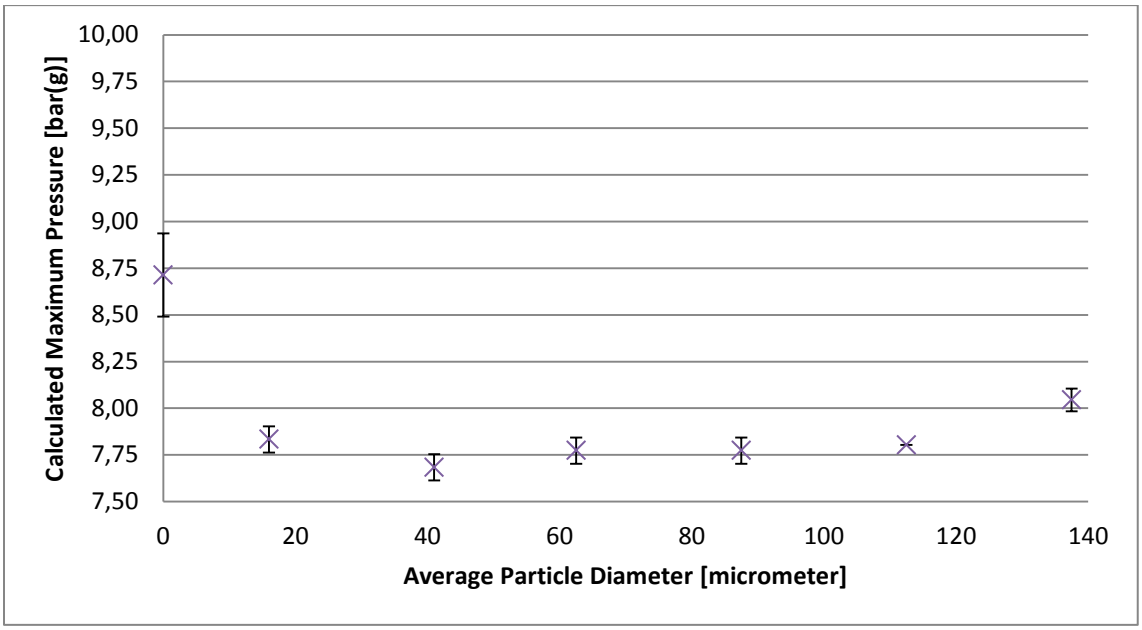

Figure 66: Relationship between average particle diameter and the calculated explosion pressure for experiments done with a propane-air mixture with 4.2vol% propane.

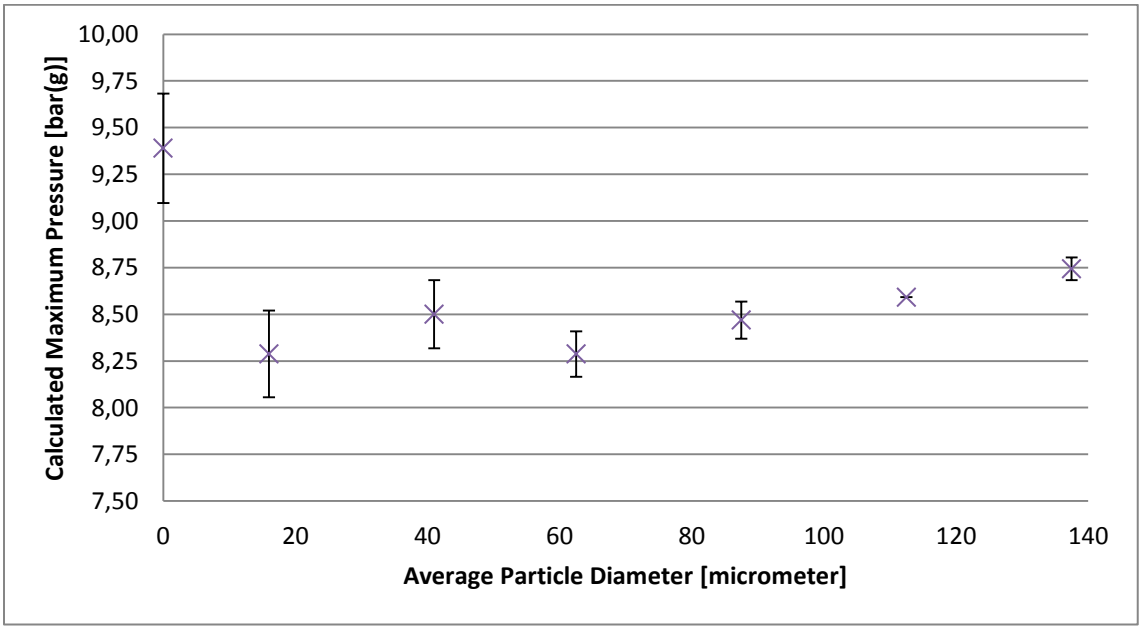

Figure 67: Relationship between average particle diameter and the calculated explosion pressure for experiments done with a propane-air mixture with 5.25vol% propane.

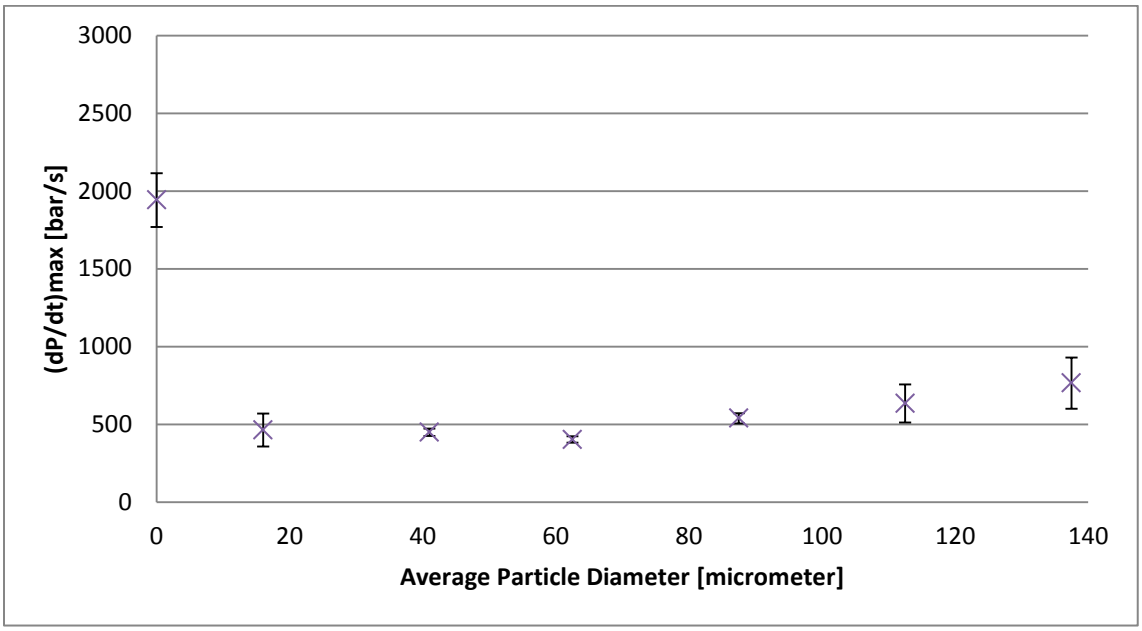

Figure 68: Relationship between average particle diameter and maximum rate of pressure rise for experiments done with a propane-air mixture with 4.2vol% propane.

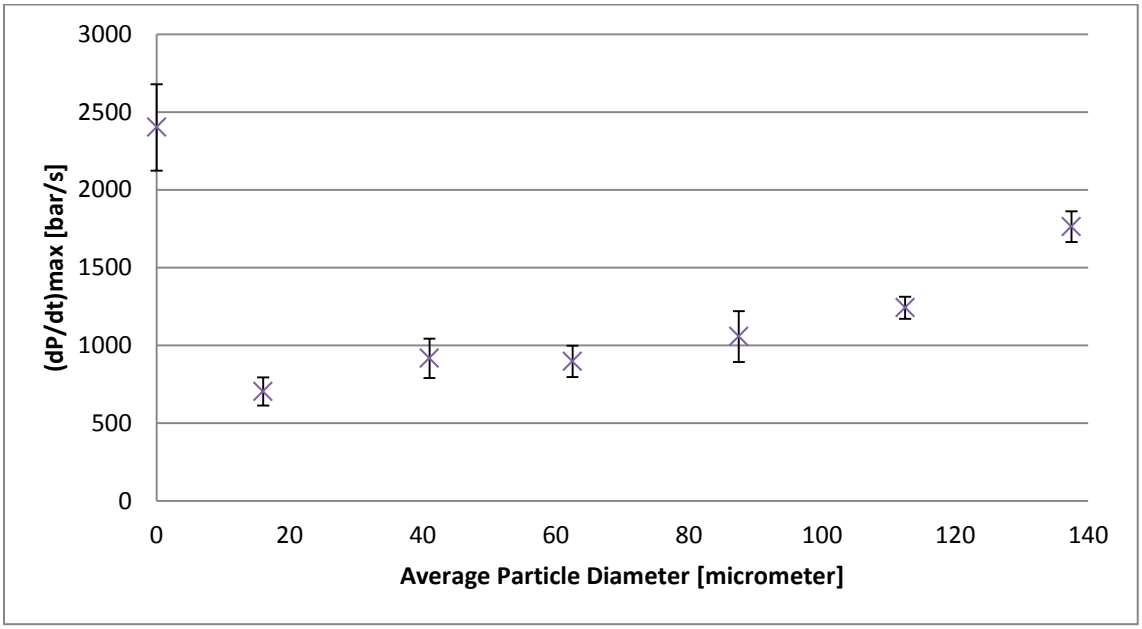

Figure 69: Relationship between average particle diameter and maximum rate of pressure rise for experiments done with a propane-air mixture with 5.25vol% propane.

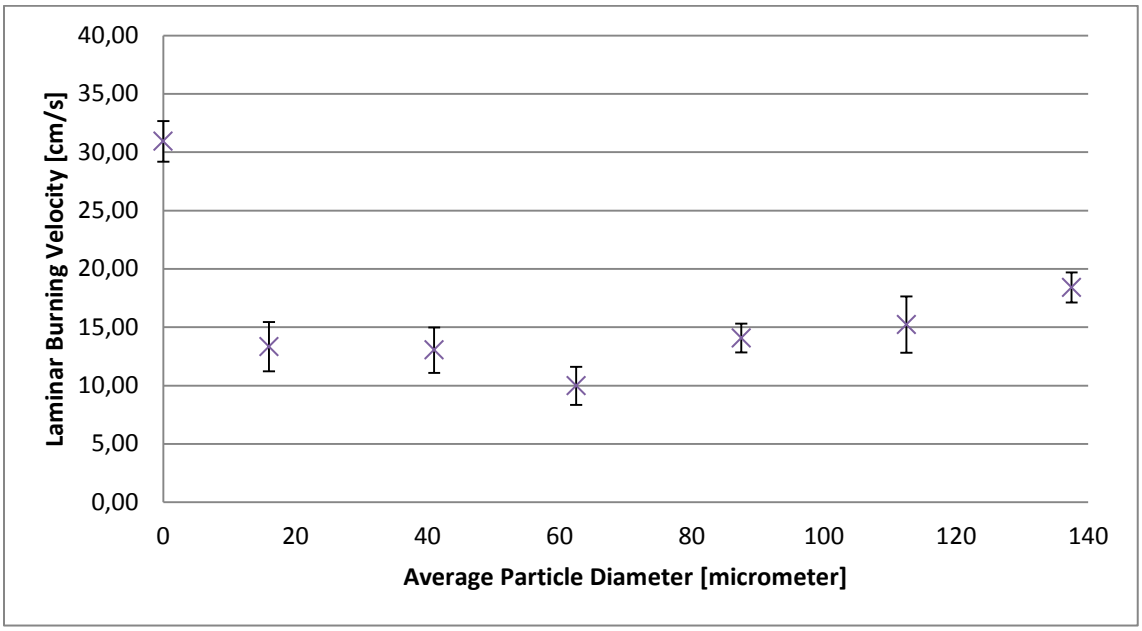

Figure 70: Relationship between average particle diameter and the laminar burning velocity for experiments done with a propane-air mixture with 4.2vol% propane.

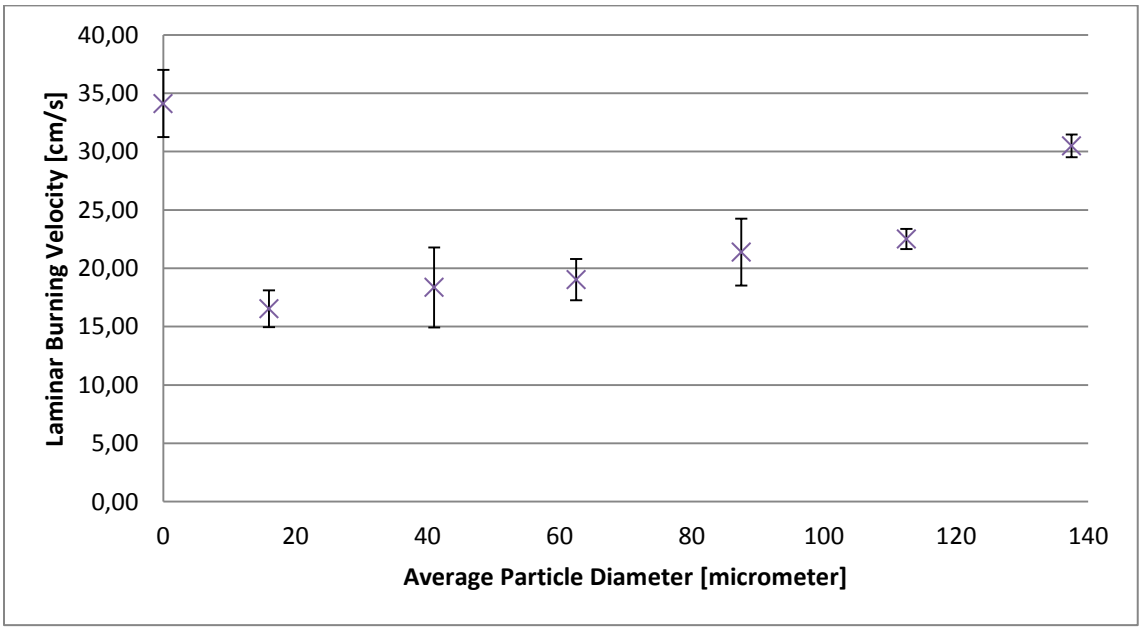

Figure 71: Relationship between average particle diameter and the laminar burning velocity for experiments done with a propane-air mixture with 5.25vol% propane.